# Interaction entre (Ru(bpy)2dppz(2+ et un brin court d'ADN : étude thermodynamique et structurale

Fuchao Jia

DISSERTATION

# THERMODYNAMIC AND STRUCTURAL STUDY OF THE INTERACTION BETWEEN $Ru(bpy)_2dppz^{2+}$ AND DNA

SPECIALTY: PHYSICS AND PHYSICAL CHEMISTRY

SUBMITTED BY

FUCHAO JIA

FOR THE DEGREE OF DOCTEUR OF THE UNIVERSITY OF STRASBOURG, FRANCE

DEFENDED NOVEMBER 22ND 2013
IN FRONT OF THE COMMITTEE:

| | |
|---|---|
| JEAN-PIERRE MÜNCH | ADVISOR |
| MING LI | EXTERNAL REFEREE |
| XINGGUO LIANG | EXTERNAL REFEREE |
| PHILIPPE TUREK | EXAMINER |
| WILFRIED GRANGE | EXAMINER |
| PASCAL HÉBRAUD | EXAMINER |

# Resumé

Dans une première partie, nous mesurons l'affinité de l'interaction entre $[Ru(pby)_2dppz]^{2+}$ et l'ADN en utilisant la luminescence induite lors de la complexation. Nous étudions l'évolution de l'affinité lorsque la force ionique de la solution augmente. Dans une deuxième partie, nous modifions les extrémités d'un double brin d'ADN en y greffant des fluorophores. De la mesure de transfer d'énergie non-radiative entre ces fluorophores, nous étudions l'évolution de la longueur du complexe.

Nous effectuons un dosage d'un double brin de 15 paires de bases d'ADN par le complexe ruthénié. Nous nous servons de la luminescence induite par l'intercalation du groupement dppz. Cependant, l'incrément de luminescence par groupement intercalé n'est pas connu, et nous ne pouvons pas le mesurer en saturant le brin d'ADN. Nous utilisons alors une technique mise au point par Nishida [Method for Measuring the Binding of Small Molecules to Proteins from Binding-Induced Alterations of Physical-Chemical Properties], dans laquelle deux titrations de deux solutions d'ADN de deux concentrations différentes sont effectuées. En utilisant le fait que, lorsque deux solutions d'ADN complexé par le composé ruthénié, possèdent la même luminescence par paire de base , le taux de complexation de ces deux solutions doit être le même, nous pouvons alors déterminer, sans hypothèse supplémentaire, le taux de complexation de l'ADN. De l'évolution de ce taux en fonction avec la concentration de ligand, nous déduisons son affinité pour l'ADN.

Nous étudions maintenant le changement de longueur d'un double brin d'ADN de 15 paires de bases, modifié à ses deux extrémités par deux fluorophores : Alexa488 et Alexa568. Lorsque Alexa 488 est porté dans un état excité, il peut se désexciter en transférant de l'énergie de manière non-radiative à Alexa568, qui se désexcite alors en émettant des photons de plus faibles énergie que ceux émis par Alexa488. L'efficacité de ce transfer d'énergie peut être quantifié à partir de la mesure des intensités émises à

basse et haute énergie. Elle dépend a priori de l'efficacité couplage (et en conséquence de la distance) entre les deux fluorophores. Nous effectuons des mesures de temps de vie des états excités de chacun des fluorophores. Nous avons observé que l'addition de ligand a pour conséquence une forte inhibition quenching des fluorophores. De l'analyse de l'évolution du temps de vie du fluorophore donneur d'une part et de celui du fluorophore accepteur d'autre part, nous déduisons l'évolution de l'efficacité du transfer d'énergie en fonction de la concentration de ligand. Nous confrontons les résultats obtenus par chacune de ces analyses, et en déduisons finalement, en nous servant de l'analyse de l'équilibre effectuée dans la première partie, l'évolution de la longueur de la chaîne en fonction du taux de complexation

# Abstract

This Ph.D thesis is mainly divided in to 2 parts. The first part is luminescence study, we are interested in the affinity constant (Ka) change under different salinity environments when the complexation of $[Ru(bpy)_2dppz]^{2+}$-DNA arrive equilibrium. In the second part, we focus our attention on the kinetic study by fluorescence which comes from the fluorophore. The distance change between 2 fluorophores is explored when $[Ru(bpy)_2dppz]^{2+}$ intercalates into DNA, which lead to the variation of DNA conformation. Any changes in DNA conformation will be reflected by the efficiency change of fluorescence resonance energy transfer (FRET). Quantitative analysis on the $Ru(bpy)_2dppz]^{2+}$-DNA interaction will be built in the second part.

In the first part, the interaction of $[Ru(bpy)_2dppz]^{2+}$ with DNA is studied in a wide range of DNA / $[Ru(bpy)_2dppz]^{2+}$ ratios by using the luminescence signal which comes from complex. The affinity constant (Ka) is explored under different chloride sodium concentration (NaCl=[0, 100 mM]), when the complexation reaches equilibrium. Nishida method is employed to compute the value of Ka without any hypothesis. The value of affinity constant is at the level scale of $10^6$ $M^{-1}$ which is basically identical to the other researcher's results. Ka decreased with increasing the

concentration of NaCl as we expected.

Quantitative analysis on the $Ru(bpy)_2dppz]^{2+}$-DNA interaction will be done in the second part. DNA was modified by different fluorophores at its extremities, 5' end and 3' end were labeled with alexa488 (seen as donor) and alexa568 (seen as acceptor), respectively. Our goal is to study the efficiency change of FRET and the change of distance between 2 fluorophores with fluorescence technique when one Ruthenium molecule intercalate in to DAN base pair. Two methods will be employed to achieve our idea. One is that the efficiency of FRET can be computed from the donor emission (alexa488), the other is the efficiency of FRET can be calculated from the acceptor emission (acceptor), the efficiency of FRET is highly dependent on the distance of 2 fluorophores ($E = \frac{1}{1+(\frac{r}{R_0})^6}$), any changes in distance will cause the efficiency change. The FRET efficiency decreased when the $[Ru(bpy)_2dppz]^{2+}$ intercalated into DNA structure, which also meant that the distance between 2 fluorohore increased.

# Acknowlegements

While many of the relationships that I have established during my graduate career were solely professional, some of them transited onto personal level and they have provided a lot more than just learning a particular set of skills or technical information. Nevertheless, I would like to take the opportunity and thank many people, who assisted me at some point along my career in one way or another, and without whom this work would not have been possible.

First of all, I would like to pay my deepest thank to my PhD advisor: Jean-Pierre Münch, for the support you provided. You helped and taught me how to solve scientific problems and fight with French administration when needed, your rigorous scientific attitude plays a very important role in my later research life. Many thanks for encouraging me to come to Strasbourg and to begin Ph.D thesis, which turned out to be one of the most challenging adventures so far. . .

Let me reveal my special appreciation to Pascal Hébraud. Sincerely appreciate your patience and enormous help in completing this project. You not only helped and taught me how to solve scientific problems and fight with French administration when needed, but you also give me uncountable support and great guidance for solving experimental and scientific problems, you always and immediately pull me back when my study is offset track, congratulations sent by you always arrive in time when I get progress in my study. Greatly appreciate your uncountable help, without you this work would not have been possible.

Many thanks to China Scholarship Council (CSC) for providing the financial support to me, for studying and living at Strasbourg.

I am also grateful to my close friends: Stéphane Despax, Alban Debacker, Maxime Liard and Damien Cianfarani who shared office and lab space with me, who helped me to deal with everyday challenges. Same grateful is sent to Marcelina Joanna Klajner and Piotr Klajner, thanks to whom my faith in people is still strong and steadfast.

Another uncountable debt of thanks is due to my Chinese friends: Yunjie Xiang, Quan Li, Fu Li, Xiaofeng Lin, Yuefeng Liu, Jingjie Luo, Xuemei Liao, Xiaojie Liu, Wei Yu, Wen Luo, Yang Zhou, Lei Wang, whose presence around me helped to avoid homesickness. Connected by the same choice of place to live or work, we spent together many moments discussing, helping each other or just having fun.

Many thanks are equally addressed to people who I have a great pleasure to work with: Sebastien Harlepp, Gilles Versini, and Jean-Pierre Vola. Thank you for your help and nice cooperation.

Out of all these people, above all I would like to thank my family; my marvelous Wife Dianli Cao, for continuously encouraging me towards finishing the thesis and never losing faith in me. I will keep everything you have given me in my life forever! My parents Mom—Renrong Zhang, Dad—Jinqing Jia and Sisters—Fuju Jia and Fuhua Jia for their never-ending help and support.

**Thank you!**

# Contents

# Chapter 1

## 1 Introduction

### 1.1 DNA and $Ru(bpy)_2dppz^{2+}$

$Ru(bpy)_2dppz^{2+}$ is an organometallic molecule (Figure 1.1), centered around a Ru atom bound with three ligands, whose one of them dipyridophenazine (dppz) allow for its strong interaction with DNA: it intercalates between DNA base pair. It exhibits the unique property of being luminescent when intercalation occurs. As a consequence, it plays an important role in exploring the structure and properties of DNA. It can be seen as a reporter of DNA structure, so it is very interesting to study on the interaction between the $Ru(bpy)_2dppz^{2+}$ and DNA.

Firstly, a general overview of DNA, structure and physical properties, is presented in the introductory part. Secondly, complexation of ruthenium and DNA is introduced in introduction.

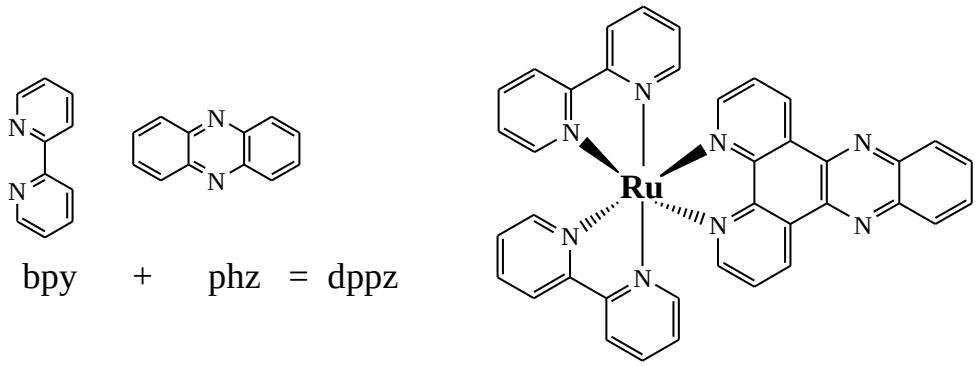


$[Ru(bpy)_2dppz]^{2+}$

**Figure 1.1:** Chemical structure of ligand (dppz) fragments and $[Ru(bpy)_2dppz]^{2+}$.

## 1.2 Deoxyribonucleic acid (DNA)

DNA is a very long, threadlike macromolecule built form a large number of dexoyribonucleotides, each composed of a base, a sugar, and a phosphate group. The bases of DNA molecules carry genetic information, whereas their sugar and phosphate group perform a structural role. All living cells on Earth, without any known exception, store their hereditary information in the universal language of DNA sequences. These monomers string together in a long linear sequence that encodes the genetic information.

## 1.2.1 Chemical structure of DNA

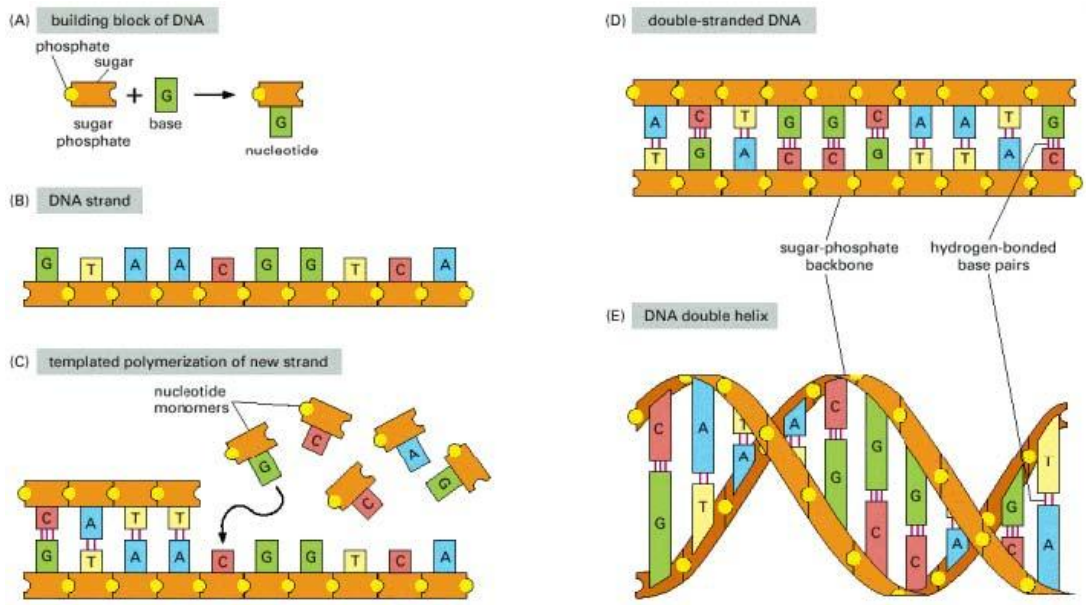


**Figure 1.2: (A)** Building block of DNA. **(B)** DNA strand. **(C)** Templated polymerization of new strand. **(D)** Double-stranded DNA. **(E)** DNA double helix [1].

DNA is made up of simple subunits, called nucleotides (Figure 1.2A and Figure 1.4), each consisting of a sugar-phosphate molecule with a nitrogen-containing sidegroup, called base, attached to it [2]. The bases are of four types (adenine, guanine, cytosine, and thymine), corresponding to four distinct nucleotides, labeled A, G, C, and T, the chemical structure of these bases is shown in Figure 1.3. A single strand of DNA consists of nucleotides joined together by sugar-phosphate linkages (Figure 1.2B). Note that the individual sugar-phosphate units are asymmetric, giving the backbone of the strand a definite directionality, or polarity. The backbone has two important features: it is highly flexible and is highly charged (in water, at room temperature). The negative charge of the backbone is due to the fact that the phosphate groups in water or under physiological pH are fully dissociated. Through template

polymerization (Figure 1.2C), the sequence of nucleotides in an existing DNA strand controls the sequence in which nucleotides are joined together in a new DNA strand; T in one strand pairs with A in the other, and G in one strand pairs with C in the other. The new strand has a nucleotide sequence complementary to that of the old strand, and a backbone with opposite directionality, i.e. GTAA. . . of the original strand, and . . .TTAC in complementary one. Normally DNA molecule consists of two complementary strands (Figure 1.2D). The nucleotides within each strand are linked by strong (covalent) chemical bonds; the complementary nucleotides on opposite strands are held together more weakly, by hydrogen bonds. The two strands twist around each other forming a double helix (Figure 1.2E)--a strong structure that can accommodate any sequence of nucleotides without changing its basic structure. The bases can pair in this way only if the two polynucleotide chains that contain them are anti-parallel to each other.

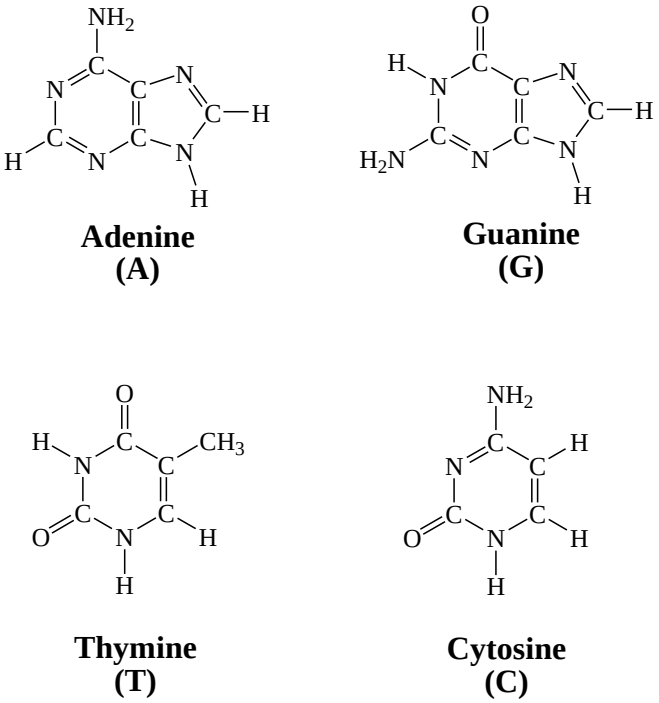


**Figure 1.3:** Chemical structure of four types of the DNA bases.

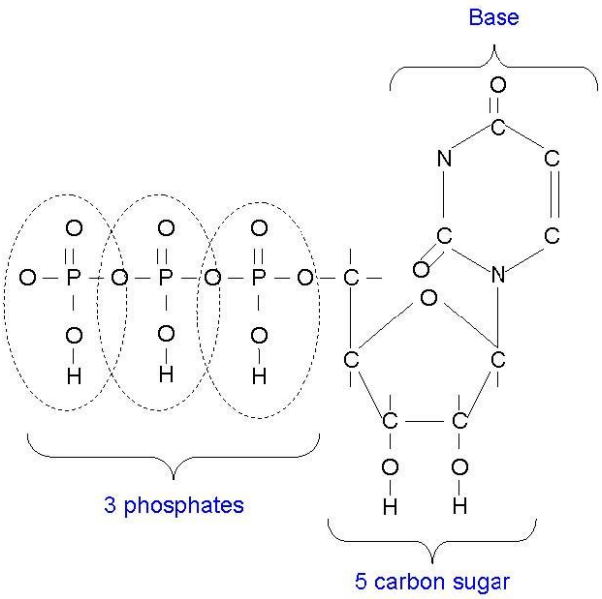


**Figure 1.4::** DNA consists of nucleotides. Single nucleotide is a sugar-phosphate molecule with attached nitrogen-containing base. Here, thymine (T) is presented [1].

## 1.2.2 Physical properties of DNA

The physical structure of double-stranded DNA is determined by the fact that its character is amphiphilic [3]. That means that one part of DNA chain (the phosphate backbone) is hydrophilic and another one (bases) is hydrophobic. Along with the flexibility of backbone, this amphiphilic character is a cause of double-helical structure of DNA. Double-stranded DNA occurs as a ladder which is twisted around its axis right-handed. The diameter of such twisted double-helix is 2.37 nm [3]. The twisting angle between adjacent base pairs is 34.6 ° and the distance between two neighbor nucleotides is 0.34 nm. The number of base pairs coinciding with the full twist (360 °) of DNA double-helix is around 10.4 [3]. That full twist repeats itself in every 3.4 nm (Figure 1.5). Between two molecules of deoxyribose attached to complementary base pairs, there is a space for creating grooves, which go along the

whole DNA chain. Both of the N-glycosidic bonds connecting deoxyribose with base pairs are on the same side of the double helix. Therefore the size of the grooves is not identical. They are 0.22 nm or 0.12 nm wide and are called major and minor groove, respectively [4].

DNA in solution is not rigid but is continually changing its conformation due to thermal fluctuations. Therefore, the bending stiffness of DNA is measured by the persistence length. It is defined as the distance over which the direction of a polymer segment persists, in the time or ensemble average, owing to limited flexibility of the polymer. It means the length of the DNA along which a thermally excited bend of 1 radian typically occurs. For DNA the persistence length is $l_p \approx$ 50 nm, ($\approx$ 150 bp). Under physiological conditions this value is larger than the persistence length of synthesized polymers: DNA is referred to as semi-flexible. The flexibility of DNA is due to fact that the covalent P-O (phosphate-oxygen) bonds can freely rotate around, so adjacent P-O (phosphate-oxygen), and deoxyribose rings can rotate freely. DNA chain may be described with the Worm-Like Chain model (WLC) [5].

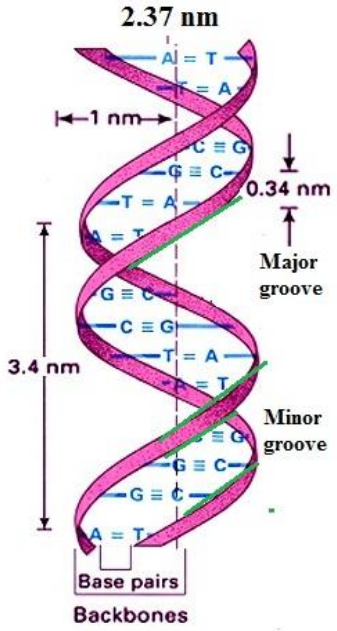


**Figure 1.5:** Physical structure of –B form DNA

## 1.2.3 Brief description of 3 kinds of DNA forms

**B-form DNA:** the most common form, present in most DNA at neutral pH and physiological salt concentrations, is B-form. That is the classic, right-handed double helical structure we have described in the previous part.

. **A-form DNA:** a thicker right-handed duplex with a shorter distance between the base pairs has been described for RNA-DNA duplexes and RNA-RNA duplexes. This is called A-form DNA.

**Z-form DNA:** a third form of duplex DNA has a strikingly different, left-handed helical structure. This Z DNA is formed by stretches of alternating purines and pyrimidines, e.g. GCGCGC, especially in negatively supercoiled DNA. A small amount of the DNA in a cell exists in the Z form.

The structure of three kinds of DNA forms is shown in Figure 1.6, and the comparison of three kinds of DNA shown in table 1.1 [6].

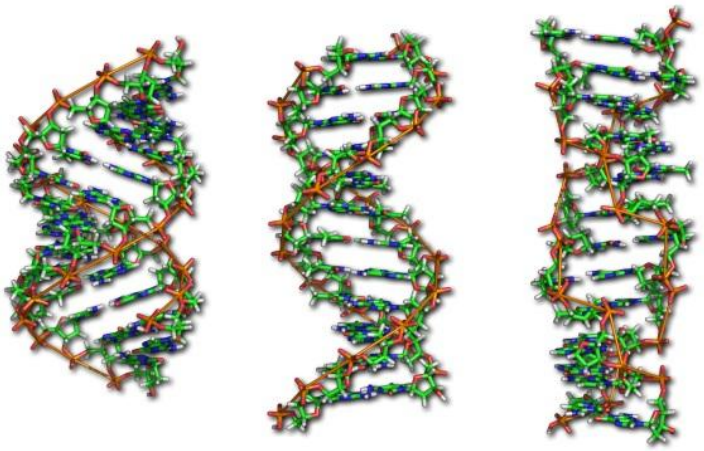

**Figure 1.6:** A-form (left), B-form (middle) and Z-DNA (right) .

**Table 1.1:** Comparison of A-, B-, and Z-DNA

| | Helix type | | |
|---|---|---|---|
| | A | B | Z |
| Shape | Broadest | Intermediate | Narrowest |
| Rise per base pair | 2.3 Å | 3.4 Å | 3.8 Å |
| Helix diameter | 25.5 Å | 23.7 Å | 18.4 Å |
| Screw sense | Right-handed | Right-handed | Left-handed |
| Base pair per turn of helix | 11 | 10.4 | 12 |
| Pitch per turn of helix | 25.3 Å | 35.4 Å | 45.6 Å |
| Tilt of base pairs from normal to helix | 19° | 1° | 9° |
| Major groove | Narrow and very deep | Wide and quite deep | Flat |
| Minor groove | Very broad and shallow | Narrow and quite deep | Very narrow and deep |

## 1.3 Binding modes of ruthenium compound with DNA

DNA association with ruthenium complexes does not involve the formation of a covalent bound, several interactions have been established for these complexes [7-14]. Three main different non-covalent modes are induced in this part: groove binding, intercalation and insertion, which are shown in Figure 1.7 and Figure 1.8 [15,16].

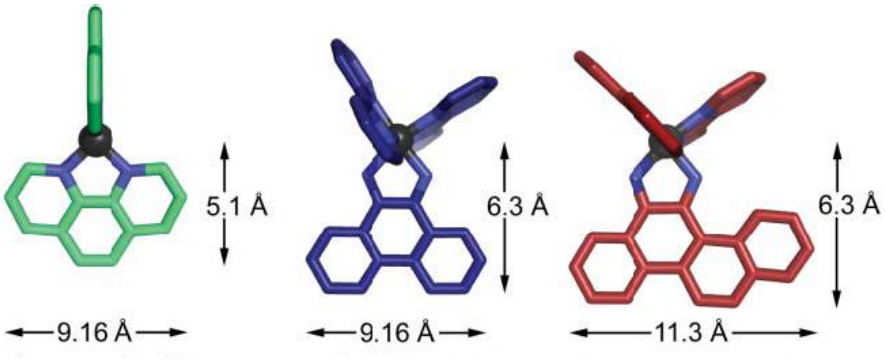


**(c) Groove binder** **(b) Metallointercalator** **(a) Metalloinsertor**

**Figure 1.7:** Geometries of (a) groove binder, (b) metallo-intercalator, (c) metallo-insertor [15].

**(a) Groove binder** **(b) Metallointercalator** **(c) Metalloinsertor**

**Figure 1.8:** The three binding modes of metal complexes with DNA: (a) groove binding, (b) intercalation, and (c) insertion [15].

***Groove binding:***

The earliest work has been performed on the DNA-binding of octahedral metal centers focused on tris(phenanthroline) complexes of ruthenium, chromium, zinc, nickel and cobalt (Figure. 1.9) [16-23]. Extensive photophysical and NMR experiments described that these complexes bind to DNA via two distinct modes: (1) hydrophobic interactions in the minor groove and (2) partial intercalation of a phenanthroline ligand into the helix in the major groove. Perhaps more important than the discovery of these dual binding modes, however, was the revelation these complexes provided regarding the importance of chirality in DNA-binding [24]. In the case of $[Ru(phen)_3]^{2+}$, for instance, the $\Delta$-enantiomer is found in the intercalative binding mode, while the complementary $\Lambda$-enantiomer is favored in the minor groove binding mode. In subsequent years, it was discovered that metal centers bearing more sterically demanding phenanthroline ligand derivatives, such as diphenylphenanthroline (DIP), display even more dramatic chiral discrimination. Luminescence and hypochromism assays have revealed enantioselective binding on the part of $[Ru(DIP)_3]^{2+}$; the $\Delta$-enantiomer binds enantiospecifically to right-handed B-DNA and the $\Lambda$-enantiomer binds only to left-handed Z-DNA [23]. This enantiospecificity has been exploited to map left-handed Z-DNA sites in supercoiled plasmids using $[\Lambda\text{-}Co(phen)_3]^{3+}$ [22]. Indeed, this trend in enantiomeric selectivity for octahedral tris(chelate) complexes, matching the symmetry of the complex to that of the DNA helix, has repeatedly and consistently been observed for non-covalent DNA-binding complexes developed in the years since these initial discoveries [25-27].

These earliest tris (phenanthroline) complexes do not, of course, represent the only examples of complexes that bind DNA via the minor or major grooves. For instance, the extensively studied $[Cu(phen)_2]^{+}$, has been shown to bind DNA via the minor groove. Indeed, these groove-binding complexes not only bind DNA but also cleave the macromolecule in the presence of hydrogen peroxide [28-30]. Metal complexes that bind in the groove have come a long way since these first studies and are now

quite sophisticated. Turro and co-workers, for instance, developed an artificial photonuclease by linking the metallo-groove-binder $[Ru(bpy)_3]^{2+}$ to an electron-acceptor chain containing two viologen units. Interestingly, the chemistry of metallo-groove-binders also extends to supramolecular self-assembly. Following the initial work of Lehn on the interaction and cleavage of DNA with a cuprous double-helicate [31], Hannon and co-workers designed a triple-helicate capable of recognizing three-way junctions in DNA. This intricate recognition has recently been characterized by single crystal X-ray crystallography [32-35].

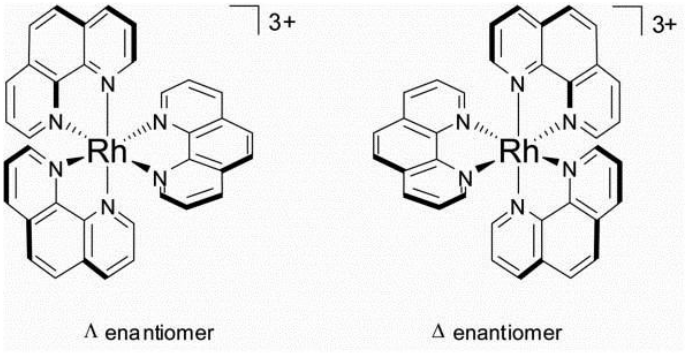


**Figure 1.9:** $\Lambda$ - and $\Delta$ -enantiomers of $[Rh(phen)_3]^{3+}$

***Metallo-intercalators between mismatched DNA base pairs:***

Intercalators are small organic molecules or metal complexes that unwind DNA in order to $\pi$-stack between two base pairs (Figure. 1.8). Metallo-intercalators, it then follows, are metal complexes that bear at least one intercalating ligand (Figure. 1.7). As their name suggests, these ligands, oriented parallel to the base pairs and protruding away from the metal center, can readily $\pi$-stack in the DNA duplex. Furthermore, upon binding, the ligands behave as a stable anchor for the metal complex with respect to the double helix and direct the orientation of the ancillary ligands with respect to the DNA duplex. Two well known examples of intercalating ligands are phi (9,10- phenanthrenequinone diimine) and dppz (Figure. 1.10) [25].

Ligand intercalation was first demonstrated by photophysical studies [8,16-22,36-40]. However, it was not until extensive NMR studies [41-44] and high

resolution crystal structures had been performed that the structural details of this binding mode were properly illuminated (Figure. 1.11) [45]. Metallo-intercalators intercalate into the double helix from the major groove, with the intercalating ligand acting in effect as a new base pair. No bases are ejected out of the duplex. Further, intercalation leads to a doubling of the rise and a widening of the major groove at the binding site. Importantly, this interaction distorts only minimally the structure of DNA. In the case of B-DNA, for example, the sugars and bases all maintain their original $C_2$' endo and anti conformations, respectively. Indeed, only the opening of the phosphate angles, not any base or sugar perturbations, is necessary for intercalation.

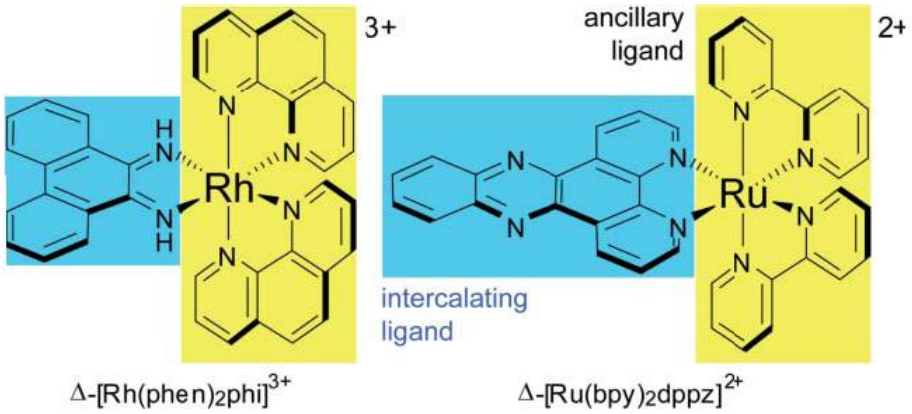


**Figure 1.10:** Chemical structure of two common metallo-intercalators: Δ -$[Rh(phen)_2(phi)]^{3+}$ (left) and Δ-$[Ru(bpy)_2(dppz)]^{2+}$ (right). The intercalating ligands are highlighted in blue, the ancillary ligands in yellow.

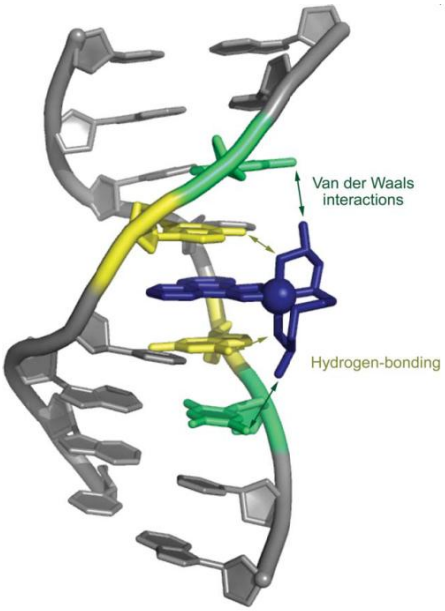


**Figure 1.11:** Crystal structure of the metallo-intercalator Δ - $\alpha$ -Rh[(R,R)-$Me_2$trien](phi)$^{3+}$ bound to its target sequence, 5'-TGCA-3'[15].

***Metallo-intercalators between mismatched DNA:***

The vast majority of non-covalent, DNA binding metal complexes are either groove-binders or intercalators. However, the nonexistence of complexes that bind DNA via other ways does not necessarily exclude the existence of alternative modes. Indeed, L. S. Lerman, in his article proposing intercalation as the DNA-binding mode for organic dyes, presciently proposed a third non-covalent binding mode: insertion [46]. He pointed that a molecule, may bind ''a DNA helix with separation and displacement of a base-pair.'' Metallo-insertors, like metallo-intercalators, contain a planar aromatic ligand that extends into the base-stack upon DNA-binding. However, while metallo-intercalators unwind the DNA and insert their planar ligand between two intact base-pairs, metallo-insertors eject the bases of a single base-pair, with their planar ligand acting as a $\pi$-stacking replacement in the DNA base stack. Until recently, no examples of DNA-binding insertors, neither metal-based nor organic, had been reported. However, the research of J Barton's on mismatch-specific DNA-binding agents has led to the discovery of a family of rhodium complexes that

bind DNA via this unique mode. These complexes have been dubbed metallo-insertors (Figure. 1.12), and the crystal structure of the metallo-insertor (red) bound to a target CA mismatch is given in Figure 1.13.

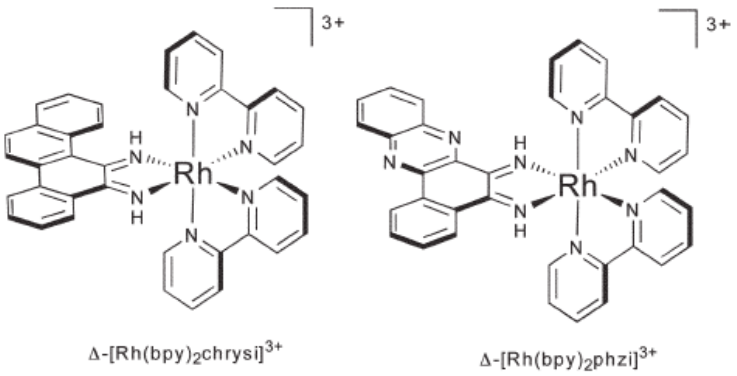


**Figure 1.12:** Chemical structures of mismatch-specific metallo-insertors.

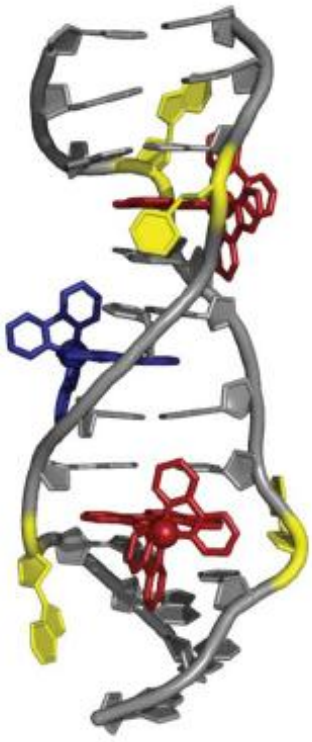

**Figure 1.13:** Crystal structure of the metallo-insertor (red) bound to a target CA mismatch [15].

## 1.4 Interaction between $Ru(bpy)_2dppz^{2+}$ and DNA

When the first observation of molecular "light switch" of $Ru(bpy)_2dppz^{2+}$ for DNA was discovered, intense studies were explored on the interaction between them [11,36,47-51]. In this part, we will briefly and mainly introduce some studies of J K Barton because of her excellent work in the developing of probing the structure of DNA.

1). *First observation of molecular "light switch" for DNA: $Ru(bpy)_2dppz^{2+}$ [36]:*

In this study, they find $Ru(bpy)_2dppz^{2+}$ to be a highly sensitive spectroscopic reporter of double-helical DNA by using steady-state emission spectra technique [36]. In aqueous solution, luminescence is detectable only when $Ru(bpy)_2dppz^{2+}$ intercalates into the nucleic acid structure. The emission characteristics furthermore sensitively distinguish both in terms of intensity and emission maximum the different helical forms of the polynucleotide (Figure 1.14). $Ru(bpy)_2dppz^{2+}$ was useful as a sensitive, nonradioactive, luminescent DNA probe in both heterogeneous and homogeneous assays.

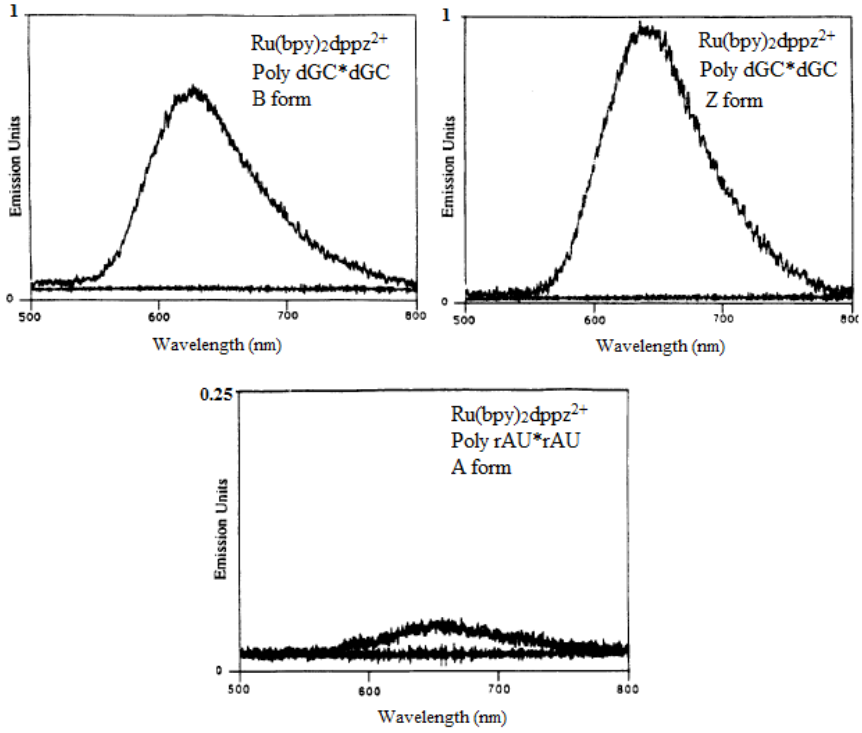


**Figure 1.14:** Steady-state emission spectra of $Ru(bpy)_2(dppz)^{2+}$(10 μM) in the absence and presence of B-form (top left), Z-form (top right), and A-form (bottom) double-helical DNA [36].

2). $Ru(bpy)_2dppz^{2+}$--*the light switch effect as a function of nucleic acid sequence and conformation [37]:*

The spectroscopic propeties for $Ru(bpy)_2dppz^{2+}$ and $Ru(phen)_2dppz^{2+}$ on binding to nucleic acids of different sequences and conformations have been explored by spectroscopic measurements. Both complexes ($Ru(bpy)_2dppz^{2+}$ and $Ru(phen)_2dppz^{2+}$) serve as "molecular light switch" for DNA, luminescing intensely in the presence of DNA but no photoluminescence in aqueous solution. The luminescent enhancement observed upon binding is attributed to the sensitivity of the excited state to quenching by water; the metal complex, upon intercalation into the DNA helix, is protected from the aqueous solvent, thereby preserving the luminescence. Correlations between the extent of protection (depending upon the DNA conformation) and the luminescence parameters are observed. Indeed, the strongest luminescent enhancement is observed for intercalation into DNA conformations which afford the greatest amount of overlap

with access from the major groove, such as in triple helices. Differences are observed in the luminescent parameters between the two complexes which also correlate with the level of water protection. In the presence of nucleic acids, these two complexes exhibit biexponential decays in emission. Quenching studies are consistent with two intercalative binding modes for the dppz ligand from the major groove: one in which the metal-phenazine axis lies along the DNA dyad axis and another where the metal-phenazine axis lies almost perpendicular to the DNA dyad axis. $Ru(bpy)_2dppz^{2+}$ and $Ru(phen)_2dppz^{2+}$ can be seen as unique reporters of nucleic acid structures and may become valuable in the design of new diagnostics for DNA.

3). *Sensitivity of $Ru(bpy)_2dppz^{2+}$ luminescence to DNA defects [50]:*

$Ru(bpy)_2dppz^{2+}$, upon binding to DNA contained a defect, exhibits significant luminescent enhancements above then well matched DNA. In the presence of a single base mismatch, large luminescent enhancements are evident when ruthenium bound to an oligonucleotide containing an abasic site (Figure 1.15). Titrations with hairpin oligonucleotides containing a variable mismatch site exists correlation between the level of luminescent enhancement and the thermodynamic destabilization associated with the mismatch. This correlation is reminiscent of that found earlier for a bulky rhodium complex that binds mismatched DNA sites through metalloinsertion, where the complex binds the DNA from the minor groove side, ejecting the mismatched bases into the major groove. This metalloinsertion mode for the dppz complex at the defect site is proved by differential quenching studies with minor and major groove quenchers and time-resolved emission studies. For sure, the utility of $Ru(bpy)_2dppz^{2+}$ can be seen as a sensitive reporter of DNA structure with defect site.

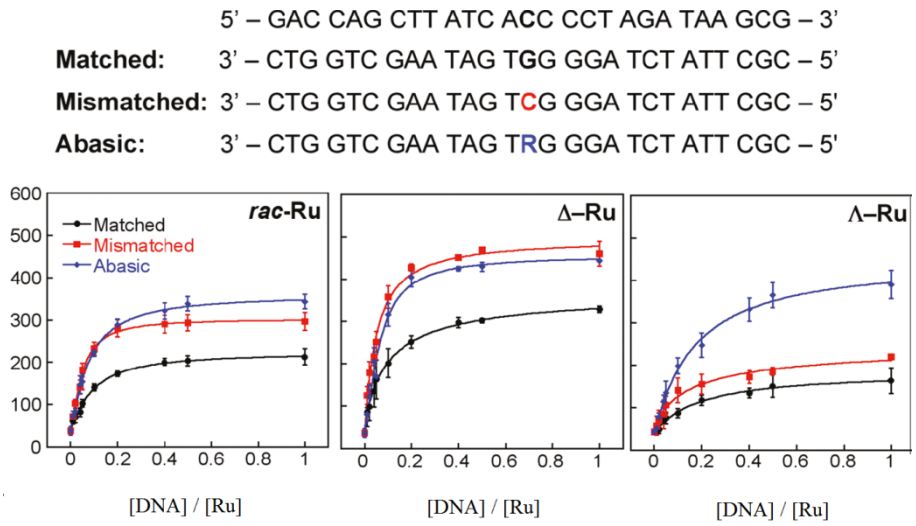


**Figure 1.15:** Titrations of $Ru(bpy)_2dppz^{2+}$ with DNAs containing defects. Top: DNA sequences of matched, mismatched and abasic 27-mer duplex DNA (R denotes a tetrahydrofuranyl abasic site). Bottom: plots of the integrated emission intensity ($\lambda_{ex}$ = 440 nm) of rac- (left), Δ- (middle), and Λ-$Ru(bpy)_2dppz^{2+}$ (right) (100 nM) upon increasing the concentration of DNA in 50 mMNaCl, 5 mM Tris, pH7.5 [50].

4). *Crystal structure of Δ-$Ru(bpy)_2dppz^{2+}$ bound to mismatched DNA reveals side-by-side metalloinsertion and intercalation [11]:*

The versatile binding modes attainable for octahedral metal complexes bearing an intercalating ligand are depicted in detail. Here it is shown that two independent views of metalloinsertion in this work, two of intercalation and one of end-capping (Figure 1.16 and 1.17). The metal complex binds with DNA through metalloinsertion in the minor groove at destabilized regions of the DNA, accompanied by extrusion of the mismatched bases. This binding mode has been observed previously with a sterically expansive ligand, but this structure clearly demonstrates that a narrower ligand such as dppz is equally capable of recognizing mismatches by the means of metalloinsertion, pointing to the generality of this binding mode. The smaller size of the dppz ligand also allows the ruthenium complex to bind through classical intercalation between two consecutive well-matched base pairs. Curiously, intercalated complexes are also located in the minor groove, which they hypothesize is stabilized by extensive ancillary interactions. This discrepancy notwithstanding, the

crystal structure attests to the remarkable structural flexibility of DNA upon high-density ligand binding, illustrates the nuanced binding geometries sampled by a non-covalently bound small molecule, and highlights the dominance of metalloinsertion as the preferred binding mode to destabilized regions of DNA. These newly obtained structural understandings will help guide the development of future generations of metal complexes as chemical tools and medicinal agents.

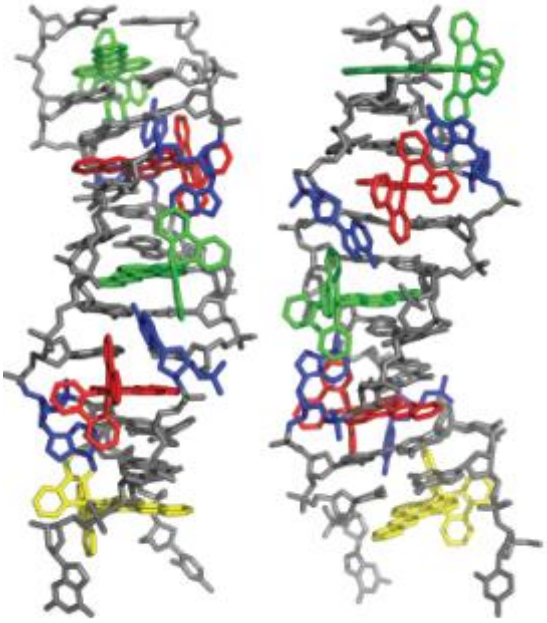

**Figure 1.16:** Structure of Δ -$[Ru(bpy)_2dppz]^{2+}$ bound to the mismatched oligonucleotide 5′-CGGAAATTACCG-3′. Front view (left) and view rotated 90 degrees (right) around the helix axis. Three DNA-binding modes are observed: (1) metalloinsertion, whereby the ruthenium complex (red) inserts the dppz ligand into the DNA duplex (grey) at the mismatched sites through the minor groove, extruding the mispaired adenosines (blue); (2) metallointercalation, whereby the complex (green) binds between two well-matched base pairs; (3) end-capping, whereby the complex (yellow) stacks with the terminal Watson–Crick pair of the duplex [11].

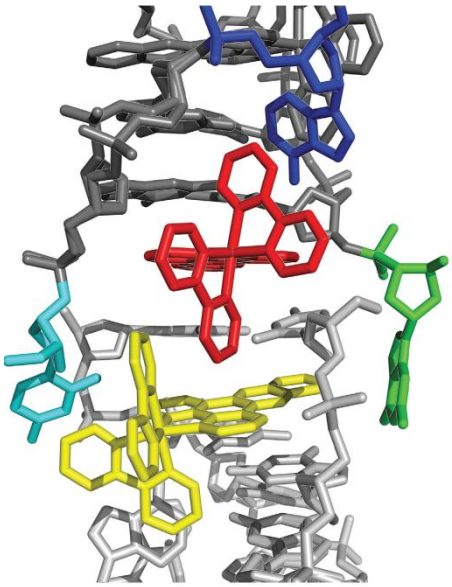

**Figure 1.17:** The end-capping complex. The duplex (dark grey) is end-capped by the ruthenium complex (red), which stacks between an extruded adenosine (blue) and the first complex (yellow) in a crystallographically related duplex (light grey). The last GC base pair (cytidine, cyan; guanosine, green) forms a frayed end [11].

## 1.5 Characterization of $Ru(bpy)_2dppz^{2+}$ and DNA interaction

$Ru(bpy)_2dppz^{2+}$ exhibits intense luminescence when upon binding to DNA due to the ligand part (dppz) intercalation into intact DNA base pair. There are two very interesting questions which deserve to be determined by their interactions as the interaction between them reaches equilibrium, these will help us to understand the interaction modes and the structural changes of DNA.

1) Determination of affinity constant ( $K_a$ )

$$Ru + \mathrm{DNA_{bp}} \overset{K_a}{\rightleftharpoons} [Ru - \mathrm{DNA_{bp}}]$$

A series of titrations are performed in our study, the luminescence intensity increases with the increase of ruthenium concentration ($C_{Ru}$), there exists linear

relationship between luminescence and rate of complexation at lower ruthenium concentration, which will be presented in the experimental part of chapter 2. In order to compute the affinity constant and complexation degrees without any hypothesis, in particular without assuming that the concentration at which DNA is saturated is known, a analysis method given by C. J. Halfman and T. Nishida is employed to calculate them according to the luminescence intensity change induced by $Ru(bpy)_2dppz^{2+}$ intercalation [52]. The values of affinity constant (be of the order of $10^6$ $M^{-1}$ at [NaCl] = 10 mM) gotten from Nishida method is similar with that value computed from the other scientists.

2) Dynamical changes of DNA helix

Although it is well known that the length of DNA increases approximately, when one $Ru(bpy)_2dppz^{2+}$ molecule intercalates into DNA base pair [53]. The induced dynamical changes, in terms of DNA, fluctuations are not established. In Chapter 3 of this manuscript, we will quantify the change of flexibility induced by the intercalation of $Ru(bpy)_2dppz^{2+}$, of a short dsDNA (15 base paris long). What about the kink when the binding of DNA with $Ru(bpy)_2dppz^{2+}$ occurs?

## Outline of the manuscript

In chapter 2, the interaction between $Ru(bpy)_2dppz^{2+}$ and DNA will be reported. We are going to follow the evolution of the luminescence intensity to compute the affinity constant $K_a$ and the number of base pair occupied by one ruthenium molecule with Nishida method. The dependence of $K_a$ on ionic strength is also explored. The results we get from chapter 2 will also be used in chapter 3 in order to quantify the dynamic changes.

In chapter 3, we use Fluorescence Resonance Energy Transfer (FRET) in order to monitor the average distance between the extremities of a 15 bp dsDNA modified with 2 fluorophores at its extremities. In this chapter, both ends of dsDNA are modified by two types of fluorophores: Alexa488 and Alexa568. When Alexa488 is excited to an excited state, it can decay by transferring non-radiative energy to Alexa568, which then de-excites by emitting photons of lower energy than those emitted by Alexa488. The efficiency of this energy transfer can be quantified from the measurement of intensities emitted at low and high energy. It depends on a priori of the coupling efficiency (and therefore the distance) between the two fluorophores. We will show that the increase of the average distance between the DNA extremities is incompatible with the assumption of a rigid and straight DNA/$Ru(bpy)_2dppz^{2+}$ complex.

# Chapter 2

## 2 Luminescence study

### 2.1 A brief introduction of luminescence

Since the elucidation of the structure of anti-parallel double helical DNA, intense research has focused on the development of nonradioactive probes for nucleic acids [15,54-58]. The construction of small molecules that recognize and react at specific DNA sites has been an area of intense interest. In particular, the study of transition metal complexes that bind DNA with specificity has been a burgeoning field. This growth has been due in large part to the useful properties of metal complexes, which possess a wide array of photophysical attributes and allow for the modular assembly of an ensemble of recognition elements [15,59].

There has been considerable interest in $Ru(bpy)_2dppz^{2+}$ as a luminescent probe of DNA over the past few decades since the first observation of molecular "light switch" for DNA [36]. The chemical structure of the ruthenium complex was shown in Figure 2.1. In particular, this complex is brightly luminescent when bound to DNA, but it is non-emissive in aqueous solution [36,37,47-49,60]. The "light-switch" effect originates from hydrogen bond formation with water, which quenches the excited-state luminescence and reduces the quantum yield by 2-3 orders of magnitude. In the bound form, the dppz ligand is intercalated into the DNA strand. Intercalation shields the phenazine nitrogens from the solvent and results in a luminescent excited state [61-64].

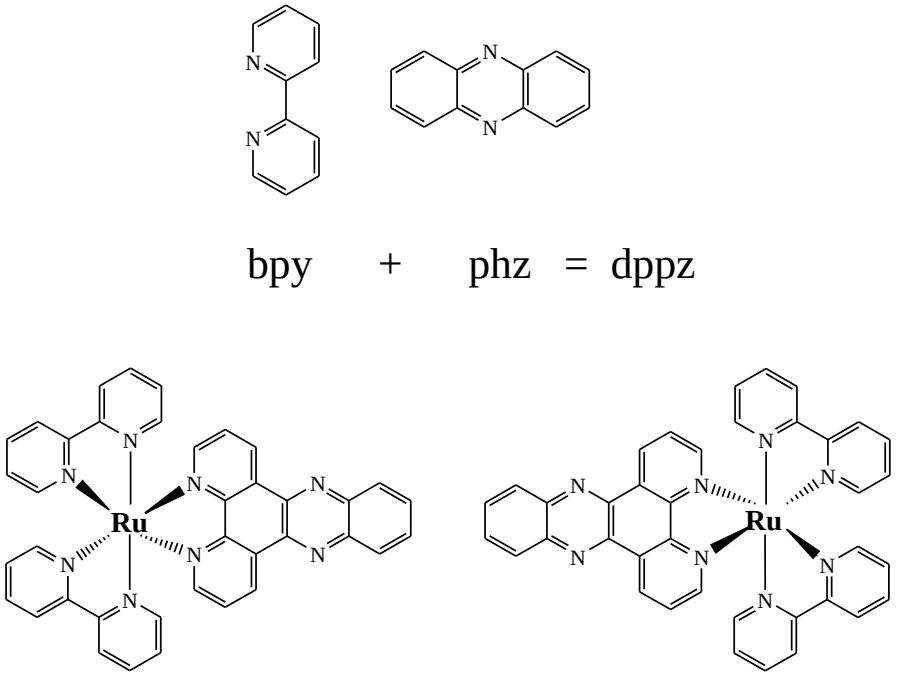


**Figure 2.1:** Chemical structure of ligand (dppz) fragments and $[Ru(bpy)_2dppz]^{2+}$.

## Our goal of luminescence study

The goal in this part is to study the interaction of $Ru(bpy)_2dppz^{2+}$ with DNA in a wide range of DNA / $Ru(bpy)_2dppz^{2+}$ ratios by using the luminescence signal which comes from the complex. The interaction of ruthenium-based compound with DNA has been studied in the limit of smaller concentrations of ruthenium derivatives than DNA base pairs. Luminescence studies have shown that ruthenium complexes exhibit high affinity with DNA and can recognize specific DNA sequences. Several tools have been employed to study the interaction between DNA and organometallic compound: spectroscopic measurements, such as absorption or emission spectroscopy [7,8,13,65], dichroic activity, either circular [9], that uses the chiral properties of DNA and of studied complexes or linear [10], as well as single molecule manipulations [53,66].

The equilibrium may be described by a single adsorption equilibrium:

$$Ru + \mathrm{DNA}_{bp} \underset{}{\overset{K_a}{\rightleftharpoons}} [Ru - \mathrm{DNA}_{bp}] \quad (2.\ 1)$$

$$\text{with} \quad K_a = \frac{[Ru - DNA_{bp}]}{[DNA_{bp}]_f [Ru]_f} \quad (2.\ 2)$$

We define the complexation ratio:

$$v = \frac{[Ru]_b}{\left[\mathrm{DNA}_{bp}\right]_t} \quad (2.\ 3)$$

Where $K_a$ is the affinity constant when the association reaches equilibrium, $[Ru - DNA_{bp}]$ is the concentration of complex, $[DNA_{bp}]_f$ and $\left[\mathrm{DNA}_{bp}\right]_t$ represent the free concentration and total concentration of DNA, respectively. Here $[Ru]_f$ and $[Ru]_b$ are the free concentration and bound concentration of $Ru(bpy)_2dppz^{2+}$, separately. $v$, the binding ratio, is equal to the bound ruthenium ($[Ru]_b$) over the total concentration of nucleic acid ($\left[\mathrm{DNA}_{bp}\right]_t$). How to build the relationship between luminescence intensity and binding intensity ($v$)? A linear relationship ($v \propto$ intensity) is often assumed, and the linear coefficient is determined when a plateau of the intensity is observed at high concentration of ligand. Nevertheless these 2 hypothesis ( linearity and $v = 1$ at the intensity plateau) have proven not to be correct for similar molecules and we will analyze our titration without any further hypothesis [67].

In this study, we follow the evolution of luminescence intensity when we add ruthenium compound into DNA solution, but we do not know the relationship between the change of luminescence intensity and binding intensity ($v$). Our purpose in this study is thus to find out the relationship between them. Any changes in luminescence intensity stem from the bound ruthenium ($[Ru]_b$), and $K_a$ has a relationship with bound ruthenium $[Ru]_b$. So if we can successfully build a

relationship between $K_a$ and $v$, the question will be answered. Now we reorganize the $K_a$ equation with consideration of $v$:

$$K_a = \frac{v}{(1-v)[Ru]_f} \tag{2. 4}$$

$$\frac{v}{[Ru]_f} = K_a(1-v) \tag{2. 5}$$

This model assumes that the size of ligand is very tiny and hence one ruthenium molecule can bind to just one DNA base pair. Therefore, plotting the $\frac{v}{[Ru]_f}(v)$, we expect to obtain the linear plot whose slope would be -1 and intercept with y-axis is $K_a$. Nevertheless when we plot $\frac{v}{[Ru]_f}$ as a function of $v$, the slopes is different from -1. It means that the number of bound DNA per $Ru(bpy)_2dppz^{2+}$ is not 1 and that slope and intercept cannot be interpreted in that way, even the estimation of their linear part results in errors. In order to compute the affinity constant and comlexation degree of ruthenium with DNA, we used a method to analyze the experiment results without any hypothesis, proposed by Toshiro Nishida and Wlodzimierz Bujalowski [52,68,69]. It has been proven that it was very efficient in Nishida's and Bujalowski's study.

We design similar experiments according to their study, three titrations with different ruthenium concentrations are performed in our work. The interaction between $Ru(bpy)_2dppz^{2+}$ and DNA was explored with increasing the concentration of $Ru(bpy)_2dppz^{2+}$ in sodium chloride solvent, the evolution of luminescence intensity as a function of ruthenium concentration is recorded. The salt dependence of $K_a$ is also explrored in our study. (Salt concentration varies from 10 mM to 100 mM).

## 2.2 Description of Nishida technique

Any method used to analyze ligand binding to a macromolecule generally related the extent of the complex formation to the free ligand concentration in solution. Binding isotherms of a protein association with a nucleic acid or, in general, of ligand binding to a macromolecule represent a direct relationship between the degree of binding (moles of ligand bound per mole of a macromolecule) and the free ligand concentration [68,70-72]. Analogously, in the case of the protein (ligand) binding to a long one-dimensional nucleic acid lattice, the equilibrium binding isotherm represents the direct relationship between the binding density (moles of ligand bound per mole of bases or base pairs) and the free protein concentration [68,72-78]. A true thermodynamic binding isotherm is model-independent and reflects only this relationship. Only then, when such a relationship is available, can one proceed to extract physically meaningful interaction parameters that characterize the examined interacting systems.

This is accomplished by comparing the experimental isotherms to theoretical predictions based on specific statistical thermodynamic models that incorporate known molecular aspects of the system, such as intrinsic binding constants, cooperativity parameters, allosteric equilibrium constants, discrete character of the binding sites or overlap of potential binding sites, etc. Only then, can one make rational molecular interpretations of the nature and mechanisms of the observed phenomena.

Numerous techniques have been developed or applied to study equilibrium properties of specific and nonspecific protein-nucleic acid interactions [79-87]. In our study, we mainly use a method to analyze our results, performed by Toshiro Nishida. This method is presented for obtaining binding data in any ligand-macromolecule

system for which binding induces a measurable change in a physical property of the system. The relationship between the equivalents of ligand bound and the physical property change need not be a known theoretical function, nor need it be empirically determined at an impractically high ligand concentration. Rather, the physical property change is measured at a number of total ligand-macromolecule mole ratios at two or more protein concentrations. The number of equivalents of bound ligand and the concentration of free ligand is computed from data obtained at a minimum of two macromolecule concentrations.

Binding of small ligand to macromolecule is described by the same mass action law (Equation 2.6) that applies to the association of simpler monovalent substances[88].

$$v = \frac{nK_a c_f}{1 + K_a c_f} \tag{2. 6}$$

where $v$ is equal to the average mole ratio of bound ligand to macromolecule (also can be called as bind intensity), $c_f$ is the equilibrium free-ligand concentration, $n$ is number of binding sites on a macromolecule, and $K_a$ is the intrinsic association constant of the binding sites. This relationship describes the binding when the intrinsic association constants of all $n$ sites are equal and when binding to any one site does not influence binding to any other site.

An ideal analysis of data from binding studies would allow each $n$ and $K_a$, and be determined unambiguously. When all sites are equivalent, $n$ and $K_a$ may be determined by plotting $v^{-1}$ as a function of $c_f^{-1}$ as suggested by Klotz [89] or by plotting $\frac{v}{c_f}$ vs. $v$ suggested by Scatchard et al [90,91].

At a sufficiently low macromolecule concentration ($P$), the fraction of bound to total ligand is significantly less than 1 and the free concentration of ligand ($c_f$) can be determined from the difference between the mole ratio of total ligand to protein and $\bar{v}$ multiplied by the protein concentration, The determination was given by Equation 2.7.

$$c_f = P(\frac{c_t}{P} - v) \tag{2.7}$$

where $c_t$ is total concentration of ligand, $P$ represents the total concentration of macromolecule. Let us perform 2 titrations, a and b, at 2 macromolecule concentrations, $P_a$ and $P_b$. If the measured intensity per macromolecule is the same, then the binding ratios $\nu_a$ and $\nu_b$ are equal. Let us call $c_{ta}$ and $c_{tb}$ the total ligand concentrations corresponding to identical intensities per macromolecule. We have, from (Equation 2.7) and solving for $\nu = \nu_a = \nu_b$.

$$\nu = \frac{(c_t / P)_a - \frac{P_b}{P_a}(c_t / P)_b}{1 - \frac{P_b}{P_a}} \tag{2.8}$$

Where $(c_t / P)_a$ and $(c_t / P)_b$ are the total concentration of ligands per macromolecule added macromolecules concentrations $P_a$ and $P_b$, that leads to the same intensity per macromolecule to the same $\nu$.

from which, using Equation 2.7, and we have:

$$c_f = \frac{P_a P_b}{P_a - P_b}[(c_t / P)_a - (c_t / P)_b] \tag{2.9}$$

Our goal is to study and quantify the association between a double stranded DNA macromolecule and $Ru(bpy)_2dppz^{2+}$ with this method. DNA base pairs and $Ru(bpy)_2dppz^{2+}$ are seen as protein and ligand, respectively. We also study on the salt dependence of affinity constant $K_a$ with different concentrations of NaCl (10 mM, 20 mM, 50 mM, 100 mM) in our study.

## 2.3 Experimental part

### 2.3.1 Experimental results

Luminescence study experiments have been performed in different salinity environments (10 mM, 20 mM, 50 mM, and 100 mM of NaCl). We perform a titration of 15 base pairs dsDNA by adding $Ru(bpy)_2dppz^{2+}$ to that the DNA concentration remains constant. For each salinity, we perform titrations at $[DNA]_{strand}$ = 2.5 μM, 5 μM, and 10 μM. The luminescence intensity as a function of contrentration ratio ( $C_{Ru(bpy)_2 dppz^{2+}} / C_{DNA_{bp}}$ ) under different salinity concentrations are shown in Figure 2.2. At first glance, the luminescence intensity increases with adding more $Ru(bpy)_2dppz^{2+}$ into the DNA solution. In other words, the complexation of $Ru(bpy)_2dppz^{2+}$ with DNA increases, more and more $Ru(bpy)_2dppz^{2+}$ molecules intercalate into the DNA base pairs lead to the intensity increase up to a saturation. This saturation level is approximately proportional to the DNA strand concentration (see the plateau at high $C_{Ru}$ in Figure 2.3). Nishida's method is applied to compute the affinity constant, the binding intensity and the free concentration of $Ru(bpy)_2dppz^{2+}$ .

**Table 2.1:** Protocol of titration of luminescence measurements

| $V_{total}$ (μl) | $V_{DNA,add}$ (μl) | $V_{Ru,add}$ (μl) | [DNA] (μM) | $C_{Ru}$ (μM) |
|---|---|---|---|---|
| 10 | 0 | 0 | 2.5 | 0 |
| 14 | 1 | 3 | 2.5 | 0.01 |
| 22 | 2 | 6 | 2.5 | 0.02 |
| 27 | 1 | 4 | 2.4 | 0.031 |
| 34 | 2 | 5 | 2.5 | 0.039 |
| 43 | 1 | 8 | 2.44 | 0.05 |
| 45 | 1 | 1 | 2.55 | 0.058 |
| 46 | 0 | 1 | 2.5 | 0.068 |
| 47 | 0 | 1 | 2.44 | 0.077 |
| 50 | 1 | 2 | 2.5 | 0.093 |
| 10 | 0 | 0 | 2.5 | 0.1 |
| 15 | 1 | 4 | 2.33 | 0.2 |
| 19 | 1 | 3 | 2.36 | 0.31 |
| 25 | 2 | 4 | 2.6 | 0.4 |
| 34 | 2 | 7 | 2.5 | 0.5 |
| 35 | 0 | 1 | 2.42 | 0.62 |
| 37 | 1 | 1 | 2.56 | 0.72 |
| 38 | -0 | 1 | 2.5 | 0.842 |
| 39 | 0 | 1 | 2.43 | 0.94 |
| 41 | 1 | 1 | 2.56 | 1.02 |
| 47 | 1 | 5 | 2.44 | 1.95 |
| 10 | 0 | 0 | 2.5 | 3 |
| 13 | 1 | 2 | 2.69 | 3.84 |
| 18 | 1 | 4 | 2.5 | 5 |
| 25 | 1 | 6 | 2.6 | 6 |
| 26 | -0 | 1 | 2.5 | 7.69 |
| 33 | 1 | 6 | 2.87 | 7.87 |
| 34 | -0 | 1 | 2.79 | 9.11 |
| 35 | -0 | 1 | 2.71 | 10.28 |
| 39 | 0 | 4 | 2.43 | 19.48 |
| 49 | 3 | 7 | 2.55 | 29.79 |

Where $V_{DNA,add}$ and $V_{Ru,add}$ are the volume of added DNA and $Ru(bpy)_2dppz^{2+}$ for every single measurement to keep the DNA concentration as a constant and increase the ruthenium concentration, respectively. [DNA] and [$Ru(bpy)_2dppz^{2+}$] represent the final concentration of DNA and $Ru(bpy)_2dppz^{2+}$, respectively

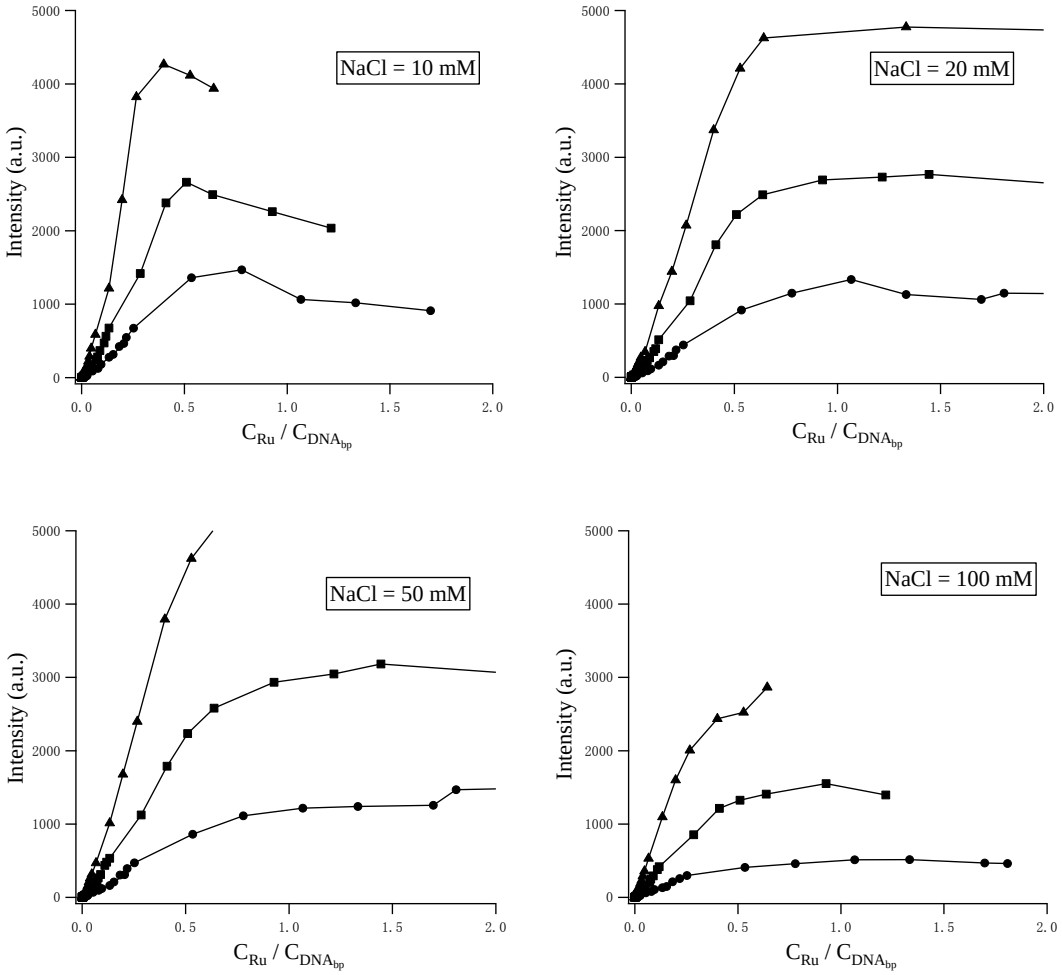


**Figure 2.2:** Evolution of luminescence intensity as a function of concentration ratio ($C_{Ru}$ / $C_{DNAbp}$)under different salinity concentrations. The concentrations of DNA strand are 2.5 μM (circle), 5 μM (square) and 10 μM (triangle), respectively.

## 2.3.2 Data analysis and results

To obtain reliable results from this treatment of the data, it is necessary that the binding doesn't involve DNA concentration effects and that intercalation-induced luminescence change is not dependent upon DNA concentration, so the luminescence intensity was normalized firstly. Then we plot the normalized intensity versus concentration of ruthenium ($C_{Ru}$), one group titration results with 0.01 M of NaCl

were shown in Figure 2.3. In order to correctly apply Nishida technique on our experiment result, valid range for intensity should be chosen between 0 and plateau value which depends on the concentration of Ruthenium and DNA. After choosing the valid range, a linear approximation is done between successive points, the points with the same intensity per DNA strand are picked up (Figure 2.3 circles), but this method creates unphysical changes of curvature when at each experimentally measured value. So we keep only these pair of points where one of the points is a real experimental value. Series of binding intensity ($v$) and free concentration of ruthenium ($c_f$) can be obtained from the following equation. The results are shown in Figure 2.4.

$$v = \frac{(c_t / P)_a - \frac{P_b}{P_a}(c_t / P)_b}{1 - \frac{P_b}{P_a}} \tag{2.10}$$

$$c_f = \frac{P_a P_b}{P_a - P_b}[(c_t / P)_a - (c_t / P)_b] \tag{2.11}$$

Where $P_a$ and $P_b$ represent the 2 different concentrations of DNA for the 2 titrations considered, $c_f$ is the free concentration of ruthenium, and $c_t$ is total concentration of ruthenium ($C_{Ru}$) at every single measurement.

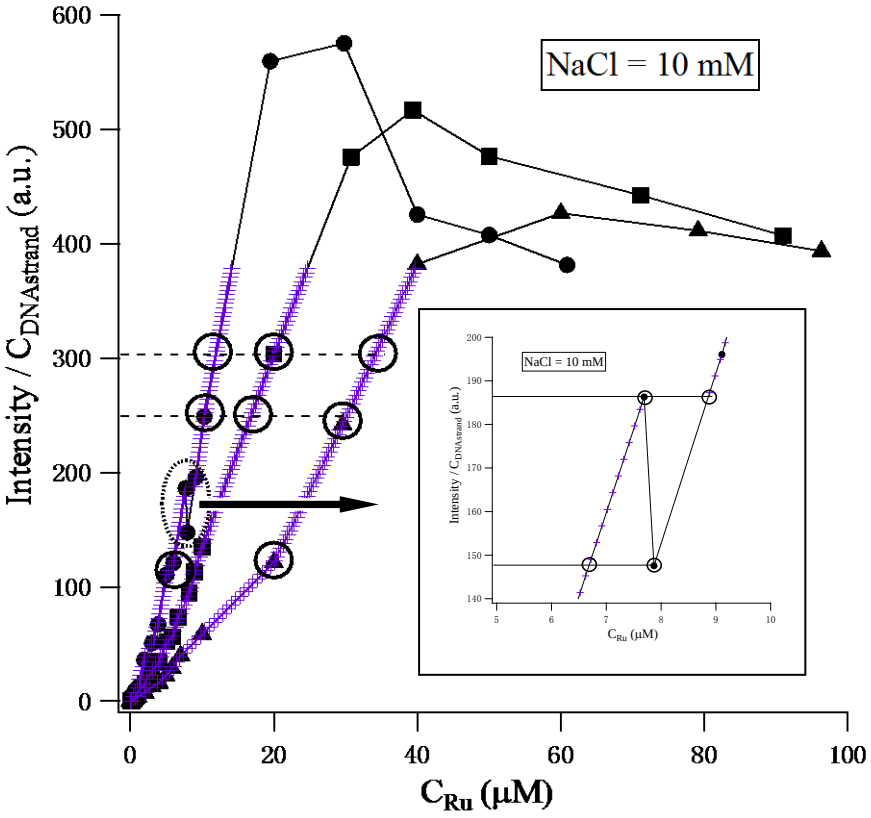


**Figure 2.3:** Evolution of intensity per DNA strand versus $C_{Ru}$ under 3 different concentrations of DNA, 2.5 μM (circle), 5 μM (square), 10 μM (triangle). A linear approximation is performed between consecutive experimental points in order to determine the ruthenium concentration at when the normalized intensities are equal. Inset: the region of unphysical change of curvature between two successive experimental points only the circled pair of points are considered .

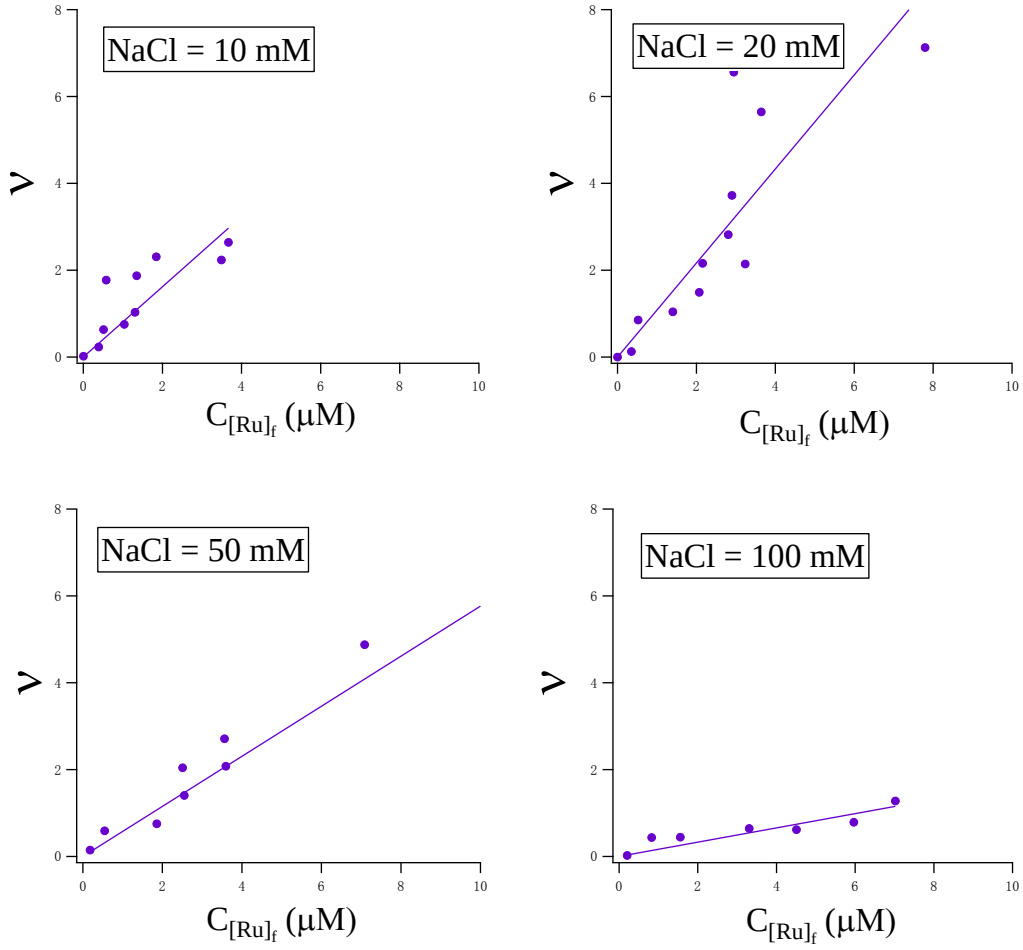


**Figure 2.4:** Binding intensity (ν) versus free concentration of ruthenium ($C_{[Ru]f}$) under different salinity concentrations.

The determination of ν can be described by the following equation:

$$\nu = \frac{nK_a c_f}{1 + K_a c_f}$$

Now if $c_f$ is very close to 0, ν can be written into the following equation:

$$\nu = nK_a c_f \tag{2.12}$$

We then perform an affine curve fitting of ν ($C_{[Ru]f}$), the slope of the curve the value of $nK_a$. The results are shown in Table 2.1. It is unambiguous that $nK_a$ value decreases with the increase of the salinity concentration.

**Table 2.2:** The values of $nK_a$ under different salinity environment.

| [NaCl] (M) | 0.01 | 0.02 | 0.05 | 0.1 |
|---|---|---|---|---|
| $nK_a$ ($M^{-1}$) | $1.18*10^6$ | $1.08*10^6$ | $0.58*10^6$ | $0.17*10^6$ |
| $\frac{1}{nK_a}$ (M) | $0.85*10^{-6}$ | $0.92*10^{-6}$ | $1.74*10^{-6}$ | $6.06*10^{-6}$ |

The $nK_a$ value is gotten from the first approximation, but the individual value of $n$ and $K_a$ are unknown, they can be obtained after reorganizing the Equation 2.6:

$$\frac{1}{v}=\frac{1}{nK_a}\frac{1}{c_f}+\frac{1}{n} \tag{2.13}$$

If we make a plot of $\frac{1}{v}$ as a function of $\frac{1}{c_f}$, and perform linear fit (Figure 2.5). The slope of the fitting curve is $\frac{1}{nK_a}$ and the intercept is $\frac{1}{n}$, affinity constant ($K_a$) and binding sites ($n$) can be easily obtained by getting reverse of $\frac{1}{nK_a}$ and $\frac{1}{n}$. The values of $K_a$ and $n$ under different salinity environment are shown in Table 2.2. The value of $K_a$ decreased with the increase of salinity concentration. But we have no idea about the variation trend of $n$.

The *n* value can't be determined with accuracy, as it is a limit value at $1/c_f$ is close to 0. It is expected not to depend on the salinity. Taking the average value over all experiments, have $\bar{n}=3.76\pm1.965$. This value agrees with the size of sites occupied by similar binding ligand and measured with single molecule from spectroscopy [53].

**Table 2.3:** The value of $K_a$ and $n$ under different salinity environments.

| [NaCl] (M) | 0.01 | 0.02 | 0.05 | 0.1 |
|---|---|---|---|---|
| $n$ | 2.86±2.02 | 5.95±3.26 | 4.59±2.17 | 1.64±0.41 |
| $K_a$ ($M^{-1}$) | $7.37*10^5$ | $2.85*10^5$ | $2.44*10^5$ | $2.2*10^5$ |
| $nK_a$ ($M^{-1}$) | $2.11*10^6$ | $1.69*10^6$ | $1.12*10^6$ | $3.6*10^5$ |

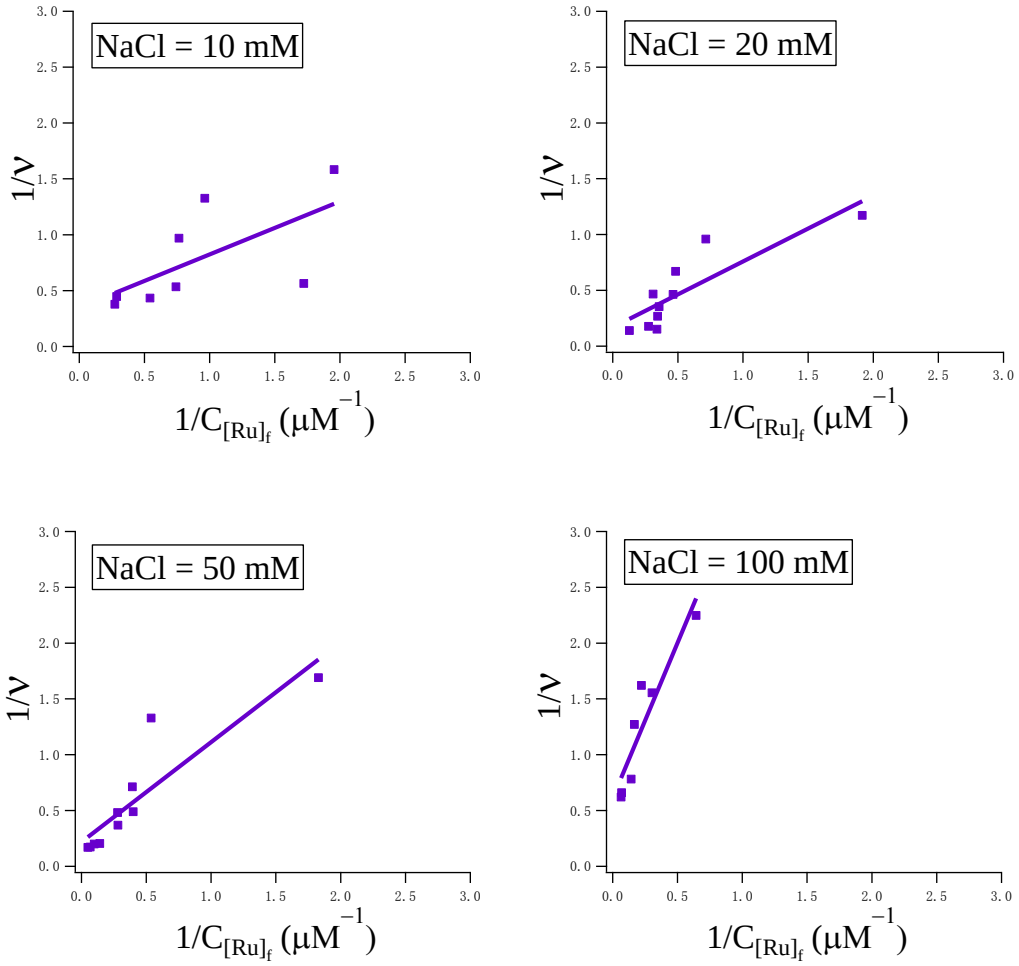


**Figure 2.5:** $\frac{1}{\nu}$ as function of $\frac{1}{c_{[Ru]f}}$ under different salt concentrations. Solid lines are the linear fits of data.

## 2.3.3 Discussions: salt dependence of $K_a$

It is known that simple monovalent counterions (like $Na^+$) interact with polyelectrolyte such as DNA by direct condensation. This reduces the axial charge density of the polyelectrolyte. According to Manning's theory not all of the charges are neutralized, but only a fraction of them, so that, the unneutralized polyelectrolyte charges are screened from each other [92-94]. Let us call $\psi$ is the ratio of neutralized charges along the DNA chain. For dsDNA $\psi = 0.88$ [95].

We write the equilibrium between $[Ru(bpy)_2dppz]^{2+}$ and $DNA_{bp}$. Where ruthenium complex binds to DNA, $\psi$ sodium ions is displaced, we have:

$$(DNA_{bp}Na^+_{\psi}) + Ru \underset{\nwarrow}{\overset{K_a^*}{\rightleftharpoons}} DNA_{bp}Ru + \psi Na^+ \qquad (2.14)$$

where $K_a^*$ is the thermodynamic constant of this equilibrium. $K_a^*$ may be expressed as:

$$K_a^* = \frac{[DNA_{bp}Ru][Na^+]^{\psi}}{[DNA_{bp}Na^+_{\psi}]_f [Ru]_f} \qquad (2.15)$$

Our previous analysis of the experimental data leads to an apparent $K_a$:

$$K_a = \frac{[Ru - DNA_{bp}]}{[DNA_{bp}]_f [Ru]_f}$$

so $K_a^*$ might be then written as:

$$K_a^* = K_a[Na^+]^{\psi} \tag{2.16}$$

$$K_a = K_a^*[Na^+]^{-\psi} \tag{2.17}$$

$$\log K_a = log\ K_a^* - \psi \log [Na^+] \tag{2.18}$$

At constant temperature and pressure, under conditions of excess $Na^+$, variations of $K_a$ with $Na^+$ concentrations are written:

$$\frac{\partial \log K_a}{\partial \log[Na^+]} = -\psi \tag{2.19}$$

In deriving this relationship, we neglected the change in chemical activity of DNA and Ruthenium due to addition of salt into the solution. A general derivation is given in [95].

It is thus expected that the affinity decreases with salt concentration with a logarithm, slope equals to -0.88. Our experiments indeed show such a decrease, the *nK* values obtained from the fitting of ν( $c_f$ ), which gives the more reliable slopes lead to a logarithm slope of -0.82 (Figure 2.6) in good agreement with Manning's theory. The values of $K_a$ computed in this chapter will be used in the next chapter in order to analyze the dynamical and structural changes induced by the binding of $Ru(bpy)_2dppz^{2+}$.

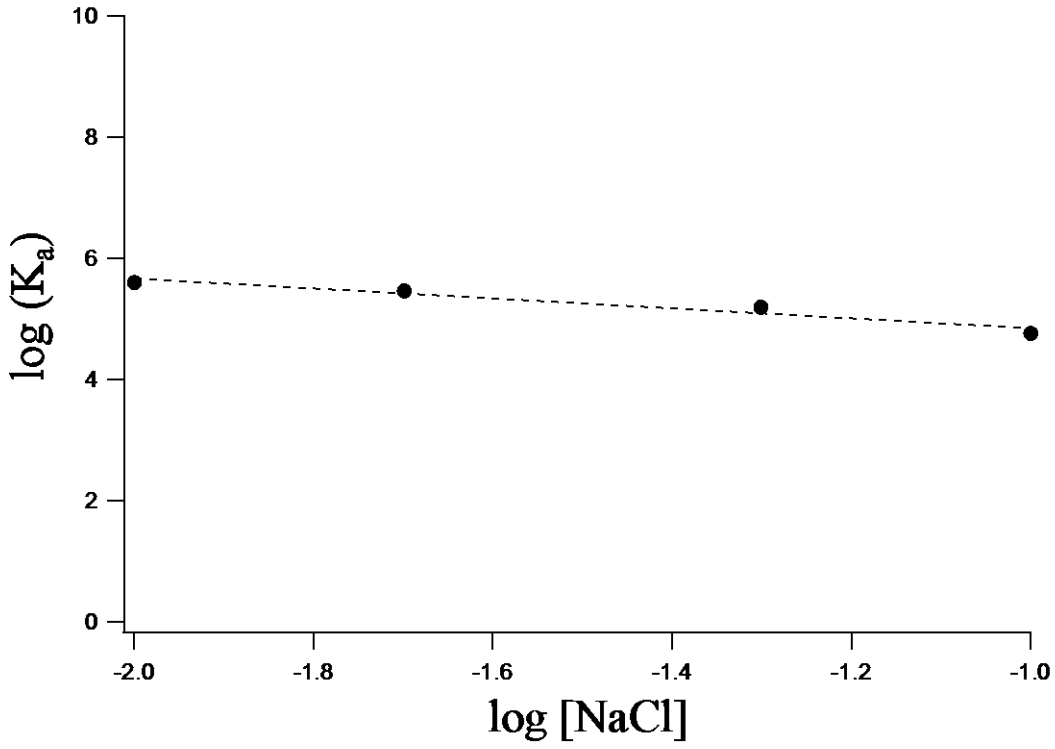


**Figure 2.6:** Logarithm of $K_a$ values as a function of logarithm of salt concentration. The slope is equal to -0.82 with a linear fit.

# Chapter 3

## 3 Fluorescence resonance energy transfer (FRET) study

## Outline

In this chapter, we will study the length change of double strand DNA (dsDNA) with 15 base pairs long, both ends of dsDNA being modified by a fluorophore: Alexa488 at one end and Alexa568 at the other extremity. When Alexa488 is excited to an excited state, it can decay by transferring non-radiative energy to Alexa568, which then de-excites by emitting photons of lower energy than those emitted by Alexa488. The efficiency of this energy transfer can be quantified from the measurement of intensities emitted at low and high energy. It depends on the coupling efficiency (and therefore the distance) between the two fluorophores.

Lifetimes measurements of excited states of each fluorophore are performed. We observed that the addition of ligand results in a strong quenching of fluorophores. From the analysis of the evolution of the lifetime of the donor on one hand, and that of the acceptor on the other hand, we deduce the evolution of the efficiency of energy transfer in the concentration of function ligand. We compare these results obtained by each of these analyses, and finally deduce, using our analysis of the balance made in the first part, the evolution of the chain length on the rate of complexation.

# 3.1 Relaxation process of excited fluorophore molecule

## 3.1.1 Fluorescence

During the past 20 years fluorescence has been widely used in the biological sciences. Fluorescence spectroscopy and time-resolved fluorescence are considered to be primarily research tools in biochemistry and biophysics. This emphasis has changed, and the use of fluorescence has expanded. Fluorescence now becomes a dominant methodology and is used extensively in biotechnology, such as flow cytometry [96,97], medical diagnostics [98,99], DNA sequencing [100-102], and genetic analysis [103,104], to name a few. Fluorescence detection is highly sensitive, and there is no longer the need for the expense and difficulties of handling radioactive tracers for most biochemical measurements. There has been dramatic growth in the use of fluorescence for cellular and molecular imaging [105-107]. Fluorescence imaging can reveal the location and measurements of intracellular molecules, sometimes at the level of single-molecule detection [108,109].

### 3.1.1.1 Phenomenon of Fluorescence

Luminescence is the emission of light from any substance, and occurs from electronically excited states. Luminescence is formally divided into two categories, *fluorescence and phosphorescence*, which depends on the nature of the excited state.

***Fluorescence*** is the emission of the light from the excited singlet states, in which the electron in the excited orbital is paired (by the opposite spin) with the second

electron in the ground-state orbital. The process of returning to the ground state of the electron is spin allowed and occurs rapidly by emission of a photon. The emission rates of fluorescence are typically $10^{-8}$ $s^{-1}$, so that a typical fluorescence lifetime is near 10 ns ($10^{-9}$ s). The lifetime (presented as $\tau$) of a fluorophore is the average time between its excitation and return to the ground state. It is valuable to consider a 1 ns lifetime within the context of the speed of light. Light travels 30 cm, or about one foot, in 1 ns. A lot of fluorophores display sub-nanosecond lifetimes. The measurement of the time-resolved emission requires sophisticated optics and electronics due to the short timescale of fluorescence. In spite of the added complexity, time-resolved fluorescence is widely used because of the increased information available from the data when compared with stationary or steady-state measurements. Additionally, advances in technology have made time-resolved measurements easier, even when using microscopes.

***Phosphorescence*** is emission of light from triplet excited states, in which the electron in the excited orbital has the same spin orientation as the ground-state electron. Transitions to the ground state are forbidden and the emission rates are slow ($10^{3}$ to $10^{0}$ $s^{-1}$), so that phosphorescence lifetimes are typically milliseconds to seconds. Even longer lifetimes are possible, as is seen from "glow-in-the-dark" toys. Following exposure to light, the phosphorescence substances glow for several minutes while the excited phosphors slowly return to the ground state. Phosphorescence is not usually seen in fluid solutions at room temperature. This is because there exist many deactivation processes that compete with emission, such as non-radiative decay and quenching processes. It should be noted that the distinction between fluorescence and phosphorescence is not always clear. Transition metal-ligand complexes (MLCs), which contain a metal and one or more organic ligands, display mixed singlet – triplet states. These MLCs display intermediate lifetimes of hundreds of nanoseconds to several microseconds.

The processes that occur between the absorption and emission of light are usually illustrated by the Jablonski diagram, one form of a Jablonski diagram is shown in Figure3.1. Jablonski diagrams are often used as the starting point for discussing light

absorption and emission. These diagrams are used in a variety of forms, to illustrate various molecular processes that can occur in excited states. These diagrams are named after Alexander Jablonski. He is regarded as the father of fluorescence spectroscopy because of his many accomplishments, including descriptions of concentration depolarization and defining the term anisotropy to describe the polarized emission from solutions.

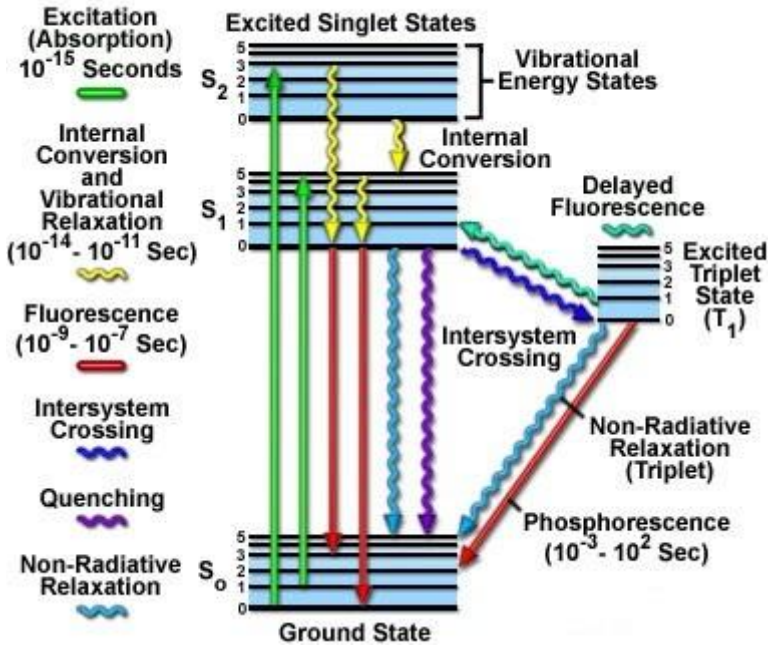


**Figure 3.1:** One form of Jablonski diagram, when the molecule is excited from ground state to the excited state, there exists several ways of relaxation processes. As depicted in the figure, fluorescence, quenching, phosphorescence, intersystem crossing and nor-radiative relaxations happen to the excited molecules. They have different relaxation time which can help us to understand the energy state of the molecule.

Fluorescence typically occurs from aromatic molecules. In our study, Alexa488 and Alexa568 are employed because of their unique features and according to the requirements of the laser experiments, they are labeled at 2 ends of the DNA, respectively. They are shown in Figure 3.2.

Alexa488 dye is by far the best fluorescein substitute available for most applications [110-112]. It is probably the best dye available for single-molecule detection of bio-conjugates. This green-fluorescent dye exhibits several unique features. Fluorescence spectra is almost identical to those of fluorescein, it has excitation and emission maxima at 495/519 nm (shown in Figure 3.3) and a fluorescence lifetime around 4.1 nanoseconds; It exhibits strong absorption, with an extinction coefficient greater than 65000 $cm^{-1}M^{-1}$; And a much greater photostability than fluorescein, allowing more time for observation and image capture.

Alexa568 Dye: the excitation and emission maxima locate at 578 and 603 nm (shown in Figure 3.3), respectively [112].

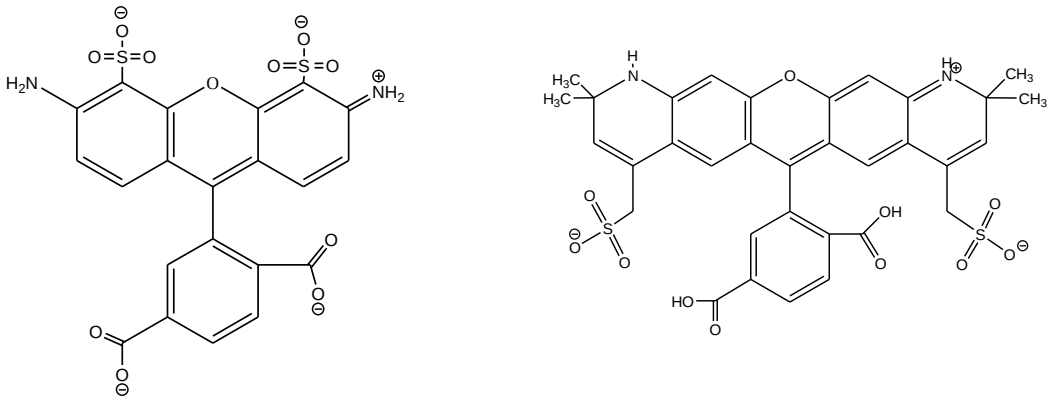

Alexa Fluorophore 488 Alexa Fluorophore 568

**Figure 3.2:** Chemical structure of alexa fluorophores used in our study.

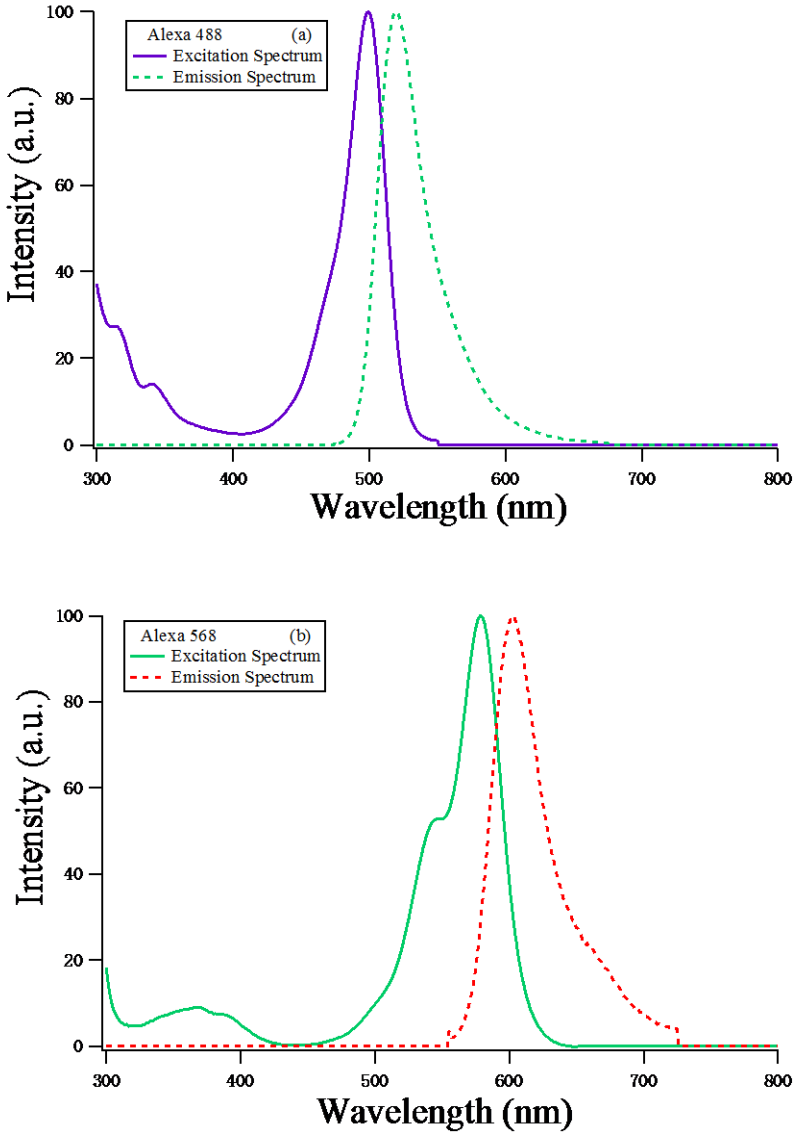


**Figure 3.3:** (a) Excitation and emission spectrum of Alexa488, (b) Excitation and emission spectrum of Alexa568.

### 3.1.1.2 Fluorescence lifetimes and quantum yields

The fluorescence lifetime and quantum yield (presented by $\tau$ and $\psi$) are perhaps the most important characteristics of a fluorophore. Quantum yield is the ratio of emitted photons relative to the number of absorbed photons. The lifetime is also important, as it determines the time available for the excited fluorophore to interact with or diffuse in its environment, and hence the information available from its emission.

The lifetime ($\tau$) of the excited state is defined by the average time the molecule spends in the excited state prior to return to the ground state (Equation. 3.1).

$$\tau = \frac{1}{\Gamma + \mathrm{k}_{nr}} \tag{3.1}$$

$\Gamma$ is the emissive rate, and $\mathrm{k}_{nr}$ is rate of all possible non-radiative decay, they both depopulate the excited state, and can be easily presented by a very simplified Jablonski diagram (Figure 3.4). Now we assume that there are $F^*$ excited fluorophores at time t. One population of excited molecule corresponds to one relaxation time, so the decay process can be expressed by the following Equation 3.2

$$\frac{dF^*}{dt} = -\frac{F^*}{\tau} \tag{3.2}$$

Perform integration to Equation 3.2, the exponential decay equation will be gotten in terms of lifetime τ and also be a function of time (t).

$$F^*(t) = F_0^* e^{-t/\tau} = F_0^* e^{-t/(\Gamma + k_{nr})} \tag{3.3}$$

Where $F_0^* = F^*(0)$ is the number of excited fluorophores at time 0.

The fluorescence quantum yield ($\psi$) is the ratio of the number of photons emitted by the fluorophores to the total number of excited fluorophores. $\psi$ can be seen as the probability that an excited fluorophore relaxes back to its ground state by emitting a photon, it can be described by Equation 3.4

$$\psi = \frac{1}{F_0^*} \int_0^\infty F^*(t) \Gamma dt \tag{3.4}$$

where $\Gamma$ is the rate of photon emission.

Substitute eq. 3.3 into eq. 3.4 and get integration, finally we get:

$$\psi = \frac{\Gamma}{\Gamma + k_{nr}} \tag{3.5}$$

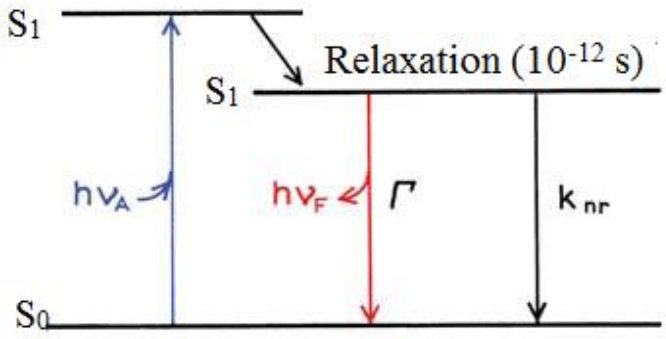


**Figure 3.4:** A simple Jablonski diagram to illustrate quantum yields and lifetimes. $\nu_A$is the frequency of absorbed photon, $\nu_F$ is the frequency of emitted photon when the excited molecule relaxes from the excited states to the ground state, Γ is the emissive rate, and $\kappa_{nr}$ is rate of all possible non-radiative decay.

### 3.1.1.3 Fluorescence quenching

The processes that refer to a decrease of the fluorescence intensity of a molecular can be called quenching. Quenching can occur by different mechanisms. A variety of molecular interactions can result in quenching, for instance, ground-state complex formation, collisional quenching, energy transfer, excited-state reactions and molecular rearrangements. In our study, we will be concerned primarily about two types of quenching:

One is *dynamic quenching*, which results from collisional encounters between the fluorophore and quencher, the other that will be discussed is s*tatic quenching*, where of binding between the fluorescent sample and the quencher occurs.

Two simplified sketches are shown in Figure 3.5 to describe collisional quenching and static quenching. For collisional quenching, the fluorophore at the ground state will jump to the excited state (presented by $F^*$ in the sketch) by absorbing fixed energy. The relaxation process of excited fluorophore is normally divided into two ways, one process of relaxation goes to ground state by emitting a photon due to the collision between the excited fluorophore and quencher, the other without photon emission can be seen as non-radiative decay process due to collision. For static quenching, the quenching can occur as a result of the formation of a non-fluorescent ground-sate complex (described with [F-Q]) between the fluorophore and quencher, when this complex absorbs light it immediately returns to the ground state without emission of a photon. Of course, except for the processes described above, quenching can also occur by a variety of trivial effects, such as attenuation of the incident light by the fluorophore itself or other absorbing species, but we will assume and very that such trivial effects are not the cause of the decreases in fluorescence intensity in this thesis.

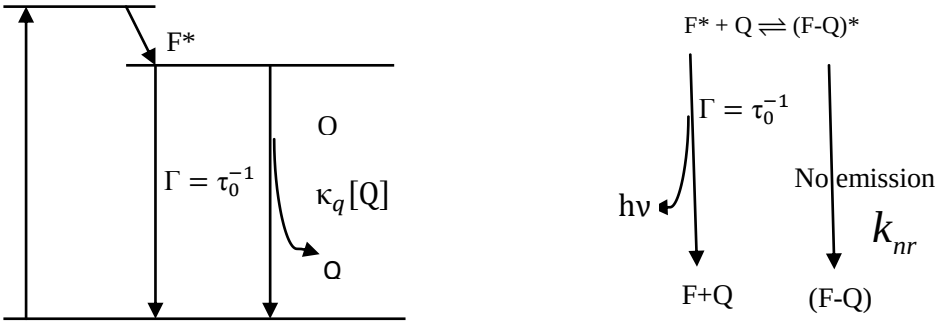


Collisional Quenching Static Quenching

**Figure 3.5:** Two simplified sketches of quenching. Left is collisional quenching, Γ is the emissive rate, [Q] is the concentration of the quencher, $\kappa_q$ is the prefactor of the quencher. The right is static quenching, Γ is the emissive rate, ν is the frequency of photon emitted by excited fluorophore during the relaxation process, $k_{nr}$ is the non-emissive rate of decay process.

a) Theory of collisional quenching

We assume that collisional quenching happens due to the collision of two and nor more than two molecules: one fluorophore and one quencher particle, so the collisional quenching of fluorescence can be described by the Stern-Volmer equation:

$$\frac{F_0}{F} = 1 + k_q \tau_0 [Q] = 1 + K_D [Q] \tag{3.6}$$

In this equation, $F_0$ and $F$ are the fluorescence intensities in the absence and presence of quencher, respectively; $k_q$ is the bimolecular quenching constant; $\tau_0$ and $\tau$ are the lifetime of the fluorophore in the absence and presence of quencher, and $Q$ is the concentration of quencher. The Stern-Volmer quenching constant is given by $K_D = k_q \tau_0$ under the precondition which the quenching is known to be dynamic.

*Derivation of the Stern-Volmer equation:*

This equation can be derived by considering the fluorescence intensities observed in the absence and presence of quencher. The fluorescence intensity observed for a fluorophore is proportional to its concentration in the excited state, [$F^*$]. Under a continuous illumination, a constant population of excited fluorophores is established, and therefore $\frac{dF^*}{dt} = 0$. So in the absence and presence of quencher, there are two different equations to describe [ $F^*$ ]:

$$\frac{dF^*}{dt} = f(t) - \gamma[F^*]_0 = 0 \tag{3.7}$$

$$\frac{dF^*}{dt} = f(t) - (\gamma + k_q[Q])[F^*] = 0 \tag{3.8}$$

where $f(t)$ is the constant excitation function, $\gamma = \tau_0^{-1}$ is the decay rate of the fluorophore in the absence of quencher. In the absence of quenching, the excited-state population decays with a rate of $\gamma = \Gamma + k_{nr}$, where $\Gamma$ is the radiative rate and $k_{nr}$ represents all the possible way of non-radiative decay rate. In the presence of quencher, there is an additional decay rate $k_q[Q]$. The excited-state population will be a constant under the continuous excitation, so eq. 3.7 and eq. 3.8 can be set to 0. Division of eq. 3.8 and eq. 3.7 yields:

$$\frac{F_0^*}{F^*} = \frac{\gamma + k_q[Q]}{\gamma} = 1 + k_q\tau_0[Q] = 1 + K_D[Q] \tag{3.9}$$

which is the Stern-Volmer equation. Since collisional quenching is a rate process that depopulates the excited state, the lifetimes in the absence and presence of quencher

are given by:

$$\tau_0 = \gamma^{-1} \tag{3.10}$$

$$\tau = (\gamma + k_q[Q])^{-1} \tag{3.11}$$

Divided by eq. 3.10 with eq. 3.11 yields the same results of $\frac{F_0}{F}$

$$\frac{\tau_0}{\tau} = \frac{\gamma + k_q[Q]}{\gamma} = 1 + k_q\tau_0[Q] = 1 + K_D[Q] \tag{3.12}$$

It is obvious that $\frac{F_0}{F} = \frac{\tau_0}{\tau}$ which can be seen as an important characteristic of collisional quenching. The decrease in lifetime happens because quenching is an additional rate process that depopulates the excited state. The decrease in yield occurs because quenching depopulates the excited state without fluorescence emission.

b) Theory of static quenching

For static quenching, the fluorescence intensity depends upon the quencher concentration. Now we consider that one fluorophore can complex with one quencher.

$$F + Q \underset{\leftarrow}{\overset{K_S}{\rightleftharpoons}} FQ$$

The complexation between fluorophore and quencher reaches equilibrium, the association constant $K_S$ is given by equation:

$$K_S = \frac{[F-Q]}{[F][Q]} \tag{3.13}$$

where $[F-Q]$ is the concentration of the complex, [*F*] is the concentration of uncomplexed fluorophore, and $[Q]$ is the free concentration of quencher. If the complexed specy is non-fluorescent then the fraction of the fluorescence that remains (*F/F*$_0$) is given by the fraction of the total fluorophores that are not complexed: *F/F*$_0$. The total concentration of fluorophore $[F]_0$ can be written as Equation 3.14:

$$[F]_0 = [F] + [F-Q] \tag{3.14}$$

Substitute eq. 3.14 into eq. 3.13 yields equation 3.15:

$$K_S = \frac{[F]_0 - [F]}{[F][Q]} = \frac{[F]_0}{[F][Q]} - \frac{1}{[Q]} \tag{3.15}$$

Rearrange Equation 3.15, and given that the fluorescence intensity depends upon the quencher concentration, the relationship of fluorescence intensity and quencher concentration will be obtained by Equation 3.16:

$$\frac{F_0}{F} = 1 + K_S [Q] \tag{3.16}$$

Note that the dependence of $\frac{F_0}{F}$ versus $[Q]$ is also linear, which is identical to dynamic quenching. $K_S$ represents the association constant, which is given by Equation 3.13.

For static quenching, the lifetime does not decrease because only the fluorescent molecules are observed, and the uncomplex fluorophores have the unquenched lifetime $\tau_0$.

c) How to distinguish dynamic quenching and static quenching?

The most definitive method to distinguish static and dynamic quenching is the measurement of fluorescence lifetimes. Static quenching removes a fraction of the fluorophores from observation. The complexed fluorophores are not fluorescent any more, and the observed fluorescence is only from the uncomplexed fluorophores. The uncomplexed fraction is unperturbed, and hence the lifetime is still $\tau_0$. Therefore, for static quenching $\frac{\tau_0}{\tau}=1$. In contrast, for dynamic quenching, $\frac{F_0}{F}=\frac{\tau_0}{\tau}$. This distinguishment will be shown in Figure 3.6. Lastly and importantly, we should note that the above two quenching and the relationships of fluorescence intensity and decay time we discussed are under the low concentration of quencher. In other words, every equation is obtained from the perspective of one fluorophore versus one quencher particle. In the experimental part of this chapter, we will mainly discuss the results at low concentration of $[Ru(bpy)_2dppz]^{2+}$.

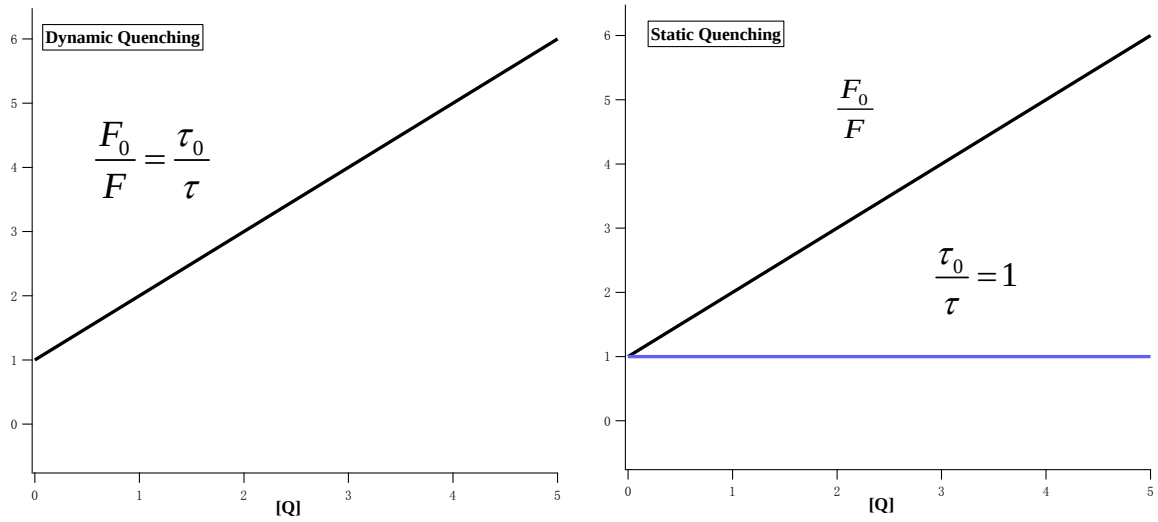


**Figure 3.6:** Two simple plots of dynamic quenching (left) and static quenching (right). $F_0$ and $F$ represent the fluorescence intensity in the absence and presence of quencher. $\tau_0$ is and $\tau$ are the decay times in the absence and presence of quencher. $[Q]$ is the concentration of quencher

## 3.1.2 FRET

### 3.1.2.1 General description of FRET

Fluorescence resonance energy transfer (FRET) has become widely used in biology and biotechnology [113].This process occurs between a donor (D) molecule in the excited state and an acceptor (A) molecule in the ground state and strongly depends on the distance between them, typically in a range of 5 to 100 Å. A FRET Jablonski diagram is shown in Figure 3.7. The energy will be transferred without the appearance of a photon and is the result of long range dipole–dipole interactions between the donor and acceptor. This process is non-radiative, which means that the energy is not emitted or absorbed as photons [113].The rate of energy transfer depends upon the extent of spectral overlap of the emission spectrum of the donor with the absorption spectrum of the acceptor, the quantum yield of the donor, the relative orientation of the donor and acceptor transition dipoles, and the distance between the donor and acceptor molecules [114-117]. The distance dependence of FRET allows measurement of the distances between donors and acceptors. So the most common application of FRET is to measure the distances between two sites on a macromolecule by labeling it with a donor and a acceptor.

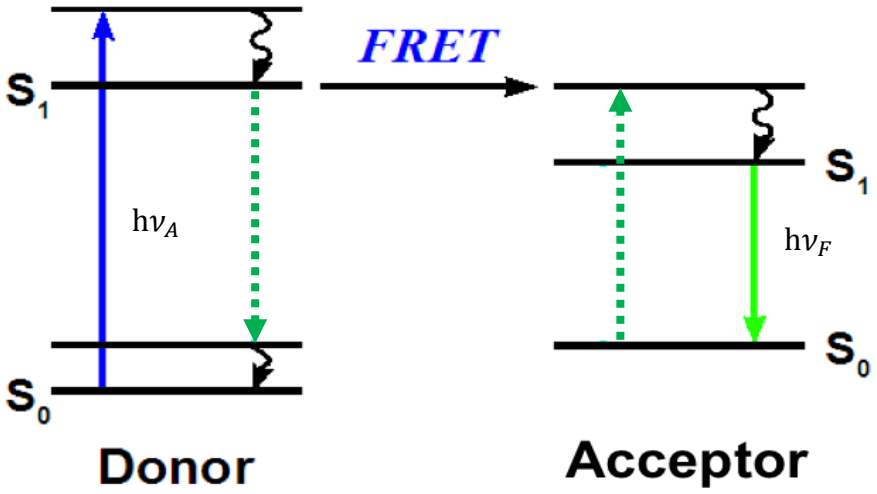


**Figure 3.7:** FRET Jablonski diagram, $S_0$ and $S_1$ represent the ground state and excited state, respectively. $\nu_A$ is the frequency of the photon absorbed by donor, $\nu_F$ is the frequency of the photon emitted by the excited acceptor.

### 3.1.2.2 Measurement of FRET efficiency

The most important factor we care in FRET process is the transfer efficiency, there are two main independent ways of measuring efficiency. Before describing these two methods of measuring efficiency, three assumptions will be introduced in this part. All of the statements about these two methods assume that these three assumptions are satisfied.

1) The presence of acceptor neither change nor add any relaxation process except FRET process.
2) The number of excited donor molecules at a given excitation wavelength is the same in the absence and presence of the acceptor.
3) The number of excited acceptor molecules at a given excitation wavelength is the same.

The transfer efficiency is the probability that an excited donor fluorophore comes

back to its ground state by FRET process. This can be expressed as:

$$E = \kappa_T \tau^{DA} \tag{3.17}$$

Where $\kappa_T$ is the transfer rate of FRET, and $\tau^{DA}$ is the overall characteristic decay time of the donor molecule in the presence of acceptor. $\tau^{DA}$ is directly measured in our experiment: it is the decay time of the fluorophore emission. Under the first assumption, the presence of acceptor doesn't change any relaxation process except for FRET process, thus FRET process is defined with the following equation:

$$\frac{1}{\tau^{DA}} = \frac{1}{\tau^{D}} + \kappa_T \tag{3.18}$$

Where $\tau^{D}$ is the characteristic time in the absence of acceptor, it can be measured directly from measurement in our study. Then the transfer efficiency can be rewritten as:

$$E = 1 - \frac{\tau^{DA}}{\tau^{D}} \tag{3.19}$$

## 3.1.2.2.1 Dynamic measurement-donor emission

**Molecular description from the donor point of view**

When FRET occurs, at least two mechanisms of donor relaxation coexist. The first one is the emission process with a decay time $\tau^{D}$, the other, relaxation through FRET

process, whose rate is presented by $\kappa_T$. We thus have

$$\frac{dD^*}{dt} = -\frac{1}{\tau^{DA}} D^* \tag{3.20}$$

And given Equation 3.18 $$\frac{1}{\tau^{DA}} = \frac{1}{\tau^{D}} + \kappa_T$$

Equation 3.18 is valid if the relaxation process described by $\tau^D$ doesn't change when the acceptors are present. So the evolution of the number of excited donors at a given excitation wavelength, can be obtained with following equation:

$$D^*(t) = D^*_{02} e^{-t/[(\tau^D)^{-1}+\kappa_T]} = D^*_{02} e^{-t/\tau^{DA}} \tag{3.21}$$

Where $D^*$ is the number of excited donors at time t, $D^*_{02}$ is the initial population of excited donors in the presence of acceptor, $\tau^{DA}$ and $\tau^D$ are the lifetimes in the presence and absence of acceptor, respectively.

**Evolution of the emitted intensity**

We do not measure the number of excited donors, but the emitted intensity. The total number of photons emitted by the donor with two different wave lengths 517 nm ($N^D_{517}$ and $N^{DA}_{517}$) and 600 nm ($N^D_{600}$ and $N^{DA}_{600}$) in the presence and absence of acceptor can be written as:

$$N^D_{517} = \int_0^\infty \frac{1}{\tau^D_{517}} D^*_{01} e^{-t/\tau^D} dt = D^*_{01} \frac{\tau^D}{\tau^D_{517}} \tag{3.22}$$

$$N_{600}^{D} = \int_0^{\infty} \frac{1}{\tau_{600}^{D}} D_{01}^{*} e^{-t/\tau^{D}} dt = D_{01}^{*} \frac{\tau^{D}}{\tau_{600}^{D}} \tag{3.23}$$

$$N_{517}^{DA} = \int_0^{\infty} \frac{1}{\tau_{517}^{D}} D_{02}^{*} e^{-t/\tau^{DA}} dt = D_{02}^{*} \frac{\tau^{DA}}{\tau_{517}^{D}} \tag{3.24}$$

$$N_{600}^{DA} = \int_0^{\infty} \frac{1}{\tau_{600}^{D}} D_{02}^{*} e^{-t/\tau^{DA}} dt = D_{02}^{*} \frac{\tau^{DA}}{\tau_{600}^{D}} \tag{3.25}$$

Where $\tau^{D}$ and $\tau^{DA}$ represent the overall decay time in the absence and presence of acceptor. $\tau_{517}^{D}$ and $\tau_{600}^{D}$ are the characteristic decay times of photon emission at 517 nm and 600 nm by the donor, whatever in the absence or presence of acceptor, the decay times do not change. $D_{01}^{*}$ and $D_{02}^{*}$ are the initial number of excited donors by the laser in the absence and presence of acceptor.

By dividing Equation 3.24 with Equation 3.22, we obtain Equation 3.26

$$\frac{N_{517}^{DA}}{N_{517}^{D}} = \frac{D_{02}^{*}}{D_{01}^{*}} \frac{\tau^{DA}}{\tau^{D}} \tag{3.26}$$

The values of $N_{517}^{D}$, $N_{517}^{DA}$, $\tau^{D}$ and $\tau^{DA}$, are directly obtained from the measurement. Moreover, if the number of excited donors does not change in the presence of acceptor (hypothesis: number 2), that is $D_{01}^{*} = D_{02}^{*}$, we get:

$$\frac{N_{517}^{DA}}{N_{517}^{D}} = \frac{\tau^{DA}}{\tau^{D}} \tag{3.27}$$

When Equation 3.27 is valid, and the transfer efficiency can also be rewritten as:

$$E = 1 - \frac{\tau^{DA}}{\tau^{D}} = 1 - \frac{N_{517}^{DA}}{N_{517}^{D}} \tag{3.28}$$

## 3.1.2.2.2 Dynamic measurement-acceptor emission

**Molecular description from the point of view of the acceptor**

The acceptor can be excited following two different mechanisms. One process is excited through the energy transfer, the other excitation process is attributed to the laser. let us call $\tau^{A}$ the overall relaxation time of acceptor in the presence of donor molecule, the existence of FRET doesn't change the relaxation path of an excited acceptor, and $\tau^{A}$ is identical to the relaxation time of acceptor excited by the laser in the absence of donor. From the perspective of the acceptor, the FRET process can be determined by the following equation:

$$\frac{dA^{*}}{dt} = \kappa_T D^{*}(t) - \frac{1}{\tau^{A}} A^{*}(t) \tag{3.29}$$

and with $D^{*}(t) = D_{02}^{*} e^{-t/\,[\tau^{D})^{-1} + \kappa_T\,]} = D_{02}^{*} e^{-t/\tau^{DA}}$

Where the first term represents the excitation through FRET and the second one represents the excitation by the laser.

With initial condition: $A^{*}(t=0) = A_{02}^{*}$ (where $A_{02}^{*}$ is the number of excited acceptor molecules excited by the laser), the solution of Equation 3.29 is:

$$A^{*}(t) = D_{02}^{*} \kappa_T \frac{1}{(\tau^{A})^{-1} - (\tau^{DA})^{-1}} e^{-t/\tau^{DA}} + [A_{02}^{*} - D_{02}^{*} \kappa_T \frac{1}{(\tau^{A})^{-1} - (\tau^{DA})^{-1}}] e^{-t/\tau^{A}} \tag{3.30}$$

Where $A_{02}^{*}$ is the number of acceptor molecules excited by the laser at time 0. This result states that the $A^{*}(t)$ should exhibit a two-time relaxation process , the first one equals to the relaxation time of the donor population in the presence of acceptor, $\tau^{DA}$, and the second one equals to the relaxation time of the acceptor in the absence of a donor, $\tau^{A}$. Let us moreover notice that if $\frac{1}{(\tau^{A})^{-1}-(\tau^{DA})^{-1}}<0$, the amplitude of the acceptor decay over $\tau^{DA}$ is negative.

**Evolution of the emitted intensity**

The number of photon emitted ( $N_{600}^{AD}$ ) by the acceptor can now be obtained:

$$N_{600}^{AD}=\int_{0}^{\infty}\frac{1}{\tau_{600}^{A}}(D_{02}^{*}\kappa_{T}\frac{1}{(\tau^{A})^{-1}-(\tau^{DA})^{-1}}e^{-t/\tau^{DA}}+\frac{1}{\tau_{600}^{A}}[A_{02}^{*}-D_{02}^{*}\kappa_{T}\frac{1}{(\tau^{A})^{-1}-(\tau^{DA})^{-1}}]e^{-t/\tau^{A}})dt \tag{3.31}$$

$$N_{600}^{AD}=D_{02}^{*}\kappa_{T}\frac{1}{(\tau^{A})^{-1}-(\tau^{DA})^{-1}}\frac{\tau^{DA}}{\tau_{600}^{A}}+(A_{02}^{*}-D_{02}^{*}\kappa_{T}\frac{1}{(\tau^{A})^{-1}-(\tau^{DA})^{-1}})\frac{\tau^{A}}{\tau_{600}^{A}} \tag{3.32}$$

$$N_{600}^{AD}=A_{02}^{*}\frac{\tau^{A}}{\tau_{600}^{A}}+D_{02}^{*}\kappa_{T}\tau^{DA}\frac{\tau^{A}}{\tau_{600}^{A}} \tag{3.33}$$

Where $\tau_{600}^{A}$ is the characteristic time of photon emission at 600 nm from the acceptor, and $\tau^{A}=\tau^{AD}$, since the presence of the donor doesn't change the relaxation processes of the acceptor.

Finally, using:

$$E=\kappa_{T}\tau^{DA}$$

Rearrange Equation 3.33:

$$N_{600}^{AD} = (A_{02}^{*} + D_{02}^{*}E)\frac{\tau^{A}}{\tau_{600}^{A}} \tag{3.34}$$

where $A_{02}^{*}$ is the number of excited acceptor stem from laser's excitation, $D_{02}^{*}E$ represent the number of acceptor excited by the FRET process.

### 3.1.3 Relationship of efficiency with the donor-acceptor distance

In our study, the organometallic compound will form a complex with DNA when we perform the titration, meanwhile, this lead to the change of distance between two fluorophores. If we want to quantify the variation of the amount of energy transfer between the donor and acceptor when complex done. It becomes essential to know the relationship of transfer efficiency and donor-acceptor distance.

The distance at which FRET is 50% efficient is called the Föster distance and the rate of energy transfer from a donor to an acceptor $\kappa_T(r)$ is normally written as a simplified equation:

$$\kappa_T(r) = \frac{1}{\tau^{D}}\left(\frac{R_0}{r}\right)^{6} \tag{3.35}$$

Where $\tau^{D}$ is the decay time of the donor in the absence of acceptor, $R_0$ is the Föster distance, and $r$ is the donor-to-acceptor (D-to-A) distance. Hence, the rate of transfer is equal to the decay rate of the donor ($\frac{1}{\tau^{D}}$) when the D-to-A distance ($r$) is equal to the $R_0$, and the transfer efficiency is 50%. At this distance ($r = R_0$) the donor emission

would be decreased to half its intensity in the absence of acceptors, $R_0$ is dependent on the spectroscopic properties of fluorophore in the used environment.

In order to better understand the relationship of transfer efficiency and D-to-A distance, we start back with the equation of transfer rate written in terms of Föster distance $R_0$, assuming that the donor and the acceptor separated by a distance $r$ :

$$\kappa_T(r) = \frac{\mathcal{Q}_D \kappa^2}{\tau^D r^6} \frac{9000(\ln 10)}{128\pi^5 N n^4} \int_0^\infty F_D(\lambda)\varepsilon_A(\lambda)\lambda^4 d\lambda$$

$$= \left(\frac{\mathcal{Q}_D \kappa^2}{\tau^D r^6} \frac{0.529}{N n^4}\right) \int_0^\infty F_D(\lambda)\varepsilon_A(\lambda)\lambda^4 d\lambda \qquad (3.36)$$

where $\mathcal{Q}_D$ is the quantum yield of the donor in the absence of acceptor, $n$ is the refractive index of the medium, $N$ is Avogadro's number, $r$ is the distance between the donor and acceptor, and $\tau^D$ is the lifetime of the donor in the absence of acceptor. $F_D(\lambda)$ is the corrected fluorescence intensity of the donor in the wavelength range $\lambda$ to $\lambda + \triangle\lambda$ with the total intensity normalized to unity. $\varepsilon_A(\lambda)$ is the extinction coefficient of the acceptor at $\lambda$, which is in units of $M^{-1}$ $cm^{-1}$. The term $\kappa^2$ is a factor describing the relative orientation in space of the transition dipoles of the donor and acceptor. $\kappa^2$ is usually assumed to be equal to 2/3, which is appropriate for dynamic random averaging of the donor and acceptor.

The overlap integral, we call it $\mathcal{J}(\lambda)$, represents the degree of spectral between the donor emission and the acceptor absorption:

$$\mathcal{J}(\lambda) = \int_0^\infty F_D(\lambda)\varepsilon_A(\lambda)\lambda^4 d\lambda \qquad (3.37)$$

Substitute Equation 3.37 in to Equation 3.36, we obtain equation 3.38

$$\kappa_T(r) = (\frac{Q_D \kappa^2}{\tau^D r^6} \frac{0.529}{Nn^4}) J(\lambda) = (\frac{1}{\tau^D r^6})(Q_D \kappa^2 \frac{0.529}{Nn^4}) J(\lambda) \quad (3.38)$$

As depicted at the beginning, the transfer rate is presented by the form of Föster distance, Föster distance $R_0$ can be finally gotten:

$$(R_0)^6 = \frac{0.529 Q_D \kappa^2}{Nn^4} J(\lambda) \quad (3.39)$$

$$R_0 = [\frac{0.529 Q_D \kappa^2}{Nn^4} J(\lambda)]^{1/6} \quad (3.40)$$

Where the $J(\lambda)$ is in unit of $M^{-1}$ $cm^3$, the wavelength is expressed in cm.

Once the value of $R_0$ is known, the transfer rate can be easily calculated by Equation 3.35. The efficiency of energy transfer ($E$) is the fraction of photons absorbed by donor which are transferred to the acceptor. It is already given by the Equation 3.19:

$$E = 1 - \frac{\tau^{DA}}{\tau^D}$$

And with Equation.3.18 $$\frac{1}{\tau^{DA}} = \frac{1}{\tau^D} + \kappa_T$$

Substitute Equation 3.18 into Equation 3.19 yields

$$E = \frac{\kappa_T}{(\tau^D)^{-1} + \kappa_T} \quad (3.41)$$

Substitute Equation 3.35 into Equation 3.41 yields

$$E = \frac{1}{1+(\frac{r}{R_0})^6} \tag{3.42}$$

Equation 3.42 shows that the transfer efficiency is strongly dependent on distance between the donor and acceptor, especially when the distance is close to the Föster distance $R_0$, the unambiguous dependence is shown in Figure 3.8. On basis of the spectroscopic properties of fluorophores (Alexa488 and Alexa568) we used in our study and the typical distance of FRET happening, our experiments are built with 15 base pairs dsDNA, which are chemically linked with Alexa488 and Alexa568 at 5' end and 3' end, respectively. The Föster distance of Alexa488-Alexa568 fluorophore pair is around 6.2 nm [118]. Titrations were performed by adding $[Ru(bpy)_2dppz]^{2+}$ in to DNA solution. Any variations in DNA conformation, will cause the change of distance between two fluorophores and consequently on the efficiency of FRET measurements.

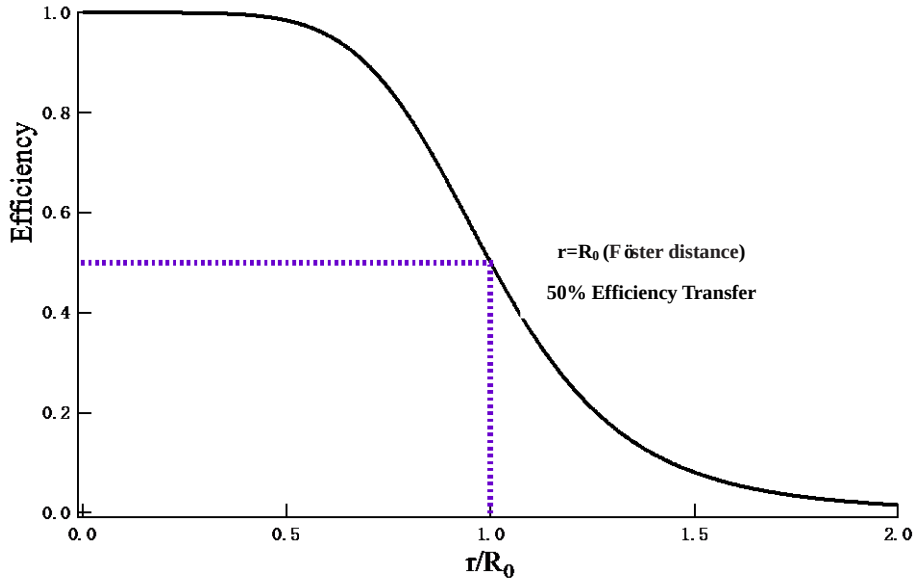


**Figure 3.8:** Dependence of the energy transfer efficiency on distance. $R_0$ is Föster distance, r is the distance between 2 fluorophores (donor-acceptor)

# 3.2 Experimental Procedure

## 3.2.1 Experimental design

We build our experiments on the basis of the FRET theory part (Refer to Part 3.1.2.2). 15 base pair dsDNA are chosen to perform the experiment. The number of DNA base pairs is limited by the range over which the FRET can take place that is approximately 10 nm. Complementary strands were purchased from IBA (Germany company) with sequences GGA GAC CAG AGG CCT and CCT CTG GTC TCC GGA. The length of 15 base pairs is approximately 5.1 nm. The extremity of the short double-stranded DNA (dsDNA) is labeled with different kinds of fluorophores (they are shown in Figure 3.2). The first sequence is modified in three different ways. 1): 5' end is labeled with Alexa488; 2): 3' end is labeled with Alexa568; 3): 5' end and 3' end are labeled with alexa488 and Alexa568, respectively. Alexa fluorophore is chemically linked with DNA base. There is no modification on the pairing sequence. The information of modified DNA is shown in Table 3.1. A sketch that depicts the labeled dsDNA is shown in Figure. 3.9.

**Table 3.1:** Specific information of modified DNA

| dsDNA | Length of dsDNA (Base pairs) | Modified end | Labeling fluorophore |
|---|---|---|---|
| 1 labeled dsDNA | 15 | 5' | Alexa 488 |
| 1 labeled dsDNA | 15 | 3' | Alexa 568 |
| 2 labeled dsDNA | 15 | 5' and 3' | 5'-Alexa 488<br>3'-Alexa 568 |

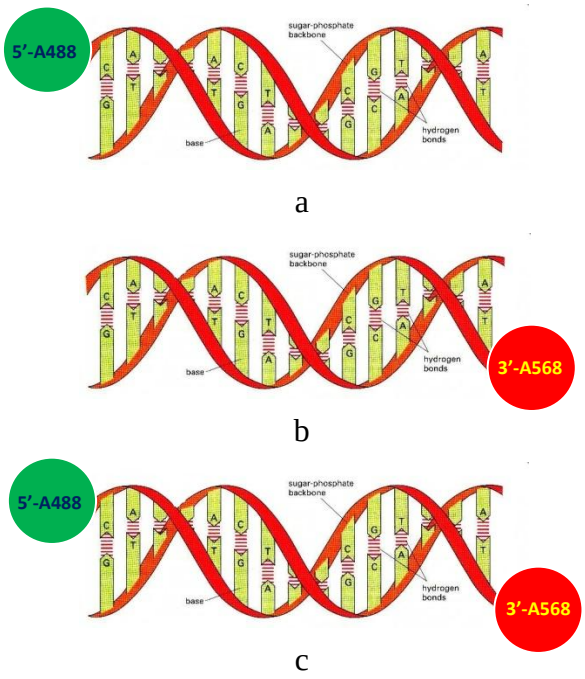


**Figure 3.9:** Three sketches of labeled dsDNA, (a) depicts single labeled dsDNA labeled with Alexa488 at 5' end, (b) draws single labeled dsDNA modified with Alexa568 at 3' end, and (c) represents the double labeled dsDNA modified with Alexa488 at 5' end and Alexa568 at 3' end.

## 3.2.2 Preparation of dsDNA and its titration

**Preparation of dsDNA**

Both two strands are resuspended to a final strand concentration 20 μM (DNA base pairs concentration is 300 μM) in NaCl of 20 mM (at 25 ℃). Next they are annealed by heating the DNA to 94 ℃ before cooling down the sample to 16 ℃ for 15 minutes, then DNA is cooled down to 16 ℃ for another 15 minutes. All of the measurements are performed at 20 ℃ to ensure the DNA remains in the double helix structure .

**Experimental titration**

The experimental titration has been carried out in salinity environment (20 mM of NaCl) with the initial volume of 1000 μL. The strand concentration of dsDNA is kept at 1 μM, which dilutes from the 20 μM of DNA stock solution with 20 mM of NaCl solution, whereas the concentration of $Ru(bpy)_2ddpz^{2+}$ ($C_{Ru}$) is being increased for every single measurement. A series of similar titrations are performed in this study: an example of the titration is displayed in table 3.2.

**Table 3.2:** Titration of lifetime measurement

| $V_{total}$ (μl) | $V_{DNA,add}$ (μl) | $V_{Ru,add}$ (μl) | [DNA] (μM) | $C_{Ru}$ (μM) |
|---|---|---|---|---|
| 1000 | 0 | 0 | 1 | 0 |
| 1006 | 1 | 5 | 1.004 | 0.005 |
| 1011 | 0 | 5 | 1 | 0.01 |
| 1016 | 1 | 4 | 1.004 | 0.05 |
| 1021 | 0 | 5 | 0.999 | 0.1 |
| 1033 | 1 | 11 | 0.997 | 0.2 |
| 1044 | 1 | 10 | 0.996 | 0.3 |
| 1069 | 3 | 22 | 1.001 | 0.5 |

Where $V_{DNA,add}$ and $V_{Ru,add}$ are the volume of added DNA and $Ru(bpy)_2dppz^{2+}$ for every single measurement to keep the DNA concentration as a constant and increase the ruthenium concentration, respectively. [DNA] and [$Ru(bpy)_2dppz^{2+}$] represent the final concentration of DNA and $Ru(bpy)_2dppz^{2+}$, respectively.

## 3.2.3 Fluorescence measurement technique

### 3.2.3.1 Time-correlated single photon counting (TCSPC) method

Time-correlated single photon counting (TCSPC) method is often employed to do lifetime measurement because of the simplified data collection and enhanced the quantitative photon counting [119]. In this study, lifetime measurements are performed with the Fluorolog-3 model FL3-22 instruments. All emission decay datas are transferred to a personal computer and fitted with a sum of exponentials convolved with the appropriate instrument response function by employing a nonlinear least-squares weighted-residuals routine. The instrument response function is measured by using a dilute suspension of latex collsional particles to scatter laser pulses in the direction of the detector.

### 3.2.3.2 Apparatus acquisition parameters

Every single measurement is performed in the same quartz cuvette. A pulsed laser with a wavelength of 495 nm and a repetition rate of 1MHZ is employed to excite the fluorophore, the photons emitted by the fluorophore are collected by the photon detector with temporal resolution defined by a channel width equal to 0.1 ns. The wavelength collected is at 517 nm (Alexa488) and 600 nm (Alexa568) with 2 nm spectral slit. The acquisition time is chosen so that the number of photons collected in the first channel is equal to $10^4$. One measurement lasts between 10 min and 120 min

under these experimental conditions. All measurements are performed at fixed ambient temperature (20 ℃). One typical emission decay curve of Alexa488 is shown in Figure 3.10, and an instrument response function reflects the distribution of photons of the excitation pulse.

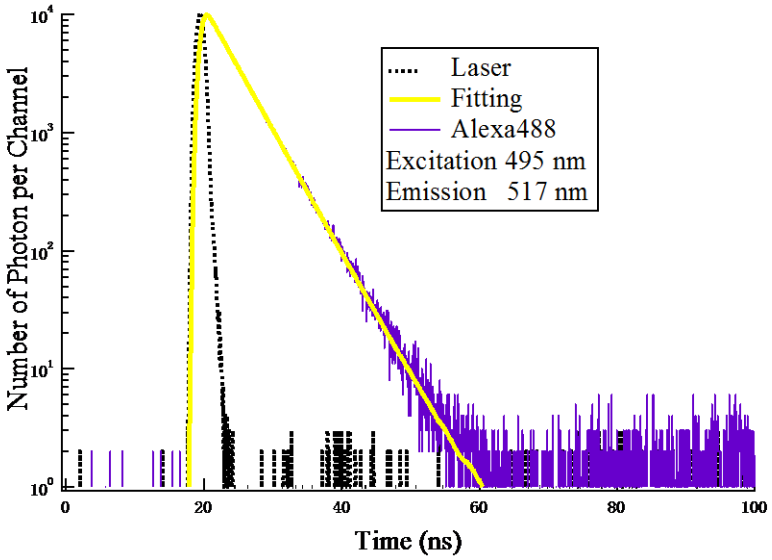


**Figure 3.10:** Typical emission decay curve obtained from a single labeled dsDNA with Alexa 488. Black: width of a laser pulse. Blue: emission of dsDNA fitted with a single exponential decay (yellow). The channel width is 0.1 ns. The decay time deduced from the single exponential is equal to 4.1 ns.

### 3.2.3.3 Description of photon collection

The fluorophore is excited with a short pulse of laser (pulse width 5 ns) which has a repetition rate equal to 1 MHZ. Photomultiplier detector is used for recording the time-dependent distribution of emitted photons after each pulse. Intensity of the laser is chosen so that the detector collects 0 or 1 photon during one internal, the collected photons are arranged in 2000 channels (the channel width is equal to 0.1 ns). The computer counts the number of photon in every channel. The experiment duration is stopped when the number of photon in the first channel is equal to $10^4$. The total

number of photon distributes along a decay curve that may obey to a multi-exponential function. Total intensity can be obtained by averaging the total number of collected photons per unit time. A simple sketch of photon acquisition is shown in Figure 3.11.

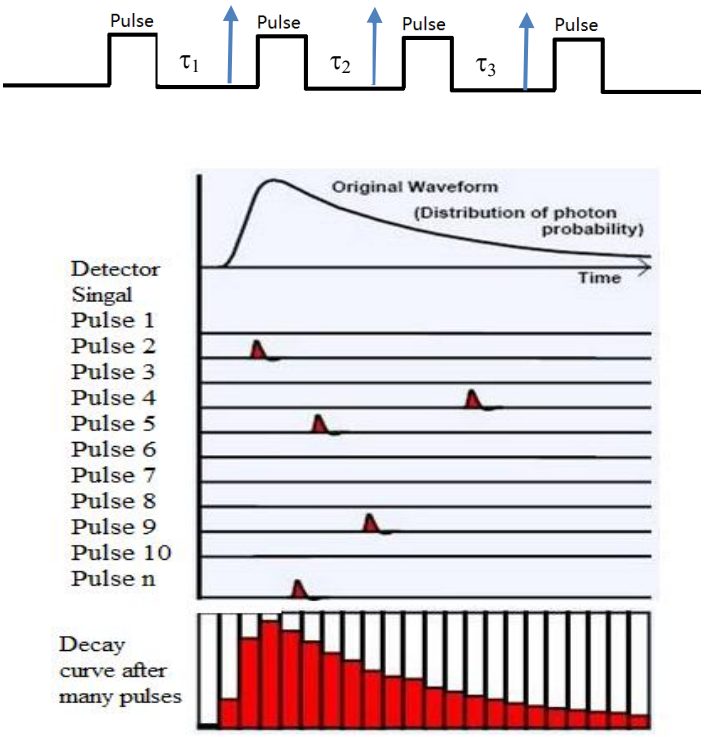


**Figure 3.11:** Photon collection after pulse excitation: 1 photon is collected after each pulse. The lapse time between the pulse and the detected photon, $\tau_1$, $\tau_2$ and $\tau_3$ is recorded. The photons are gathered in windows according to their lapse time, and then intensity decay curve is obtained.

### 3.2.3.4 Data analysis procedure

One excited population corresponds to monoexponential decay (as we show in Figure 3.10), regardless of how many kinds of decay process, the decay time is the average of all decay processes. But what we observe in our study is that there are several decay exponential when the ratio of ruthenium to $DNA_{bp}$ is over than 1

(Figure 3.12), several arguments happen next, if these amplitudes are too small or are too close to each other, how many decay times should be considered? So it is reasonable to find a proper way to get an average of decay time.

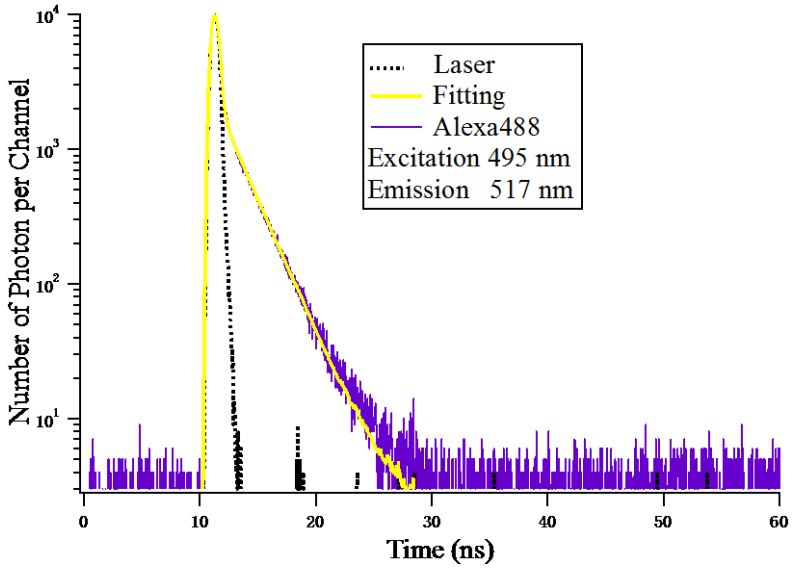


**Figure 3.12:** Typical emission decay curve obtained from a single labeled dsDNA with Alexa 488 with excess ruthenium ($C_{Ru}$ / $C_{DNAbp}$ = 20/3). Black: width of a laser pulse. Blue: emission of dsDNA fitted with 2 exponential decay (yellow). The channel width is 0.1 ns. The decay times deduced from the single exponential are equal to 0.13 ns and 3.8 ns.

DAS software is employed to fit the curve in this study, we tried 1 exponential, 2 exponential and 3 exponential function to fit the curve, it is difficult to differentiate these three kinds of exponential function at low concentration of ruthenium [0 0.5 μM], Figure 3.13 shows that there is almost no difference among three kinds of exponential fitting functions. To be strict and reasonable, 2 exponential function is employed to fit the experimental curve due to reasonable amplitude and $\psi^2$ constant which represent the quality of fitting curve result. Two characteristic decay times ($\tau_1$ and $\tau_2$ ) and two amplitudes ($\alpha_1$ and $\alpha_2$) will be directly given by the fitting results with Equation 3.43:

$$F(t) = \alpha_1 e^{-t/\tau_1} + \alpha_2 e^{-t/\tau_2} \tag{3.43}$$

where $F(t)$ describes the change of the fluorescence intensity with time t, $\alpha_1$ and $\alpha_2$ represent the amplitude, $\tau_1$ and $\tau_2$ correspond to two decay times. As we discussed in the previous paragraph, one excited population should correspond to one decay time ($\tau$), and the lifetime can be computed from equation 3.44:

$$F^{\varepsilon}(t) = \alpha e^{-t/\tau} \tag{3.44}$$

If we assume that one excited population corresponds to one decay time. This single decay time may be computed from the average of the fitted decay times $\tau_1$ and $\tau_2$.The total number of photons collected should be the same whatever the analytical description, that is:

$$\alpha_1\tau_1 + \alpha_2\tau_2 = \alpha\tau \tag{3.45}$$

Moreover using that $F^{\varepsilon}(0) = F(0)$

We have $\alpha_1 + \alpha_2 = \alpha$ (3.46)

$\tau_1$ and $\tau_2$ obtained from fitting results will be weighted by the following equation.

$$\tau = \frac{\alpha_1\tau_1 + \alpha_2\tau_2}{\alpha_1 + \alpha_2} \tag{3.47}$$

where $\tau$ will be seen as the weighted characteristic decay time, it will be used for analyzing experiment results.

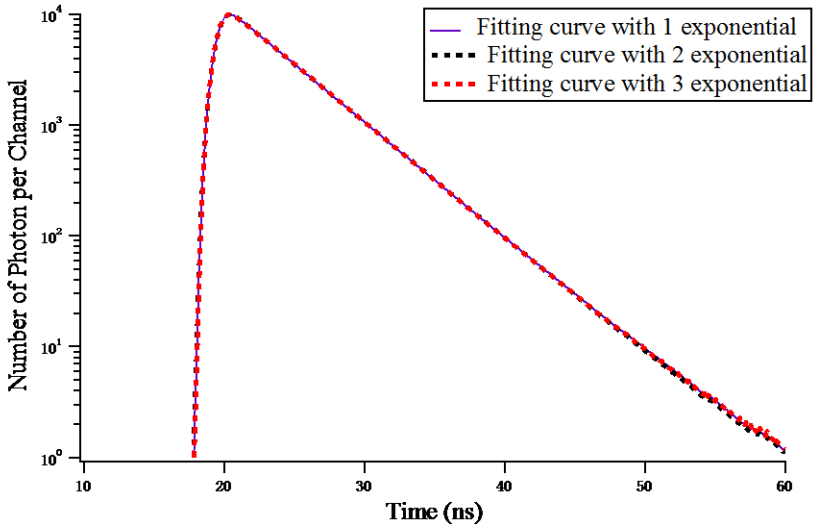


**Figure 3.13:** 1 exponential, 2 exponential and 3 exponential fitting curves from a single labeled dsDNA with Alexa488. Black dash line: width of a laser pulse. Blue solid line: 1 exponential fitting curve. Black dash line: 2 exponential fitting curve. Red dash line: 3 exponential fitting curve.

.

## 3.3 Experimental results

In this part, the lifetime of each kind of fluorophore (Alexa488-donor and Alexa568-acceptor) is measured with TCSPC technique under different experimental conditions. We observe that the addition of $Ru(bpy)_2dppz^{2+}$ results in a strong quenching of fluorophores when the ruthenium concentration is over than 1 μM. From the analysis of the evolution of the lifetime of the donor fluorophore and the acceptor fluorophore, we deduce the evolution of the efficiency of energy transfer as a function of ligand concentration. Both donor and acceptor analysis refer to Part 3.1.1.3 (page 49) and Part 3.1.2.2 (page 56) .

The titrations are performed by increasing the concentration of $Ru(bpy)_2dppz^{2+}$, the alexa fluorophore concentration is kept at 1 μM. We characterize the evolution of decay time after each single measurement, the specific information of titration is already shown in Table 3.2.

### 3.3.1 Definition of 2 regions of experimental results

The intensity of donor (alexa488) emission of single labeled dsDNA and double labeled dsDNA was measured with increasing the concentration of ruthenium, the results of emission intensity are shown in Figure 3.14. It is obvious that the intensity decreases with adding ruthenium. Strong quenching is observed when the concentration of ruthenium is over than 1 μM, so the experimental result analysis is divided into two regions. First region corresponds to  of ruthenium concentration between 0 and 1 μM, second region is determined when the concentration of ruthenium is over than 1 μM. The crossover between the two regions corresponds to 1 mol of ruthenium per 1 mol of DNA. As we are interested in the change of the dynamic of DNA upon complexation with $Ru(bpy)_2dppz^{2+}$, we will consider only the low ruthenium concentration region in the subsequent analysis.

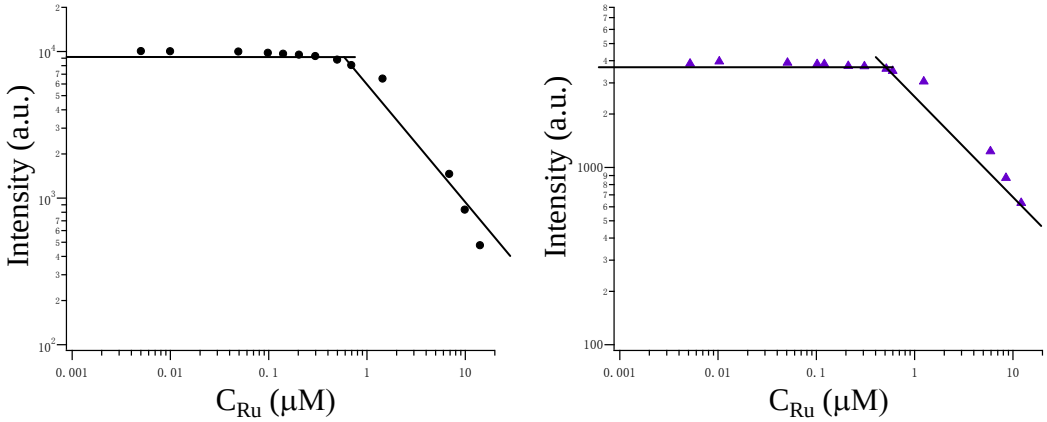


**Figure 3.14:** Evolution of Alexa488 emission intensity as a function of $C_{Ru}$. Left is the single labeled dsDNA, right is the double labeled dsDNA.

**Results of lifetime and emission intensity of donor at low ruthenium concentration region [0, 0.5 μM]**

Decay times directly given by the DAS software and weighted decay times computed with Equation. 3.47 (single labeled dsDNA and double labeled dsDNA) are shown in Table 3.3 and Table 3.4, respectively.

The plots of weighted decay time and emission intensity as a function of ruthenium concentration are shown in Figure 3.15 and Figure 3.16. The decay times decrease with increasing concentration of $Ru(bpy)_2dppz^{2+}$. The emission intensity also exhibits a linear decrease with ruthenium cocentration at low ruthenium concentration region (up to $C_{Ru}$ = 0.5 μM).

**Table 3.3:** Weighted decay time of donor of single labeled dsDNA

| $\tau_1$ (ns) | $\tau_2$ (ns) | $\alpha_1$ | $\alpha_2$ | $\tau = \frac{\alpha_1\tau_1 + \alpha_2\tau_2}{\alpha_1 + \alpha_2}(ns)$ | $C_{Ru}$ (μM) |
|---|---|---|---|---|---|
| 2.14 | 4.13 | 0.000348 | 0.0519 | 4.12 | 0 |
| 2.13 | 4.16 | 0.00235 | 0.0499 | 4.07 | 0.005 |
| 2.14 | 4.15 | 0.00177 | 0.0498 | 4.08 | 0.01 |
| 2.11 | 4.13 | 0.00188 | 0.0498 | 4.06 | 0.05 |
| 2.07 | 4.12 | 0.00297 | 0.0491 | 4.00 | 0.1 |
| 0.58 | 4.08 | 0.0087 | 0.0495 | 3.56 | 0.2 |
| 0.91 | 4.06 | 0.00708 | 0.0483 | 3.66 | 0.3 |
| 1.49 | 4.05 | 0.00937 | 0.0457 | 3.61 | 0.5 |

**Table 3.4:** Decay time of donor of double labeled dsDNA

| $\tau_1$ (ns) | $\tau_2$ (ns) | $\alpha_1$ | $\alpha_2$ | $\tau = \frac{\alpha_1\tau_1 + \alpha_2\tau_2}{\alpha_1 + \alpha_2}(ns)$ | $C_{Ru}$ (μM) |
|---|---|---|---|---|---|
| 0.87 | 2.77 | 0.0111 | 0.0519 | 2.44 | 0 |
| 1.23 | 2.83 | 0.0126 | 0.0478 | 2.5 | 0.005 |
| 1.14 | 2.83 | 0.0138 | 0.0478 | 2.45 | 0.01 |
| 1.02 | 2.8 | 0.0136 | 0.0486 | 2.41 | 0.05 |
| 1.43 | 2.89 | 0.0181 | 0.0433 | 2.46 | 0.1 |
| 1.32 | 2.86 | 0.0184 | 0.0439 | 2.41 | 0.2 |
| 1.51 | 2.93 | 0.0239 | 0.0391 | 2.39 | 0.3 |
| 1.39 | 2.87 | 0.0228 | 0.039 | 2.32 | 0.5 |

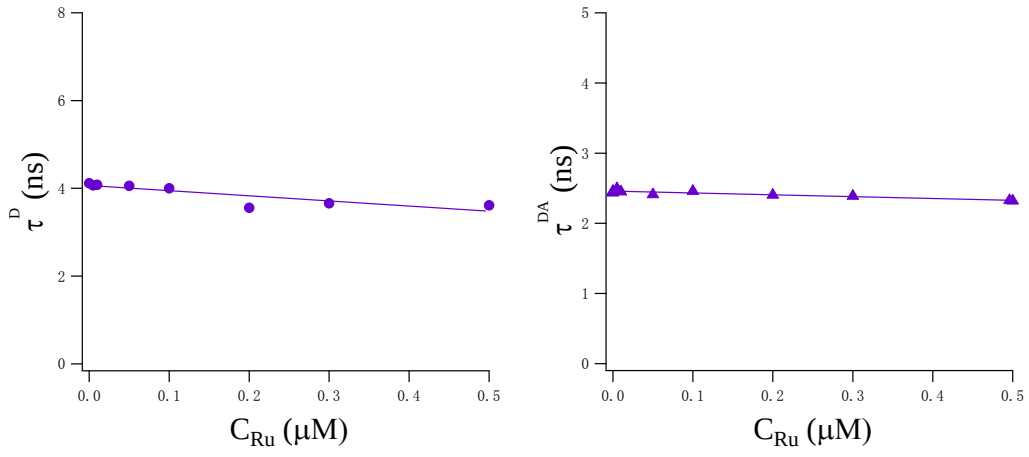


**Figure 3.15:** Evolution of decay time $\tau^D$ and $\tau^{DA}$ of donor as a function of $C_{Ru}$ in the absence (left) and presence (right) of acceptor.

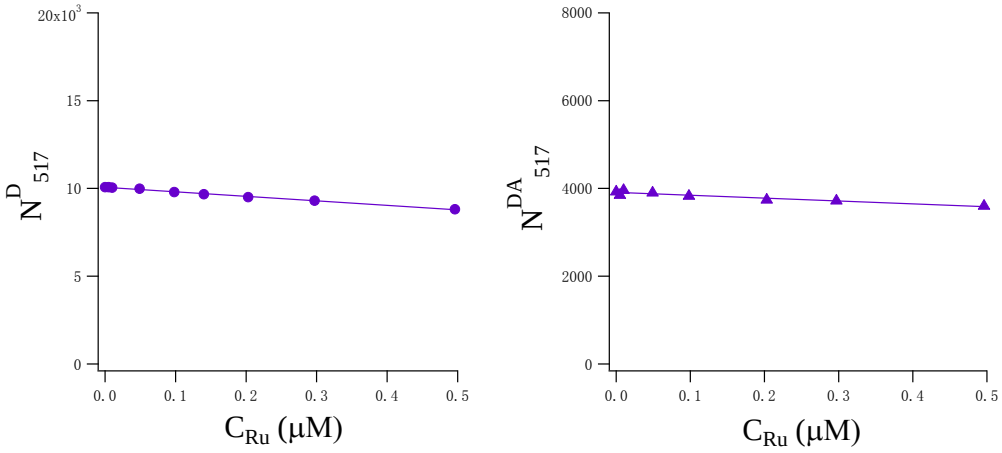


**Figure 3.16:** Number of photons emitted at 517 nm by 1μM DNA labeled with donor as a function of $C_{Ru}$. Left is single labeled dsDNA, right is the double labeled dsDNA.

## 3.3.2 Analysis of the emission at 517 nm

### 3.3.2.1 Quenching constant computation

Quenching constant is computed with Equation 3.6 and Equation 3.12 (Part 3.1.1.3 ):

$$\frac{F_0}{F} = 1 + K_D[Q]$$

$$\frac{\tau_0}{\tau} = 1 + K_D[Q]$$

We assume that the emission intensity of excited fluorophore is proportional to the total number of excited fluorophore with the time evolution, and we can not measure the number of excited fluorophore with time, As a fact of that emission intensity of fluorophore was directly measured in our experiment. So we simply use the ratio $\frac{I_0^D}{I^D}$

to compute the quenching constant, where $I^D$ is the intensity emitted by the donor and $I_0^D$ is the intensity of the donor at 0 ruthenium concentration.

The ratios of $\frac{I_0^D}{I^D}$ and $\frac{\tau_0^D}{\tau^D}$ as a function of $C_{Ru}$ are shown in Figure 3.17. The evolution obeys to a linear behavior the slope of the fitting curve leads to the quenching constant. The slopes are equal to 0.325 $\mu M^{-1}$ and 0.285 $\mu M^{-1}$, respectively. $\frac{\tau_0^D}{\tau^D}$ is not equal to 1 and the slope of fitting curve of $\frac{\tau_0^D}{\tau^D}$ is higher than the slope of $\frac{I_0^D}{I^D}$ which means that there is no static quenching at low ruthenium concentration region.

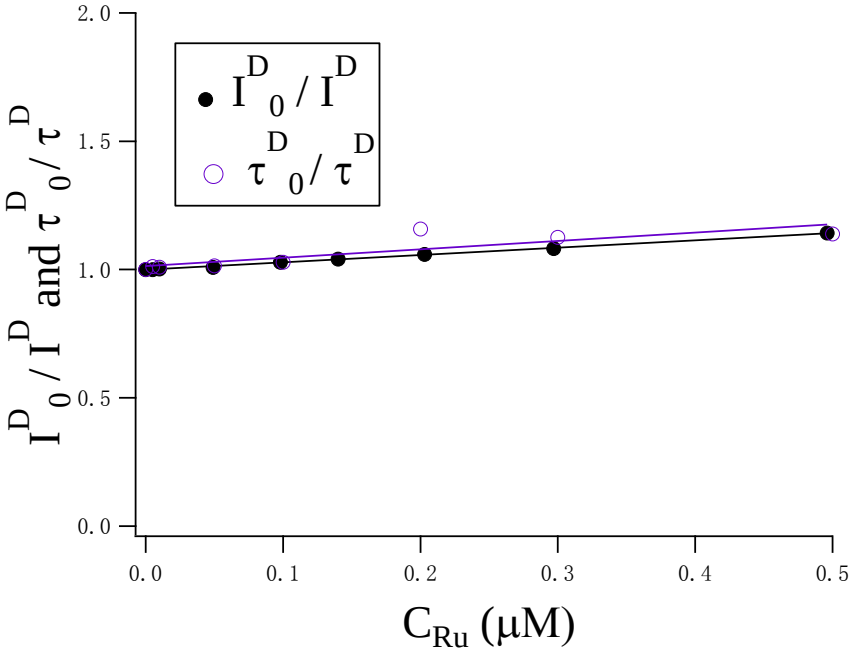


**Figure 3.17:** The ratio of $\frac{I_0^D}{I^D}$ and $\frac{\tau_0^D}{\tau^D}$ as a function of $C_{Ru}$ in the absence of acceptor. The slope of fitting curve gives the value of quenching constant.

The computation of $\frac{\tau_0^{DA}}{\tau^{DA}}$ and $\frac{I_0^{DA}}{I^{DA}}$ were done in the presence of acceptor (double labeled dsDNA), the evolution of both ratio as a function of $C_{Ru}$ are shown in Figure

3.18, the slopes of $\frac{\tau_0^{DA}}{\tau^{DA}}$ and $\frac{I_0^{DA}}{I^{DA}}$ are equally to 0.083 $\mu M^{-1}$ and 0.237 $\mu M^{-1}$, respectively. This change of slope is directly related to the appearance of a new relaxation process: FRET.

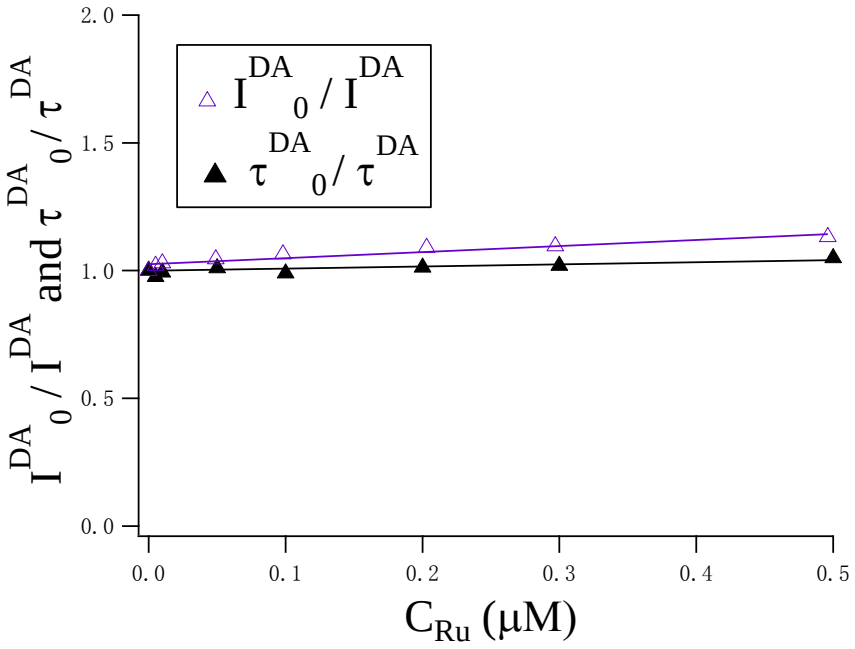


**Figure 3.18:** The ratio of $\frac{I_0^{DA}}{I^{DA}}$ and $\frac{\tau_0^{DA}}{\tau^{DA}}$ as a function of $C_{Ru}$ in the presence of acceptor.

We now are going to perform a quantitative analysis of the intensity and time changes when $Ru(bpy)_2dppz^{2+}$ complexes with DNA.

### 3.3.2.2 Evolution of the transfer rate with $C_{Ru}$

According to the theory part of measurement of FRET efficiency:

1) The presence of acceptor doesn't change nor add any relaxation process except FRET process.

2) The number of excited donor molecules at a given excitation wavelength is the same in the absence and presence of the acceptor.
3) The number of excited acceptor molecules at a given excitation wavelength is the same.

The transfer rate $\kappa_T$ and transfer efficiency *E* are separately computed from Equation 3.18 and Equation 3.19;

$$\frac{1}{\tau^{DA}} = \frac{1}{\tau^{D}} + \kappa_T$$

$$E = \kappa_T \tau^{DA} = 1 - \frac{\tau^{DA}}{\tau^{D}}$$

Where $\tau^{DA}$ and $\tau^{D}$ are already shown in the Table 3.3 and Table 3.4, so the evolution of transfer relaxation time $\tau_F$ (the inverse of $\kappa_T$ ) and transfer efficiency *E* as a function of $C_{Ru}$ can be obtained from Equation 3.18 and Equation3.19, respectively. The evolutions of $\tau^F$ and *E* as a function of $C_{Ru}$ are shown in Figure 3.19. On the whole, $\tau^F$ increases with the increase of ruthenium concentration. The transfer efficiency decreases with increasing the $C_{Ru}$.

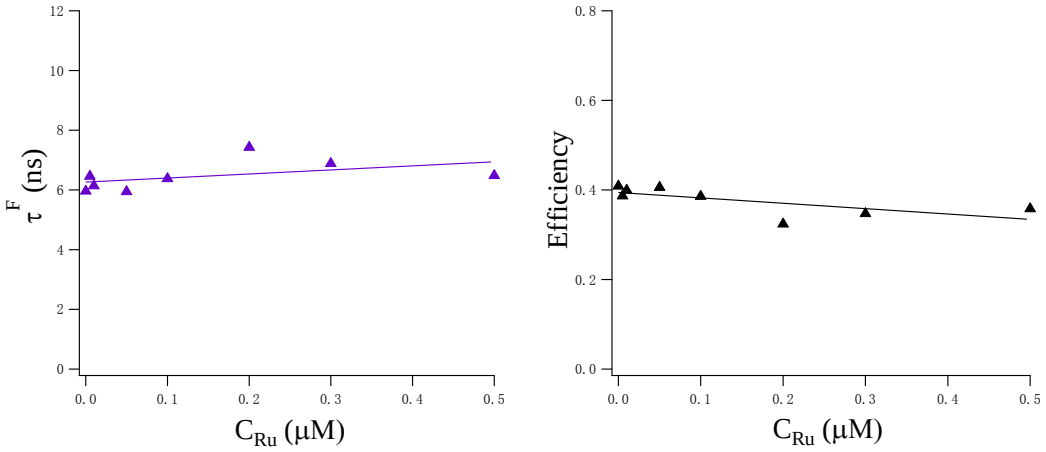


**Figure 3.19:** Evolution of $\tau^F$ (left) and $E$ (right) as a function of $C_{Ru}$. Lines are linear fitting of the data: $\tau^F = 6.257 + 1.288 C_{Ru}$, $E = 0.395 - 0.117 C_{Ru}$.

We found that the evolution of $\tau^F$ and $E$ with the Ruthenium concentration may be well described by a linear behavior. Nevertheless in order to perform this analysis, we had to compare the intensity emitted by single labeled and double labeled DNA. That is, we assume that the number of excited fluorophores is the same in the presence or absence of the acceptor ($D_{01}^* = D_{02}^*$). We will see in the next part, by showing the emission at 600 nm, this hypothesis may be avoided.

## 3.3.3 Analysis of the emission at 600 nm

We now consider the emission at 600 nm of double labeled dsDNA bound with ruthenium complex, $N_{600}$. The evolution of $N_{600}$ with $C_{Ru}$ is given in Figure 3. 20. There are three contributions to this emission.

1) Donor contribution, the total number of photon at 600 nm emitted by the donor will be called $N_{600}^{DA}$, the intensity emitted at 600 nm by the donor after a pulse will be called $I_{600}^{DA}(t)$
2) Acceptor emission, the total number of photon at 600 nm emitted by the acceptor will be called $N_{600}^{AD}$, the intensity emitted at 600 nm by the acceptor after a pulse will be called $I_{600}^{AD}(t)$
3) $Ru(bpy)_2dppz^{2+}$ contribution when it is intercalated into DNA base pair, the total number of photon at 600 nm emitted by the bound ruthenium will be called $N_{600}^{Ru}$, the intensity emitted at 600 nm by the bound ruthenium after a pulse will be called $I_{600}^{Ru}(t)$

So the total number of photons emitted at 600 nm ( $N_{600}$ ) can be expressed as:

$$N_{600} = N_{600}^{Ru} + N_{600}^{DA} + N_{600}^{AD} \tag{3.48}$$

$N_{600}$ and $N_{600}^{Ru}$ are obtained directly from experiments, whereas $N_{600}^{DA}$ and $N_{600}^{AD}$ will be obtained indirectly, we are going to analyze the emission at 600 nm term by term, the evolution of the efficiency as a function of ruthenium concentration can be finally obtained.

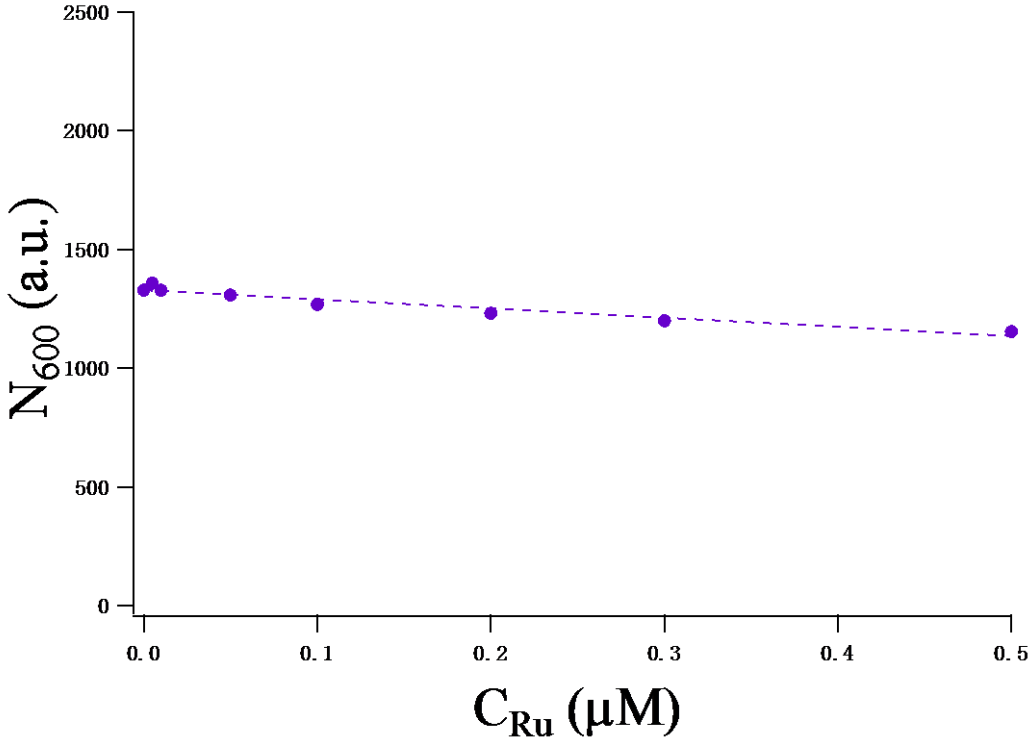


**Figure 3. 20:** Evolution of the number of photons emitted by complexed double labeled at 600 nm as a function of $C_{Ru}$. Dashed line is a linear fit of the data: $N_{600} = 1328.5 - 386.77 C_{Ru}$ .

### 3.3.3.1 Measurement of emission at 600 nm from bound $Ru(bpy)_2dppz^{2+}$ ($N_{600}^{Ru}$)

The intensity of emission at 600 nm of bound $Ru(bpy)_2dppz^{2+}$ as a function of $C_{Ru}$ has been measured when the ruthenium complex bound with non-labeled DNA, results are shown in Figure 2.2 (Chapter 2), we observe a linear region up to 0.5 bound ruthenium per DNA base pair, corresponding to the diluted region defined in Figure 3.14 in which the intensity emitted by alexa488 at 517 nm decreased linearly with ruthenium concentration. In order to compare the intensity emitted by bound ruthenium with total intensity at 600 nm, $I_{600}$, we performed 3 measurements at 3

ruthenium concentrations up to saturated region, we observe the contribution of bound ruthenium to the total intensity measured at 600 nm is always lower than 0.005. The results are shown in Table 3.5. So the contribution of bound ruthenium emitted at 600 nm is negligible.

**Table 3.5:** Intensity of emission at 600 nm of $Ru(bpy)_2dppz^{2+}$

| Intensity | Ratio of $[\frac{I_{600}^{Ru}}{I_{600}(C_{Ru}=0)}]$ | $C_{Ru}$ (μM) |
|---|---|---|
| 2.1 | 0.0016 | 1 |
| 5.6 | 0.0042 | 10 |
| 5.5 | 0.0041 | 30 |

### 3.3.3.2 Intensity emitted at 600 nm by donor ( $N_{600}^{DA}$ )

In order to obtain the emission at 600 nm from the donor, we will use the intensities emitted by DNA single labeled with Alexa488 at 600 nm and 517 nm, and the intensity emitted by double labeled DNA at 517 nm. All of these 3 quantities can be directly obtained from measurements. Indeed, we have:

$$\mathrm{N}_{517}^{D} = \int_0^\infty \frac{1}{\tau_{517}^{D}} \mathrm{D}_{01}^{*} e^{-t/\tau^{D}} dt = \mathrm{D}_{01}^{*} \frac{\tau^{D}}{\tau_{517}^{D}}$$

$$\mathrm{N}_{600}^{D} = \int_0^\infty \frac{1}{\tau_{600}^{D}} \mathrm{D}_{01}^{*} e^{-t/\tau^{D}} dt = \mathrm{D}_{01}^{*} \frac{\tau^{D}}{\tau_{600}^{D}}$$

$$\mathrm{N}_{517}^{DA} = \int_0^\infty \frac{1}{\tau_{517}^{D}} \mathrm{D}_{02}^{*} e^{-t/\tau^{DA}} dt = \mathrm{D}_{02}^{*} \frac{\tau^{DA}}{\tau_{517}^{D}}$$

$$\mathrm{N}_{600}^{DA} = \int_0^\infty \frac{1}{\tau_{600}^{D}} \mathrm{D}_{02}^{*} e^{-t/\tau^{DA}} dt = \mathrm{D}_{02}^{*} \frac{\tau^{DA}}{\tau_{600}^{D}}$$

And we have obtained Equation 3.26 from Equation 3.22 and Equation 3.24

$$\frac{N_{517}^{DA}}{N_{517}^{D}} = \frac{D_{02}^{*}}{D_{01}^{*}} \frac{\tau^{DA}}{\tau^{D}}$$

Now by dividing Equation 3.25 with Equation 3.23, we thus have:

$$\frac{N_{600}^{DA}}{N_{600}^{D}} = \frac{D_{02}^{*}}{D_{01}^{*}} \frac{\tau^{DA}}{\tau^{D}} \tag{3.49}$$

Combining Equation 3.26 and Equation 3.49, the emission at 600 nm ( $N_{600}^{DA}$) from the donor is:

$$N_{600}^{DA} = N_{517}^{DA} \frac{N_{600}^{D}}{N_{517}^{D}} \tag{3.50}$$

The evolution of $N_{517}^{D}$ and $N_{517}^{DA}$ as function of $C_{Ru}$ have been shown in Figure 3.16. The ratio $\frac{N_{600}^{D}}{N_{517}^{D}}$ doesn't depend on the ruthenium concentration, and is measured at the 0 ruthenium concentration. It is equal to 1/36.5. Thus $N_{600}^{DA}$ can be calculated as a function of $C_{Ru}$. The results are given in Figure 3.21.

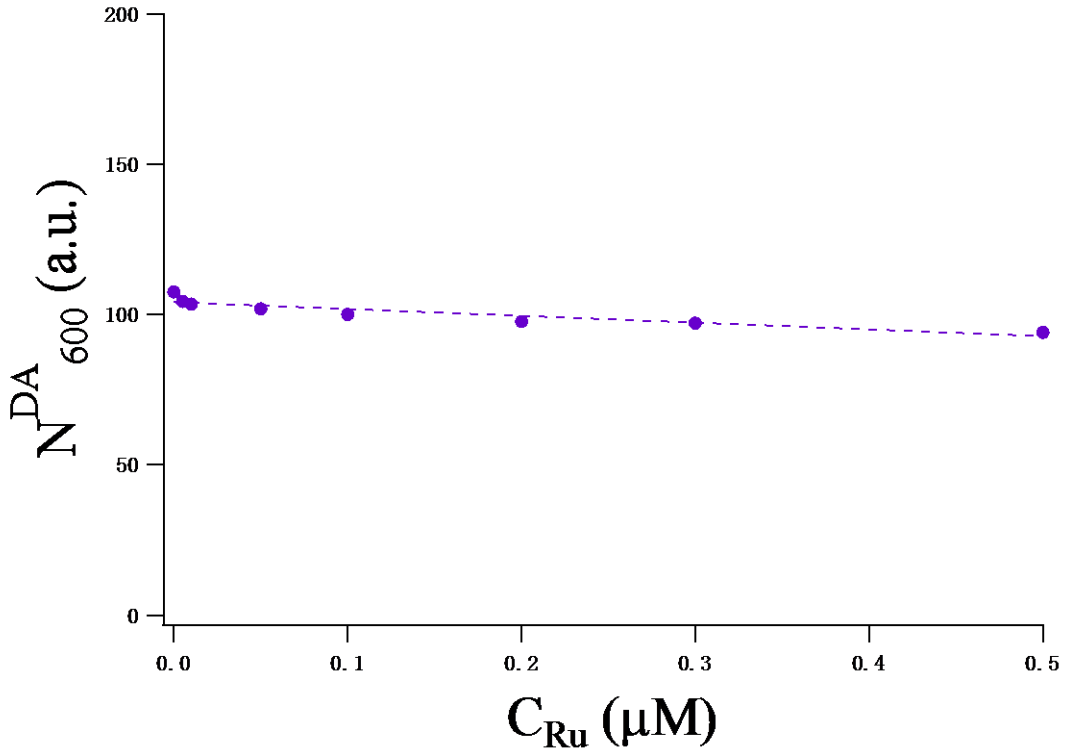


**Figure 3.21:** Evolution of the number of photons emitted by the donor ( $N^{DA}_{600}$ ) at 600 nm in the presence of acceptor as a function of $C_{Ru}$. Dashed line is a linear fit of the data: $N^{DA}_{600} = 104.1 - 22.6 C_{Ru}$.

### 3.3.3.3 Intensity emitted at 600 nm by acceptor ( $N^{AD}_{600}$ )

$N^{AD}_{600}$ can't be measured directly and is obtained from:

$$N^{AD}_{600}(C_{Ru}) = N_{600}(C_{Ru}) - N^{DA}_{600}(C_{Ru}) \quad (3.51)$$

The results are shown in Figure 3.22. $N^{AD}_{600}$ show a linear behavior with $C_{Ru}$.

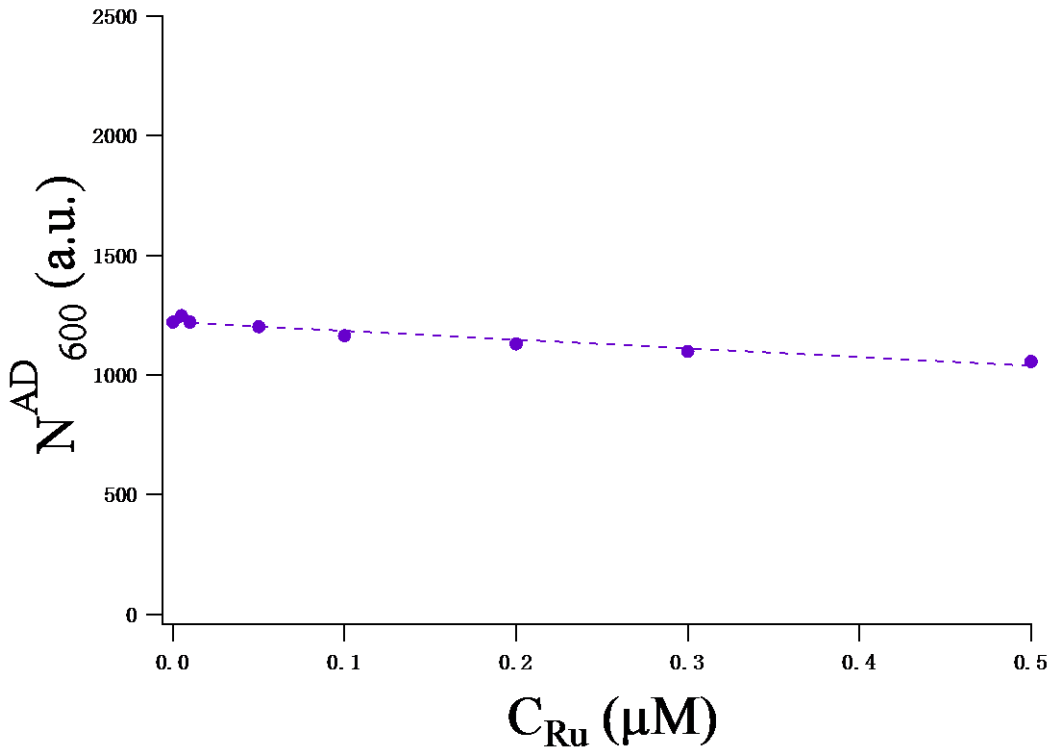


**Figure 3.22:** Evolution of the number of photons emitted by the acceptor ($N^{AD}_{600}$) at 600 nm in the presence of donor as a function of $C_{Ru}$. Dashed line is a linear fit of the data: $N^{AD}_{600} = 1220.9 - 365.5 C_{Ru}$.

### 3.3.3.4 Computation of the efficiency of energy transfer

The number of photons emitted by the acceptor is (Equation 3.34):

$$N^{AD}_{600} = (A^{*}_{02} + D^{*}_{02} E)\frac{\tau^{A}}{\tau^{A}_{600}}$$

From which we have:

$$E = \left(\frac{N^{AD}_{600}}{\tau^{A}} - \frac{A^{*}_{02}}{\tau^{A}_{600}}\right)\frac{\tau^{A}_{600}}{D^{*}_{02}} \qquad (3.52)$$

In order to compute the efficiency, we will determine the three ratios involved:

*1)* $\frac{N_{600}^{AD}}{\tau^{A}}$: $\tau^{A}$ is the fluorescence lifetime of single labeled DNA with alexa568 and is shown in Figure 3.23, and $N_{600}^{AD}$ has been obtained in the previous paragraph.

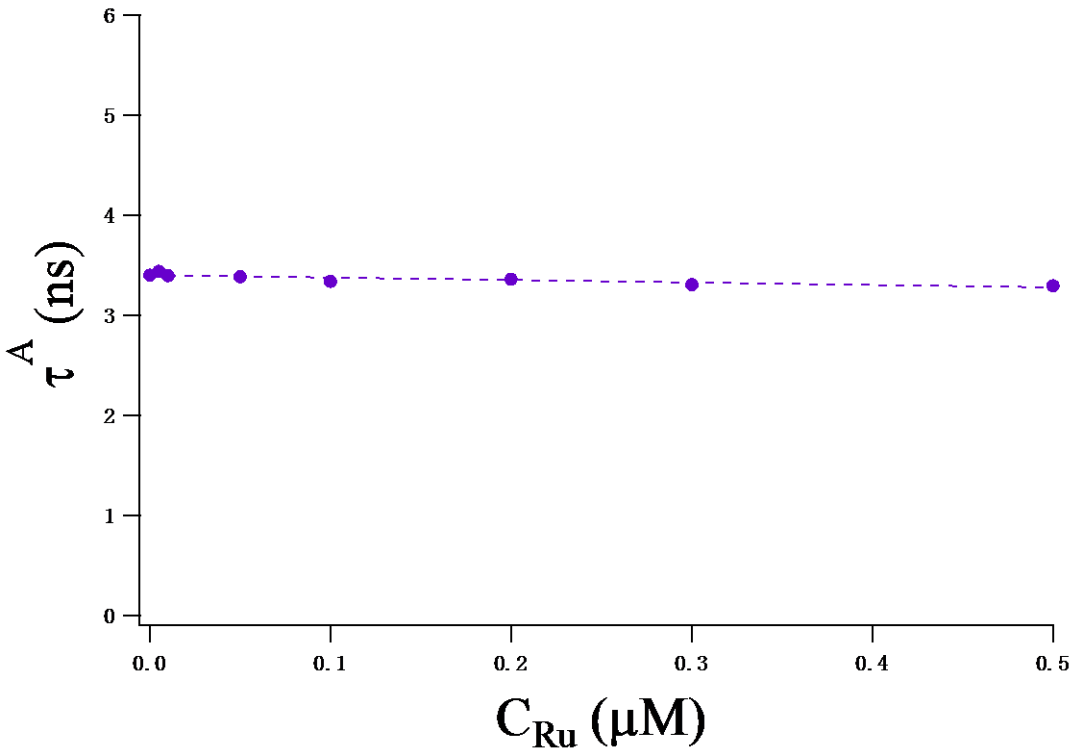


**Figure 3.23:** Evolution of decay time of acceptor as a function of $C_{Ru}$ for single labeled system. Dashed line is a linear fit of the data: $\tau^{A} = 3.4 - 0.245 C_{Ru}$.

*2)* $\frac{A_{02}^{*}}{\tau_{600}^{A}}$ is obtained from the amplitude of the 2 relaxation modes of the intensity emitted at 600 nm by two labeled DNA. This intensity is $I_{600}(t)$ :

$$I_{600}(t) = I_{600}^{AD}(t) + I_{600}^{DA}(t) \tag{3.53}$$

With $$I_{600}^{DA}(t) = \frac{D_{02}^{*}}{\tau_{600}^{D}} e^{-t/\tau^{DA}} = \frac{N_{600}^{DA}}{\tau^{DA}} e^{-t/\tau^{DA}} \tag{3.54}$$

And $$I_{600}^{AD}(t) = \frac{1}{\tau_{600}^{A}} \mathrm{A}^{*}(t) = \frac{1}{\tau_{600}^{A}} [\frac{\mathrm{D}_{02}^{*} \kappa_T \mathrm{e}^{-t/\tau^{DA}}}{(\tau^{A})^{-1} - (\tau^{DA})^{-1}} + (\mathrm{A}_{02}^{*} - \frac{\mathrm{D}_{02}^{*} \kappa_T}{(\tau^{A})^{-1} - (\tau^{DA})^{-1}}) \mathrm{e}^{-t/\tau^{A}}]$$

$$= \alpha_1 \mathrm{e}^{-t/\tau^{\mathrm{DA}}} + \alpha_2 \mathrm{e}^{-t/\tau^{\mathrm{A}}} \qquad (3.55)$$

That defines $\alpha_1$ and $\alpha_2$.

We thus obtain the ratio $\frac{\mathrm{A}_{02}^{*}}{\tau_{600}^{A}}$ from $\alpha_1 + \alpha_2 = \frac{\mathrm{A}_{02}^{*}}{\tau_{600}^{A}}$.

$\alpha_1$ and $\alpha_2$ are obtained from the measurement of $I_{600}(t)$:

$$I_{600}(t) = (\alpha_1 + \frac{N_{600}^{DA}}{\tau^{DA}}) e^{-t/\tau^{DA}} + \alpha_2 \mathrm{e}^{-t/\tau^{\mathrm{A}}} \qquad (3.56)$$

The amplitude of each relaxation mode is obtained from the fit $I_{600}(t)$, with $\tau^{DA}$ and $\tau^{\mathrm{A}}$ known from previous measurements.

The amplitudes ($\alpha_1$ and $\alpha_2$) of the two relaxation modes are given in Figure 3.24 and $\frac{N_{600}^{DA}}{\tau^{DA}}$ is equal to 41.4. $\frac{\mathrm{A}_{02}^{*}}{\tau_{600}^{A}}$ is finally obtained and given in Figure 3.25.

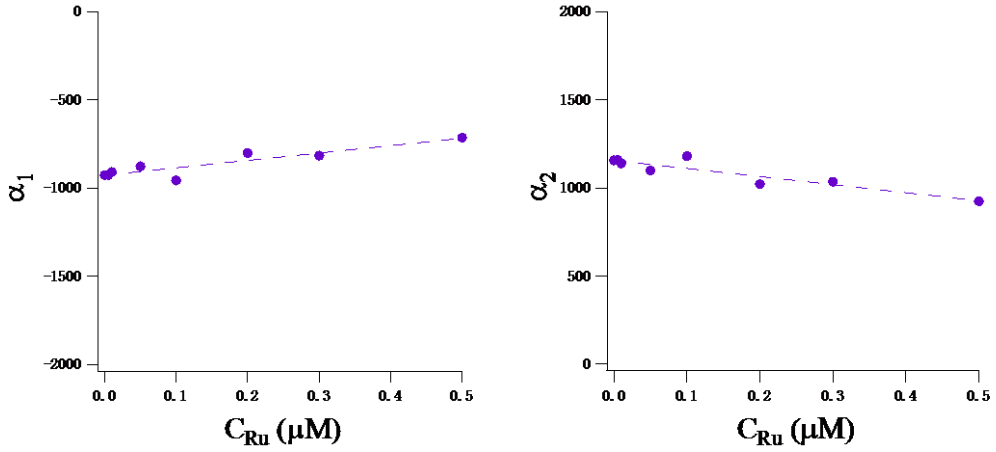


**Figure 3.24:** Evolution of $\alpha_1$ (left ) and $\alpha_2$ (right) as a function of $C_{Ru}$. Dashed lines are the linear fits of data: $\alpha_1 = -927.3 + 419.1 C_{Ru}$, $\alpha_2 = 1155.7 - 457.35 C_{Ru}$.

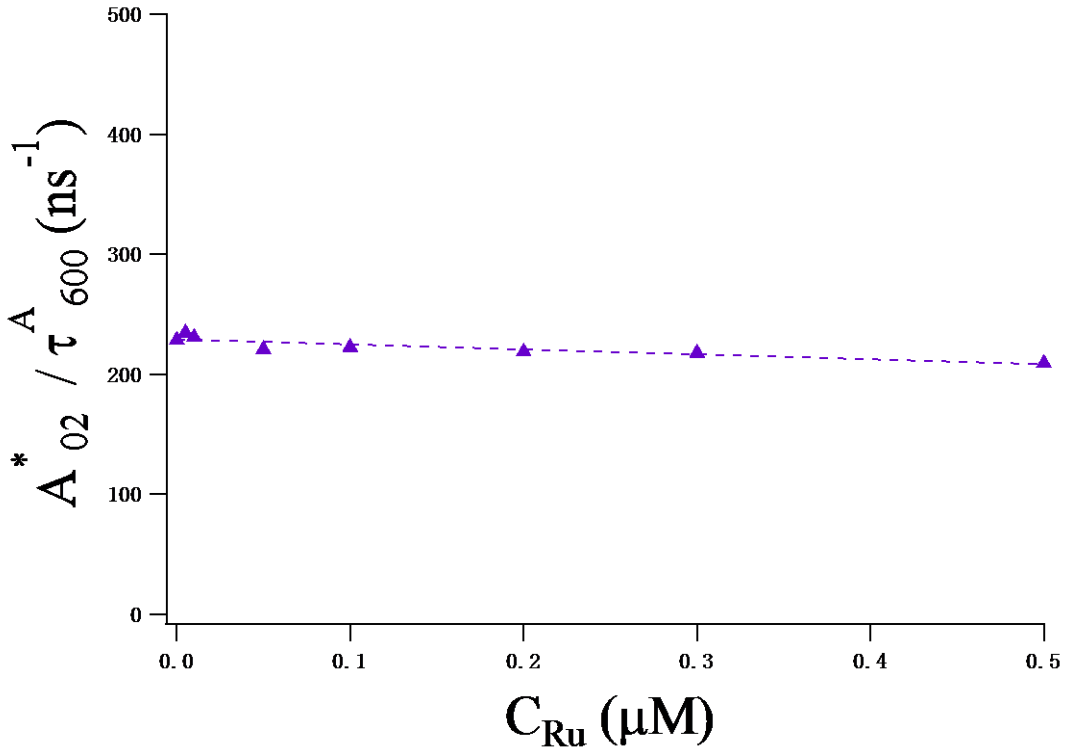


**Figure 3.25:** Evolution of $\frac{A^*_{02}}{\tau^A_{600}}$ as a function of $C_{Ru}$. Dashed line is a linear fit of data: $\frac{A^*_{02}}{\tau^A_{600}} = 228.73 - 41.33 C_{Ru}$.

*3)* $\frac{\tau_{600}^{A}}{\mathrm{D}_{02}^{*}}$ does not depend on the ruthenium concentration. Its value can not be measured from measurements of $I_{600}(t)$ as it always appears under the form $\frac{\mathrm{D}_{02}^{*}}{\tau_{600}^{A}\kappa_T}$. The evolution of the efficiency $E$ as a function of the ruthenium concentration is thus obtained up to a constant multiplication factor (Equation 3.52). In order to compare the evolution of $E$ ($C_{Ru}$) with the efficiency obtained from measurement at 517 nm, we determine this multiplication factor at $C_{Ru}$ = 0. We impose $E_{600}(C_{Ru}=0)=E_{517}(C_{Ru}=0)$, where $E_{600}$ is the efficiency measured according to the analysis above and $E_{517}$ according to Eq. 3.19. The evolution of relaxation time of FRET process $\tau^{F}$ is shown in Figure 3.26. The evolution of transfer rate $K_T$ is given in Figure 3.27. The evolution of the transfer efficiency $E$ is shown in Figure 3.28.

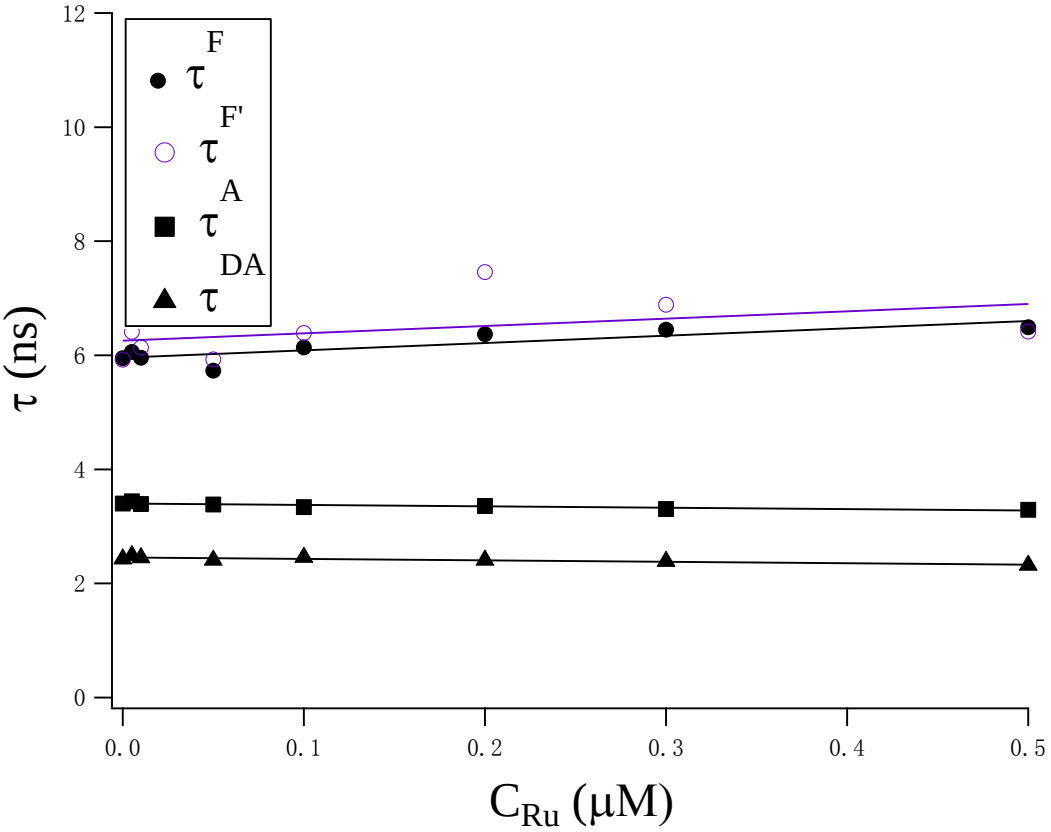


**Figure 3.26:** Evolution of relaxation time as a function of $C_{Ru}$. $\tau^{F}$ (black filled circle) and $\tau^{F'}$ (blue open circle) represent relaxation times of the FRET process obtained from donor point of view and acceptor point of view, respectively; $\tau^{A}$ (square) and $\tau^{DA}$ (triangle) represent relaxation times of acceptor in the absence and presence of donor, respectively. Dashed lines are linear fit of data: $\tau^{F} = 6.257 + 1.288 C_{Ru}$, $\tau^{F'} = 5.956 + 1.287 C_{Ru}$, $\tau^{A} = 3.4 - 0.245 C_{Ru}$, $\tau^{DA} = 2.46 - 0.255 C_{Ru}$.

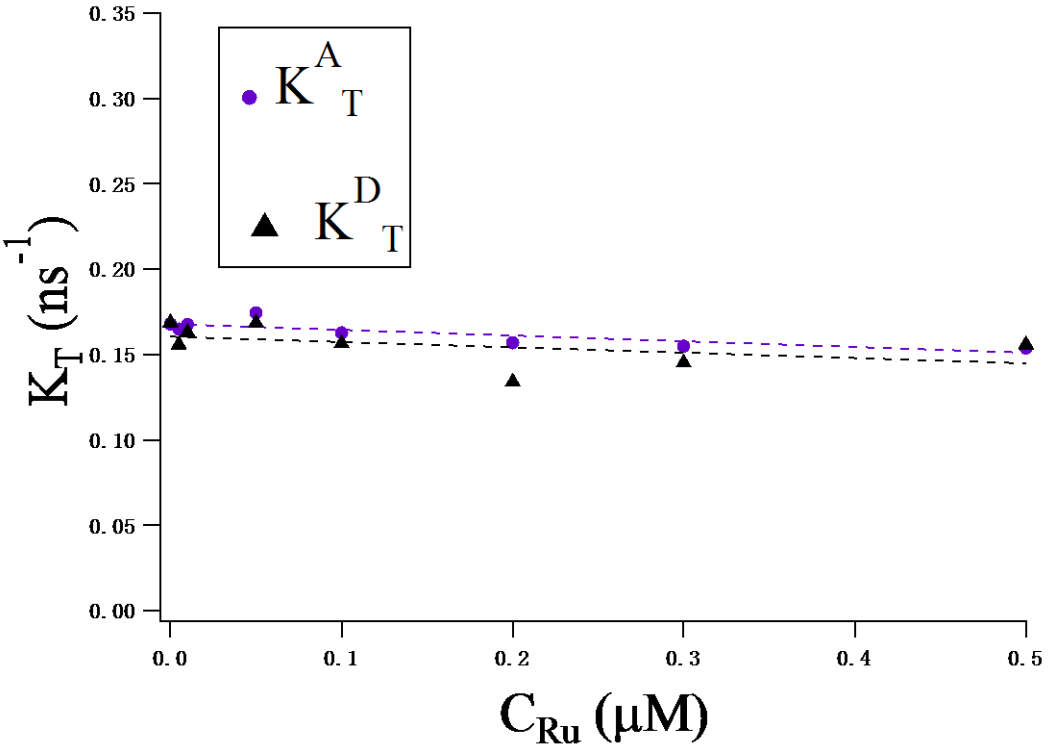


**Figure 3.27:** Evolution of transfer rate ($K_T$) as a function of $C_{Ru}$. $K_T^A$ (blue filled circle) represents the transfer efficiency from the point view of acceptor, $K_T^D$ (black triangle) represents the transfer efficiency from the point view of donor. The dashed lines are linear fit of data: $K_T^A = 0.168 - 0.033 C_{Ru}$, $K_T^D = 0.161 - 0.031 C_{Ru}$.

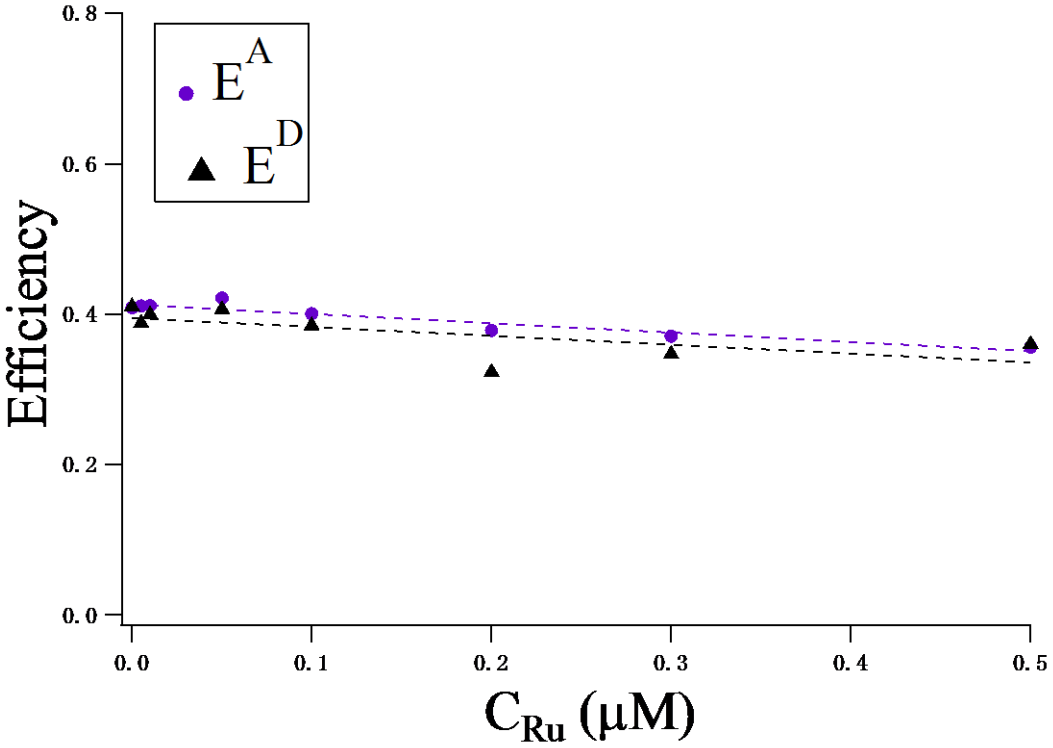


**Figure 3.28:** Evolution of transfer efficiency (*E*) as a function of $C_{Ru}$. $E^A$ (blue filled circle) represents the transfer efficiency from acceptor emission, $E^D$ (black triangle) represents the transfer efficiency from donor emission. Dashed lines are the linear fits of data: $E^A = 0.413 - 0.124 C_{Ru}$, $E^D = 0.395 - 0.117 C_{Ru}$.

### 3.3.3.5 Discussions of the efficiency

We have shown a decrease of the FRET efficiency due to the complexation of DNA with $Ru(bpy)_2dppz^{2+}$. At the ruthenium concentration under study, the average number of the ruthenium complex per DNA strand is smaller than 1.

More precisely, we have measured the affinity constant of $Ru(bpy)_2dppz^{2+}$ and DNA in Chapter 2. At 20 mM salt concentration, we have $K_a^{strand} = 2.85 * 10^5 M^{-1}$.

$$DNA_{strand} + Ru \overset{K_a^{strand}}{\rightleftharpoons} DNA_{strand} - Ru$$

Let us consider $\xi = \frac{[DNA_{strand} - Ru]}{[DNA_{strand}]}$, the fraction of dsDNA bound with one $Ru(bpy)_2dppz^{2+}$. We have :

$$K_a^{strand} = \frac{\xi}{([DNA^0_{strand}] - \xi)(C_{Ru} - \xi)}$$

where $[DNA^0_{strand}]$ is the total DNA strand concentration, and $C_{Ru}$ is the concentration of $Ru(bpy)_2dppz^{2+}$. From this equilibrium relationship, the ratio of complexed DNA strand is computed (see Figure 3.29). The ratio of complexed $DNA_{strand}$ increases up to a value of 0.55 at $C_{Ru}$ = 0.5 μM.

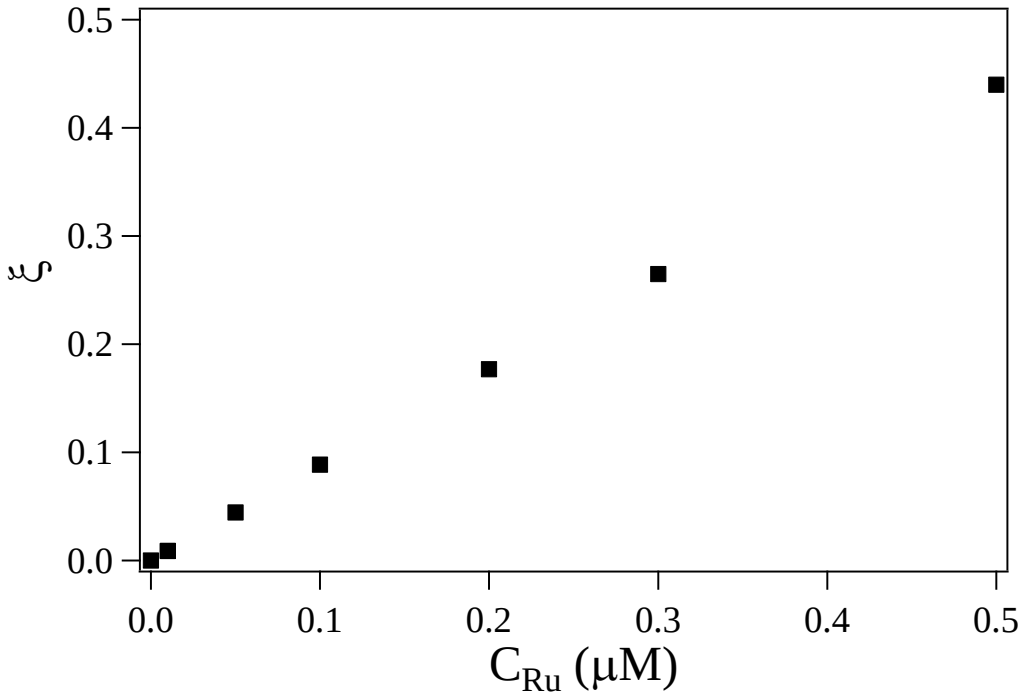


**Figure 3.29:** The fraction (ξ) of bound dsDNA as a function of $C_{Ru}$.

At the concentration under study, the fraction of DNA strand complexed by more than one ruthenium molecule may be neglected. We thus have a mixture of uncomplexed DNA and DNA strands complexed with one ruthenium molecule. Moreover this molecule may be intercalated at one or other of the 14 positions along the DNA double strand The intensities and lifetimes measured are thus average values of the intensities and lifetimes of these different complexes.

The measured lifetime may be written as:

$$\bar{\tau} = (1-\xi)\tau_0 + \xi \frac{1}{14}\sum_{n=1}^{14}\tau_{1,n} \qquad (3.57)$$

Where ξ is the fraction of DNA strands complexed with one $Ru(bpy)_2dppz^{2+}$, $\tau_0$ is the decay time of non-complexed DNA, $\tau_{1,n}$ is the decay time of DNA strand intercalated with $Ru(bpy)_2dppz^{2+}$ at the $n^{th}$ position (Figure 30). We have moreover assumed that all the intercalation positions are the same probability.

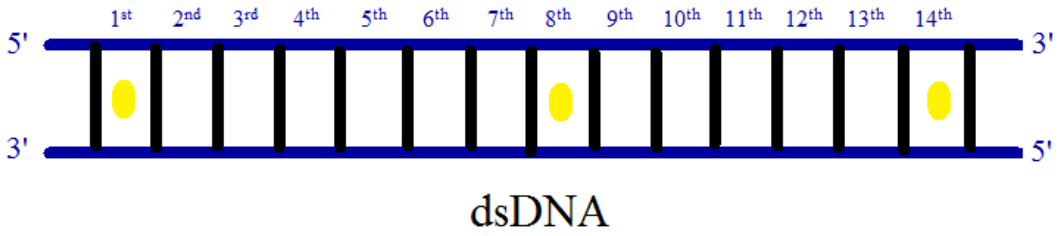


**Figure 3.30:** A sketch of the 14 intercalation positions of dsDNA (blue numbers: from 1st to 14th). The probability of ruthenium molecule intercalation into any positions is the same.

The decay time may be expressed as the consequence of the existence of two processes:

$$\frac{1}{\tau_0(C_{Ru})} = \frac{1}{\tau_0^D(C_{Ru})} + \frac{1}{\tau_0^F} \tag{3.58}$$

where $\tau_0^D$ is the donor decay time in the absence of the acceptor at concentration $C_{Ru}$, for a non-complexed dsDNA, and $\tau_0^F = \mathrm{K}_{T0}^{-1}$ is the inverse of the FRET rate in the absence of complexation. $\tau_0^F$ doesn't depend on $C_{Ru}$ and is measured at $C_{Ru} = 0$.

$$\frac{1}{\tau_{1,n}} = \frac{1}{\tau_{1,n}^D(C_{Ru})} + \frac{1}{\tau_{1,n}^F(C_{Ru})} \tag{3.59}$$

with similar notations. We have used the fact the $\tau_{1,n}^D(C_{Ru})$ doesn't depend *n*, as the observed quenching is dynamic.

We thus have:

$$\bar{\tau} = (1-\xi)\frac{\tau_0^F \tau_0^D(C_{Ru})}{\tau_0^F + \tau_0^D} + \frac{\xi}{14}\tau_1^D(C_{Ru})\sum_{n=1}^{14}\frac{1}{1+(\frac{R_0}{r_{1,n}})^6} \tag{3.60}$$

where $r_{1,n}$ is the distance between the two fluorophores when the intercalation occurs at the $n^{th}$ position.

It is known that the intercalation of the ruthenium compound induces a length increase of the DNA chain equal to the base pair distance. Let us moreover assume that the DNA double strand remains linear and rigid [53].

Then, the length of the dsDNA, complexed with one $Ru(bpy)_2dppz^{2+}$ doesn't depend on the intercalation position and we have:

$$r_{1,n} = \frac{16}{15} r_0 \tag{3.61}$$

where $r_0$ is the length of a 15bp dsDNA chain.

Let us now compute $r_1$ from the experimental measurements. We can use Equation 3.60, recognizing that:

$$(\frac{r_1}{r_0})^6 = \frac{\tau_1^F}{\tau_0^F} = \frac{\tau_1}{\tau_0^F(1-\frac{\tau_1}{\tau_n^D})} \tag{3.62}$$

We obtain $\frac{r_1}{r_0}$. The values of $\frac{r_1}{r_0}$ are plotted in Figure 3.31 as a function of $\xi$. At low $\xi$, the bound ruthenium fraction is too low and the measurement is not accurate, but for values of $\xi \geq 0.2$, $\frac{r_1}{r_0}$ saturates and its average value over the three highest complexation ratios is $\frac{\bar{r_1}}{r_0} = 1.02831$.

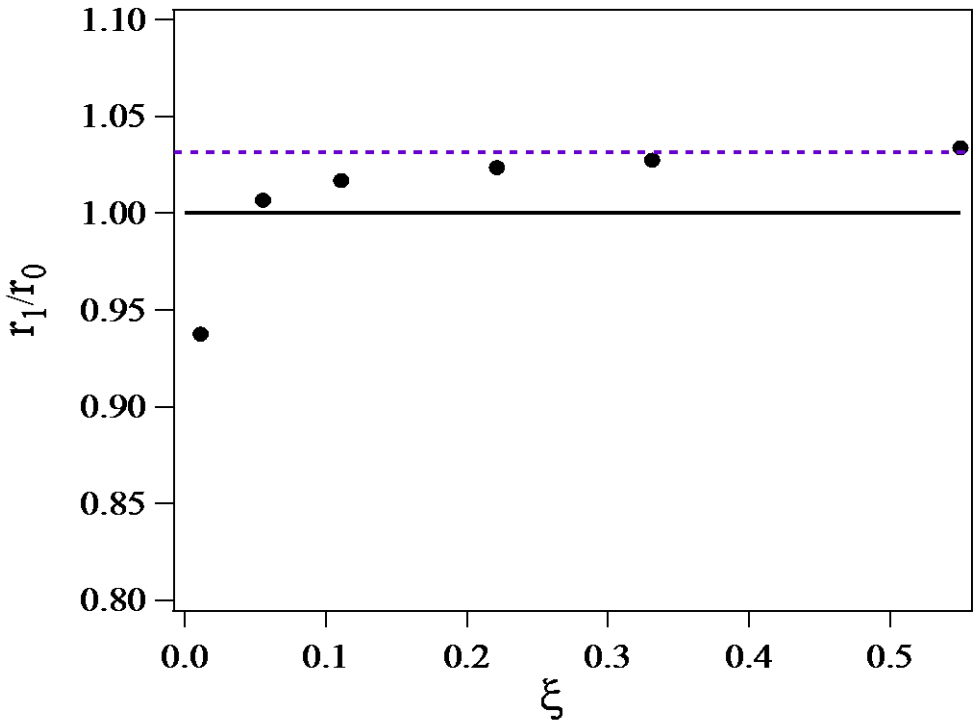


**Figure 3.31:** The evolution of $\frac{r_1}{r_0}$ as a function of $\xi$. Dash line is the average value ($\frac{\overline{r_1}}{r_0}$ = 1.02381) over the three highest complexation ratios.

This value is smaller than if the intercalation would have led to a length increase of a straight double strand, we would have: $\frac{r_{1,n}}{r_0} = \frac{16}{15} = 1.0667$. We thus conclude that the complexation induces a bending in the dsDNA. This bending may be static or dynamic, that is, due to an increase of flexibility of the DNA double strand at the intercalation. Let us define θ the bent angle induced by the intercalation:

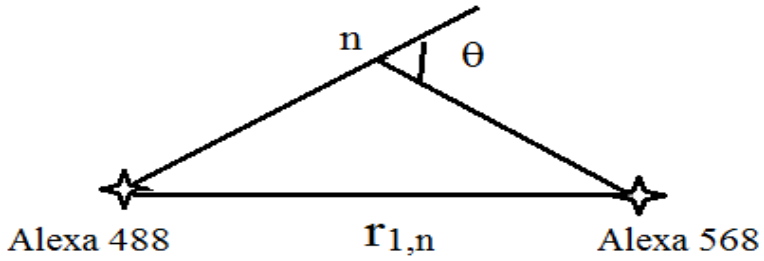


$r_{1,n}$ may be expressed as a function of $n$ and $\theta$, using Al-Khashi theorem：

$$r_{1,n}^2 = a^2[n^2 + (15-n)^2 + 2n(15-n)\cos\theta]^2$$

Equation 3.60 may be written as a function of θ, and solved for θ. The values are plotted in Figure 3.32 as a function of the fraction of complexed dsDNA, ξ.

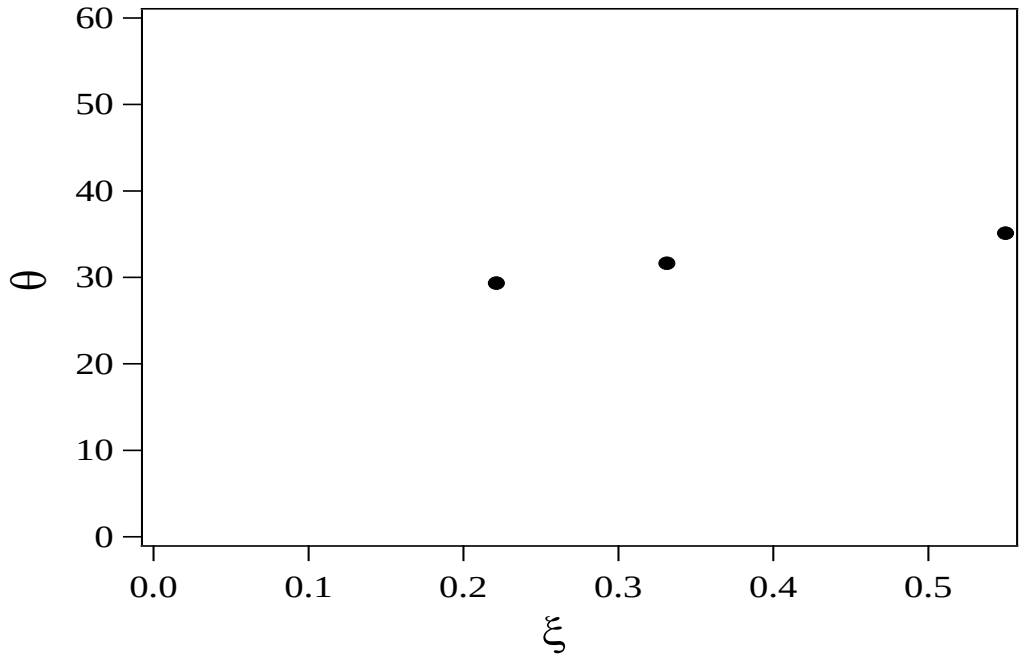


**Figure 3.32:** The values of θ as a function of ξ.

$\theta$ is found to be of the order of 30 degrees, and slightly increases when $\xi$ increases. This may be due to the presence of dsDNA complexed with 2 $Ru(bpy)_2dppz^{2+}$ which have not been taken into account in this analysis.

As a conclusion, we have observed that the end-to-end distance increase of 15bp dsDNA complexed with $Ru(bpy)_2dppz^{2+}$ is smaller than that would be increase if the DNA would remain rigid upon complexation.

We may thus conclude that DNA bends upon complexation. We have found a bending angle of the order 30 degrees. Nevertheless, our experiments cannot determine whether time–average bending is due to a local dynamic flexibility or a static kink induced by the intercalation.

# Chapter 4

## 4 Conclusion

The interactions between $Ru(bpy)_2dppz^{2+}$ and DNA under different salt concentrations (Ranging from10 mM to 100 mM) have been studied by the change of luminescence intensity when ruthenium molecule intercalates into DNA base pair. Following the evolution of the luminescence intensity, we compute the affinity constant $K_a$ and the binding sites ($n$) of ruthenium molecule to DNA double strand. Our experiments show that the affinity constant $K_a$ decrease with the increase of salt concentrations. The $nK$ values obtained from the fitting of $\nu(c_f)$, lead to a logarithm slope of -0.81 in good agreement with Manning's theory. The average binding sites ($n$) under different salt environments is equal to 3.76, which agrees with the size of sites occupied by similar binding ligand and measure with single molecule force spectroscopy.

We have used Fluorescence Resonance Energy Transfer (FRET) to monitor the average distance between the extremities of a 15 bp dsDNA modified with 2 fluorophores at its extremities. The efficiency of this energy transfer is quantified from the measurement of emitted intensities and lifetimes of donor and acceptor when one ruthenium molecule intercalates into DNA base pair. The intensities an lifetimes show a linear decrease behavior with the increase of ruthenium concentration at chosen region [0, 0.5 μM]. The efficiencies of energy transfer separately obtained from the point view of donor and the point view of acceptor display in good

agreement with each other. The efficiency shows a decrease with the intercalation of $Ru(bpy)_2dppz^{2+}$ into DNA double helix. And given the relationship of efficiency with distance of coupled fluorophores, then we get that the distance between two fluorophores increases due to the intercalation of ruthenium. But in our study, we also have observed that the end to end distance increase of 15bp dsDNA complexed with $Ru(bpy)_2dppz^{2+}$ is smaller than that would be increase if the DNA would remain rigid upon complexation. We may thus conclude that DNA bends upon the intercalation of ruthenium molecule. A bending angle was found with the order of 30 degrees. Nevertheless, our experiments can not determine whether time–average bending is due to a local dynamic flexibility or a static kink induced by the intercalation.

# Appendix

# A Sample preparation protocols

## A.1 Drugs—$Ru(bpy)_2dppz^{2+}$

Ruthenium derived compounds were prepared by the group of chemists following their protocols [120,121]. The first step consists in the synthesis of $Ru(bpy)_2Cl_2.2H_2O$. Commercial $RuCl_3.3H_20$ (1.56 g, 5.96 mmol), bipyridine (1.87 g, 12 mmol) and LiCl (1.68 g, 0.4 mmol) were refluxed in dimethylformamide (25 mL) for 8 hours. After the reaction mixture was cooled to room temperature, 150 mL of acetone was added and the resultant solution cooled to 0℃ overnight. This solution was filtered, a red-violet filtrate and a dark green-black microcrystalline product were obtained. The solid was washed three times with 25 mL portions of water and followed by three 25 mL portions of diethyl ether, and then it was dried by suction. Yield 64% (1.99 g). The second step is the coordination by dppz. A mixture of $Ru(bpy)_2Cl_2.2H_2O$ (148 mg, 0.28 mmol) and dipyridophenazine (84 mg, 0.3 mmol) in methanol / water (1 / 2, v / v, 40 mL) was refluxed for 4.5 hours. The deep red solution was concentrated to 10%, diluted with water (20 mL), boiled for 10 minutes, cooled in an ice-bath, and filtered. The tetrafluoroborate salt was precipitated by addition of 10% $NaBF_4$ (30 mL) to the filtrate. The solid was dried in vacuo, redissolved in $CH_3CN$ and then it was filtered over $Al_2O_3$ using $CH_3CN$ as eluent. A red fraction was collected and evaporated. The

resulting red solid was recrystallized from ethanol. Yield 80%.

## A.2 Protocol of preparing dsDNA for our study

The measurements were performed with 15 base pair double stranded DNA. Number of DNA base pairs is limited by the range over which the energy transfer can take place that is approximately 10 nm (100 Å). Complementary strands were purchased from IBA NAPS(Gmbh) with sequences: GGA GAC CAG AGG CCT and AGG CCT CTG GTCTCC. The length of 15 base pair DNA equal to 5.1 nm is small enough to stiffen the DNA structure. Thus any unexpected bends are not supposed to appear.

The first sequence was 5' labeled with Alexa488 and 3' labeled with Alexa568. The distance at which this fluorophores pair undergoes 50% energy transfer, $R_0$, for these pair of fluorophores is $R_0$ = 62 Å [118]. Both two strands were resuspended to a final stand concentration 20 μM (DNA base pairs concentration is 300 μM) in NaCl of 20 mM (at 25 ℃). Next they were annealed by heating the DNA to 94 ℃ before cooling down the sample to 16 ℃ for 15 minutes, then DNA was cooled down to 16 ℃ for another 15 minutes. All of the measurements were performed at 20 ℃ to ensure the DNA remain the double helix structure . To perform experiments of salt dependance, DNA was diluted in NaCl. The salinity have been increasing from 10 mM to 100 mM.

# Bibliography

[1] X-ray structure of the major adduct of the anticancer drug cisplatin with DNA: cis-[Pt (NH3) 2 (d (pGpG))]. S. E. Sherman, D. Gibson, A. Wang, S. J. Lippard. Science. 1985, 230(4724): 412-417.

[2] A. B. H. Lodish, P. Matsudaira, C. A. Kaiser, M. Krieger, M. P. Scott, L. Zipursky, J. Darnell (2003) *Molecular and Cell Biology, Fifth Edition* (W. H. Freeman and Company).

[3] R. F. Bruinsma (2002) Physics of protein-DNA interaction. *Physics of bio-molecules and cells. Physique des biomol écules et des cellules*, (Springer), pp 1-68.

[4] Crystal structure analysis of a complete turn of B-DNA. R. E. Dickerson. Nature. 1980, 287: 755.

[5] M. B. Jackson (2006) *Molecular and cellular biophysics* (Cambridge University Press).

[6] L. Stryer,D. S. Latchman (1995) *Biochemistry (4th edn)* (W. H. Freeman and Company New York) p 791.

[7] Study of the interaction between novel ruthenium (II)-polypyridyl complexes and calf thymus DNA. G. Yang, J. Z. Wu, L. Wang, L. N. Ji, X. Tian. Journal of inorganic biochemistry. 1997, 66(2): 141-144.

[8] Novel dipyridophenazine complexes of ruthenium (II): exploring luminescent reporters of DNA. R. M. Hartshorn,J. K. Barton. Journal of the American

Chemical Society. 1992, 114(15): 5919-5925.

[9] Thermodynamic and structural study of phenanthroline derivative ruthenium complex/DNA interactions: Probing partial intercalation and binding properties. E. Grueso, G. López-Pérez, M. Castellano, R. Prado-Gotor. Journal of inorganic biochemistry. 2012, 106(1): 1-9.

[10] DNA binding geometries of ruthenium (II) complexes with 1, 10-phenanthroline and 2, 2'-bipyridine ligands studied with linear dichroism spectroscopy. Borderline cases of intercalation. P. Lincoln,B. Norden. The Journal of Physical Chemistry B. 1998, 102(47): 9583-9594.

[11] Crystal structure of Δ-[Ru (bpy) 2dppz] 2+ bound to mismatched DNA reveals side-by-side metalloinsertion and intercalation. H. Song, J. T. Kaiser, J. K. Barton. Nature Chemistry. 2012, 4(8): 615-620.

[12] Crystal structures of Λ-[Ru (phen) 2dppz] 2+ with oligonucleotides containing TA/TA and AT/AT steps show two intercalation modes. H. Niyazi, J. P. Hall, K. O'Sullivan, G. Winter, T. Sorensen, J. M. Kelly, C. J. Cardin. Nature Chemistry. 2012, 4(8): 621-628.

[13] Binding modes and base specificity of tris (phenanthroline) ruthenium (II) enantiomers with nucleic acids: tuning the stereoselectivity. J. K. Barton, J. M. Goldberg, C. V. Kumar, N. J. Turro. Journal of the American Chemical Society. 1986, 108(8): 2081-2088.

[14] Neither. DELTA.-nor. LAMBDA.-Tris (phenanthroline) ruthenium (II) Binds to DNA by Classical Intercalation. S. Satyanarayana, J. C. Dabrowiak, J. B. Chaires. Biochemistry. 1992, 31(39): 9319-9324.

[15] Metallo-intercalators and metallo-insertors. B. M. Zeglis, V. C. Pierre, J. K. Barton. Chemical Communications. 2007,(44): 4565-4579.

[16] Enantiomeric selectivity in binding tris(phenanthroline)zinc(II) to DNA. J. K. Barton, J. J. Dannenberg, A. L. Raphael. Journal of the American Chemical Society. 1982, 104(18): 4967-4969.

[17] Tris(phenanthroline)ruthenium(II): stereoselectivity in binding to DNA. J. K. Barton, A. Danishefsky, J. Goldberg. Journal of the American Chemical Society. 1984, 106(7): 2172-2176.

[18] Photophysics of ruthenium complexes bound to double helical DNA. C. V. Kumar, J. K. Barton, N. J. Turro. Journal of the American Chemical Society. 1985, 107(19): 5518-5523.

[19] Binding modes and base specificity of tris(phenanthroline)ruthenium(II) enantiomers with nucleic acids: tuning the stereoselectivity. J. K. Barton, J. M. Goldberg, C. V. Kumar, N. J. Turro. Journal of the American Chemical Society. 1986, 108(8): 2081-2088.

[20] Proton NMR studies of tris(phenanthroline) metal complexes bound to oligonucleotides: characterization of binding modes. J. P. Rehmann,J. K. Barton. Biochemistry. 1990, 29(7): 1701-1709.

[21] Proton NMR studies of tris(phenanthroline) metal complexes bound to oligonucleotides: structural characterizations via selective paramagnetic relaxation. J. P. Rehmann,J. K. Barton. Biochemistry. 1990, 29(7): 1710-1717.

[22] Site-specific cleavage of left-handed DNA in pBR322 by lambda-tris (diphenylphenanthroline) cobalt (III). J. K. Barton,A. L. Raphael. Proceedings of the National Academy of Sciences. 1985, 82(19): 6460-6464.

[23] Chiral probes for the handedness of DNA helices: enantiomers of tris (4, 7-diphenylphenanthroline) ruthenium (II). J. K. Barton, L. A. Basile, A. Danishefsky, A. Alexandrescu. Proceedings of the National Academy of Sciences. 1984, 81(7): 1961-1965.

[24] Metals and DNA: molecular left-handed complements. J. K. Barton. Science. 1986, 233(4765): 727-734.

[25] Recognition and Reaction of Metallointercalators with DNA. K. E. Erkkila, D. T. Odom, J. K. Barton. Chemical reviews. 1999, 99(9): 2777-2796.

[26] Tris(phenanthroline)ruthenium(II) enantiomer interactions with DNA: Mode and specificity of binding. S. Satyanarayana, J. C. Dabrowiak, J. B. Chaires. Biochemistry. 1993, 32(10): 2573-2584.

[27] Binding of .DELTA.- and .LAMBDA.-[Ru(phen)3]2+ to [d(CGCGATCGCG)]2 Studied by NMR. M. Eriksson, M. Leijon, C. Hiort, B. Norden, A. Graeslund. Biochemistry. 1994, 33(17): 5031-5040.

[28] Artificial Nucleases. C.-h. B. Chen, L. Milne, R. Landgraf, D. M. Perrin, D. S. Sigman. ChemBioChem. 2001, 2(10): 735-740.

[29] Nuclease activity of 1,10-phenanthroline-copper ion. D. S. Sigman. Accounts of Chemical Research. 1986, 19(6): 180-186.

[30] Targeted chemical nucleases. D. S. Sigman, T. W. Bruice, A. Mazumder, C. L. Sutton. Accounts of Chemical Research. 1993, 26(3): 98-104.

[31] Interaction of Double‐Helical Polynuclear Copper (I) complexes with double‐stranded DNA. B. Schoentjes,J. M. Lehn. Helvetica Chimica Acta. 1995, 78(1): 1-12.

[32] Supramolecular DNA recognition. M. J. Hannon. Chemical Society Reviews. 2007, 36(2): 280-295.

[33] A DNA‐Binding Copper (I) Metallosupramolecular Cylinder that Acts as an Artificial Nuclease. L. J. Childs, J. Malina, B. E. Rolfsnes, M. Pascu, M. J. Prieto, M. J. Broome, P. M. Rodger, E. Sletten, V. Moreno, A. Rodger. Chemistry-A European Journal. 2006, 12(18): 4919-4927.

[34] Molecular Recognition of a Three‐Way DNA Junction by a Metallosupramolecular Helicate. A. Oleksi, A. G. Blanco, R. Boer, I. Usón, J. Aymamí, A. Rodger, M. J. Hannon, M. Coll. Angewandte Chemie. 2006, 118(8): 1249-1253.

[35] Design and DNA Binding of an Extended Triple‐Stranded Metallo‐supramolecular Cylinder. C. Uerpmann, J. Malina, M. Pascu, G. J. Clarkson, V. Moreno, A. Rodger, A. Grandas, M. J. Hannon. Chemistry-A European Journal. 2005, 11(6): 1750-1756.

[36] A molecular light switch for DNA: $[Ru(bpy)_2(dppz)]^{2+}$. A. E. Friedman, J. C. Chambron, J. P. Sauvage, N. J. Turro, J. K. Barton. Journal of the American Chemical Society. 1990, 112(12): 4960-4962.

[37] Characterization of dipyridophenazine complexes of ruthenium (II): the light switch effect as a function of nucleic acid sequence and conformation. Y. Jenkins, A. E. Friedman, N. J. Turro, J. K. Barton. Biochemistry. 1992, 31(44): 10809-10816.

[38] Photophysical Evidence That Δ- and Λ-[Ru(phen)2(dppz)]2+ Intercalate DNA from the Minor Groove. E. Tuite, P. Lincoln, B. Nordén. Journal of the American Chemical Society. 1997, 119(1): 239-240.

[39] DNA binding of .DELTA.- and .LAMBDA.-[Ru(phen)2DPPZ]2+. C. Hiort, P. Lincoln, B. Norden. Journal of the American Chemical Society. 1993, 115(9): 3448-3454.

[40] Diastereomeric DNA-Binding Geometries of Intercalated Ruthenium(II) Trischelates Probed by Linear Dichroism: [Ru(phen)2DPPZ]2+ and [Ru(phen)2BDPPZ]2+. P. Lincoln, A. Broo, B. Nordén. Journal of the American Chemical Society. 1996, 118(11): 2644-2653.

[41] Differential DNA Recognition by the Enantiomers of 1-Rh(MGP)2phi: A

Combination of Shape Selection and Direct Readout†. S. J. Franklin,J. K. Barton. Biochemistry. 1998, 37(46): 16093-16105.

[42] Solution Structure of a Metallointercalator Bound Site Specifically to DNA. B. P. Hudson,J. K. Barton. Journal of the American Chemical Society. 1998, 120(28): 6877-6888.

[43] Use of Selective Deuteration and 1H NMR in Demonstrating Major Groove Binding of .DELTA.-[Ru(phen)2dppz]2+ to d(GTCGAC)2. C. M. Dupureur,J. K. Barton. Journal of the American Chemical Society. 1994, 116(22): 10286-10287.

[44] 1H-NMR of Rh(NH3)4phi3+ Bound to d(TGGCCA)2: Classical Intercalation by a Nonclassical Octahedral Metallointercalator. J. G. Collins, T. P. Shields, J. K. Barton. Journal of the American Chemical Society. 1994, 116(22): 9840-9846.

[45] Structure of a photoactive rhodium complex intercalated into DNA. C. L. Kielkopf, K. E. Erkkila, B. P. Hudson, J. K. Barton, D. C. Rees. Nature Structural & Molecular Biology. 2000, 7(2): 117-121.

[46] Structural considerations in the interaction of DNA and acridines. L. Lerman. Journal of molecular biology. 1961, 3(1): 18-IN14.

[47] Turning the $[Ru(bpy)_2dppz]^{2+}$ light-switch on and off with temperature. M. K. Brennaman, J. H. Alstrum-Acevedo, C. N. Fleming, P. Jang, T. J. Meyer, J. M. Papanikolas. Journal of the American Chemical Society. 2002, 124(50): 15094-15098.

[48] $[Ru(bpy)_2dppz]^{2+}$ light-switch mechanism in protic solvents as studied through temperature-dependent lifetime measurements. M. K. Brennaman, T. J. Meyer, J. M. Papanikolas. The Journal of Physical Chemistry A. 2004, 108(45): 9938-9944.

[49] [Ru (bpy) 2dppz] 2+ electrochemiluminescence switch and its applications for

DNA interaction study and label-free ATP aptasensor. L. Hu, Z. Bian, H. Li, S. Han, Y. Yuan, L. Gao, G. Xu. Analytical chemistry. 2009, 81(23): 9807-9811.

[50] Sensitivity of Ru (bpy) 2dppz2+ Luminescence to DNA Defects. M. H. Lim, H. Song, E. D. Olmon, E. E. Dervan, J. K. Barton. Inorganic chemistry. 2009, 48(12): 5392-5397.

[51] Efficient DNA photocleavage by [Ru (bpy) 2 (dppn)] 2+ with visible light. Y. Sun, L. E. Joyce, N. M. Dickson, C. Turro. Chemical Communications. 2010, 46(14): 2426-2428.

[52] Measuring the binding of small molecules to protein from binding-induced alterations of physical-chemical properties. C. J. Halfman,T. Nishida. Biochemistry. 1972, 11(18): 3493-3498.

[53] Quantifying force-dependent and zero-force DNA intercalation by single-molecule stretching. I. D. Vladescu, M. J. McCauley, M. E. Nuñez, I. Rouzina, M. C. Williams. Nature methods. 2007, 4(6): 517-522.

[54] Immunological method for mapping genes on Drosophila polytene chromosomes. P. R. Langer-Safer, M. Levine, D. C. Ward. Proceedings of the National Academy of Sciences. 1982, 79(14): 4381-4385.

[55] Interaction du bromhydrate d''ethidium avec les acides nucl'eiques (AN). etude spectrofluorim'etrique. J. Le Pecq, P. Yot, C. Paoletti. CR Hebd Seances Acad Sci. 1964: 1786-1789.

[56] Fluoresence studies of nucleotides and polynucleotides III. diphosphopyridine nucleotide analogues which contain fluorescent purines. D. Ward, T. Horn, E. Reich. Journal of Biological Chemistry. 1972, 247(12): 4014-4020.

[57] Detection of two restriction endonuclease activities in Haemophilus parainfluenzae using analytical agarose-ethidium bromide electrophoresis. P. A.

Sharp, B. Sugden, J. Sambrook. Biochemistry. 1973, 12(16): 3055-3063.

[58] Enhanced chemiluminescent method for the detection of DNA dot-hybridization assays. J. A. Matthews, A. Batki, C. Hynds, L. J. Kricka. Analytical biochemistry. 1985, 151(1): 205-209.

[59] Unusual photophysical properties of a ruthenium (II) complex related to [Ru (bpy) 2 (dppz)] 2+. Y. Sun, S. N. Collins, L. E. Joyce, C. Turro. Inorganic chemistry. 2010, 49(9): 4257-4262.

[60] Proton transfer quenching of the MLCT excited state of $[Ru(phen)_2dppz]^{2+}$ in homogeneous solution and bound to DNA. C. Turro, S. H. Bossmann, Y. Jenkins, J. K. Barton, N. J. Turro. Journal of the American Chemical Society. 1995, 117(35): 9026-9032.

[61] $[Ru(phen)_2dppz]^{2+}$ luminescence: Dependence on DNA sequences and groove-binding agents. R. E. Holmlin, E. D. Stemp, J. K. Barton. Inorganic chemistry. 1998, 37(1): 29-34.

[62] Emission Spectroscopy of Ru (bpy) 2dppz2+ in Nafion. Probing the Chemical Environment in Cast Films. E. Sabatani, H. D. Nikol, H. B. Gray, F. C. Anson. Journal of the American Chemical Society. 1996, 118(5): 1158-1163.

[63] A long-lived, highly luminescent Re (I) metal–ligand complex as a biomolecular probe. X.-Q. Guo, F. N. Castellano, L. Li, H. Szmacinski, J. R. Lakowicz, J. Sipior. Analytical biochemistry. 1997, 254(2): 179-186.

[64] On the Excited States Involved in the Luminescent Probe [Ru (bpy) 2dppz] 2+. E. R. Batista,R. L. Martin. The Journal of Physical Chemistry A. 2005, 109(14): 3128-3133.

[65] DNA binding to an anticancer organo-ruthenium complex. M. Klajner, P. Hebraud, C. Sirlin, C. Gaiddon, S. Harlepp. The Journal of Physical Chemistry B.

2010, 114(44): 14041-14047.

[66] Exploring the interaction of ruthenium (II) polypyridyl complexes with DNA using single-molecule techniques. A. Mihailovic, I. Vladescu, M. McCauley, E. Ly, M. C. Williams, E. M. Spain, M. E. Nuñez. Langmuir. 2006, 22(10): 4699-4709.

[67] Spectral properties of polypyridyl ruthenium complexes intercalated in DNA: theoretical insights into the surrounding effects of [Ru (dppz)(bpy) 2] 2+. T. Very, S. Despax, P. Hébraud, A. Monari, X. Assfeld. Physical Chemistry Chemical Physics. 2012, 14(36): 12496-12504.

[68] A general method of analysis of ligand-macromolecule equilibria using a spectroscopic signal from the ligand to monitor binding. Application to Escherichia coli single-strand binding protein-nucleic acid interactions. W. Bujalowski,T. M. Lohman. Biochemistry. 1987, 26(11): 3099-3106.

[69] Full-length Dengue virus RNA-dependent RNA polymerase-RNA/DNA complexes: stoichiometries, intrinsic affinities, cooperativities, base, and conformational specificities. M. R. Szymanski, M. J. Jezewska, P. J. Bujalowski, C. Bussetta, M. Ye, K. H. Choi, W. Bujalowski. J Biol Chem. 2011, 286(38): 33095-33108.

[70] T. M. Lohman,W. Bujalowski (1991) [15] Thermodynamic methods for model-independent determination of equilibrium binding isotherms for protein-DNA interactions: Spectroscopic approaches to monitor binding. *Methods in Enzymology*, ed Robert TS (Academic Press), Vol Volume 208, pp 258-290.

[71] T. L. Hill,A. Rich (1985, Chapter 6) *Cooperativity theory in biochemistry: steady-state and equilibrium systems* (Springer-Verlag New York:).

[72] Negative cooperativity in the binding of nucleotides to Escherichia coli replicative helicase DnaB protein. Interactions with fluorescent nucleotide

analogs. W. Bujalowski,M. M. Klonowska. Biochemistry. 1993, 32(22): 5888-5900.

[73] Theoretical aspects of DNA-protein interactions: co-operative and non-co-operative binding of large ligands to a one-dimensional homogeneous lattice. J. D. McGhee,P. H. von Hippel. Journal of molecular biology. 1974, 86(2): 469-489.

[74] Cooperative and non-cooperative binding of large ligands to a finite one-dimensional lattice: A model for ligand-ougonucleotide interactions. I. R. Epstein. Biophysical chemistry. 1978, 8(4): 327-339.

[75] Interaction of recA protein with single-stranded DNA: quantitative aspects of binding affinity modulation by nucleotide cofactors. J. P. Menetski,S. C. Kowalczykowski. Journal of molecular biology. 1985, 181(2): 281-295.

[76] Cooperative and noncooperative binding of protein ligands to nucleic acid lattices: experimental approaches to the determination of thermodynamic parameters. S. C. Kowalczykowski, L. S. Paul, N. Lonberg, J. W. Newport, J. A. McSwiggen, P. H. Von Hippel. Biochemistry. 1986, 25(6): 1226-1240.

[77] Fluorescence Anisotropy Studies on the Ku-DNA Interaction ANION AND CATION EFFECTS. D. Arosio, S. Costantini, Y. Kong, A. Vindigni. Journal of Biological Chemistry. 2004, 279(41): 42826-42835.

[78] Theory of multivalent binding in one and two-dimensional lattices. E. Di Cera,Y. Kong. Biophysical chemistry. 1996, 61(2): 107-124.

[79] A gel electrophoresis method for quantifying the binding of proteins to specific DNA regions: application to components of the Escherichia coli lactose operon regulatory system. M. M. Garner,A. Revzin. Nucleic acids research. 1981, 9(13): 3047-3060.

[80] Theory and applications of the transferred nuclear Overhauser effect to the study of the conformations of small ligands bound to proteins. G. Clore,A. Gronenborn. Journal of Magnetic Resonance (1969). 1982, 48(3): 402-417.

[81] A double-filter method for nitrocellulose-filter binding: application to protein-nucleic acid interactions. I. Wong,T. M. Lohman. Proceedings of the National Academy of Sciences. 1993, 90(12): 5428-5432.

[82] RNA binding mediates the local cooperativity between the β-sheet and the C-terminal tail of the human U1A RBD1 protein. J. K. Kranz,K. B. Hall. Journal of molecular biology. 1998, 275(3): 465-481.

[83] The DinI protein stabilizes RecA protein filaments. S. L. Lusetti, O. N. Voloshin, R. B. Inman, R. D. Camerini-Otero, M. M. Cox. Journal of Biological Chemistry. 2004, 279(29): 30037-30046.

[84] Comparative Thermodynamic Analysis of DNA−Protein Interactions Using Surface Plasmon Resonance and Fluorescence Correlation Spectroscopy†. F. Schubert, H. Zettl, W. Häfner, G. Krauss, G. Krausch. Biochemistry. 2003, 42(34): 10288-10294.

[85] Equilibria and kinetics of lac repressor-operator interactions by polyacrylamide gel electrophoresis. M. Fried,D. M. Crothers. Nucleic acids research. 1981, 9(23): 6505-6525.

[86] Measurement of macromolecular equilibrium binding constants by a sucrose gradient band sedimentation method. Application to protein-nucleic acid interactions. D. E. Draper,P. H. Von Hippel. Biochemistry. 1979, 18(5): 753-760.

[87] DNA Bends in TATA-binding Protein · TATA Complexes in Solution Are DNA Sequence-dependent. J. Wu, K. M. Parkhurst, R. M. Powell, M. Brenowitz, L. J. Parkhurst. Journal of Biological Chemistry. 2001, 276(18): 14614-14622.

[88] The titration constants of multivalent substances. A. L. v. Muralt. Journal of the American Chemical Society. 1930, 52(9): 3518-3523.

[89] The application of the law of mass action to binding by proteins; interactions with calcium. I. M. KLOTZ. Archives of biochemistry. 1946, 9: 109.

[90] The attractions of proteins for small molecules and ions. G. Scatchard. Annals of the New York Academy of Sciences. 1949, 51(4): 660-672.

[91] Physical Chemistry of Protein Solutions. IV. The Combination of Human Serum Albumin with Chloride Ion1. G. Scatchard, I. H. Scheinberg, S. H. Armstrong Jr. Journal of the American Chemical Society. 1950, 72(1): 535-540.

[92] Ion effects on ligand-nucleic acid interactions. M. T. Record Jr, T. M. Lohman, P. d. Haseth. Journal of molecular biology. 1976, 107(2): 145-158.

[93] Limiting laws and counterion condensation in polyelectrolyte solutions I. Colligative properties. G. S. Manning. The Journal of Chemical Physics. 1969, 51: 924.

[94] On the application of polyelectrolyte "limiting laws" to the helix‐coil transition of DNA. I. Excess univalent cations. G. S. Manning. Biopolymers. 1972, 11(5): 937-949.

[95] Thermodynamic analysis of ion effects on the binding and conformational equilibria of proteins and nucleic acids: the roles of ion association or release, screening, and ion effects on water activity. M. T. Record, C. F. Anderson, T. M. Lohman. Quarterly reviews of biophysics. 1978, 11(02): 103-178.

[96] Analysis of bacterial function by multi-colour fluorescence flow cytometry and single cell sorting. G. Nebe-von-Caron, P. Stephens, C. Hewitt, J. Powell, R. Badley. Journal of microbiological methods. 2000, 42(1): 97-114.

[97] Flow cytometry in biotechnology. M. Rieseberg, C. Kasper, K. F. Reardon, T.

Scheper. Applied microbiology and biotechnology. 2001, 56(3-4): 350-360.

[98] S. Andersson-Engels, J. Johansson, K. Svanberg, S. Svanberg (1990) Laser-induced fluorescence in medical diagnostics. *OE/LASE'90, 14-19 Jan., Los Angeles, CA*, (International Society for Optics and Photonics), pp 76-96.

[99] New strategies for fluorescent probe design in medical diagnostic imaging. H. Kobayashi, M. Ogawa, R. Alford, P. L. Choyke, Y. Urano. Chemical reviews. 2009, 110(5): 2620-2640.

[100] A system for rapid DNA sequencing with fluorescent chain-terminating dideoxynucleotides. J. M. Prober, G. L. Trainor, R. J. Dam, F. W. Hobbs, C. W. Robertson, R. J. Zagursky, A. J. Cocuzza, M. A. Jensen, K. Baumeister. Science. 1987, 238(4825): 336-341.

[101] Fluorescence energy transfer dye-labeled primers for DNA sequencing and analysis. J. Ju, C. Ruan, C. W. Fuller, A. N. Glazer, R. A. Mathies. Proceedings of the National Academy of Sciences. 1995, 92(10): 4347-4351.

[102] Automated DNA sequencing: ultrasensitive detection of fluorescent bands during electrophoresis. W. Ansorge, B. Sproat, J. Stegemann, C. Schwager, M. Zenke. Nucleic acids research. 1987, 15(11): 4593-4602.

[103] Genetic analysis of digestive physiology using fluorescent phospholipid reporters. S. A. Farber, M. Pack, S.-Y. Ho, I. D. Johnson, D. S. Wagner, R. Dosch, M. C. Mullins, H. S. Hendrickson, E. K. Hendrickson, M. E. Halpern. Science. 2001, 292(5520): 1385-1388.

[104] Allelic discrimination using fluorogenic probes and the 5′ nuclease assay. K. J. Livak. Genetic analysis: biomolecular engineering. 1999, 14(5): 143-149.

[105] Fluorescence molecular imaging. V. Ntziachristos. Annu. Rev. Biomed. Eng. 2006, 8: 1-33.

[106] Imaging intracellular fluorescent proteins at nanometer resolution. E. Betzig, G. H. Patterson, R. Sougrat, O. W. Lindwasser, S. Olenych, J. S. Bonifacino, M. W. Davidson, J. Lippincott-Schwartz, H. F. Hess. Science. 2006, 313(5793): 1642-1645.

[107] Molecular imaging in living subjects: seeing fundamental biological processes in a new light. T. F. Massoud,S. S. Gambhir. Genes & development. 2003, 17(5): 545-580.

[108] Fluorescence correlations, single molecule detection and large number screening applications in biotechnology. R. Rigler. Journal of biotechnology. 1995, 41(2): 177-186.

[109] Real-time single-molecule imaging of the infection pathway of an adeno-associated virus. G. Seisenberger, M. U. Ried, T. Endress, H. Büning, M. Hallek, C. Bräuchle. Science. 2001, 294(5548): 1929-1932.

[110] Real-time imaging of fluorescent flagellar filaments. L. Turner, W. S. Ryu, H. C. Berg. Journal of Bacteriology. 2000, 182(10): 2793-2801.

[111] Alexa and Oregon Green dyes as fluorescence anisotropy probes for measuring protein–protein and protein–nucleic acid interactions. E. Rusinova, V. Tretyachenko-Ladokhina, O. E. Vele, D. F. Senear, J. Alexander Ross. Analytical biochemistry. 2002, 308(1): 18-25.

[112] Quantitative comparison of long-wavelength Alexa Fluor dyes to Cy dyes: fluorescence of the dyes and their bioconjugates. J. E. Berlier, A. Rothe, G. Buller, J. Bradford, D. R. Gray, B. J. Filanoski, W. G. Telford, S. Yue, J. Liu, C.-Y. Cheung. Journal of Histochemistry & Cytochemistry. 2003, 51(12): 1699-1712.

[113] FRET tells us about proximities, distances, orientations and dynamic properties. R. M. Clegg. Journal of biotechnology. 2002, 82(3): 177.

[114] Theory of the energy transfer efficiency and fluorescence lifetime distribution in single-molecule FRET. I. V. Gopich,A. Szabo. Proceedings of the National Academy of Sciences. 2012, 109(20): 7747-7752.

[115] Orientation dependence in fluorescent energy transfer between Cy3 and Cy5 terminally attached to double-stranded nucleic acids. A. Iqbal, S. Arslan, B. Okumus, T. J. Wilson, G. Giraud, D. G. Norman, T. Ha, D. M. Lilley. Proceedings of the National Academy of Sciences. 2008, 105(32): 11176-11181.

[116] Orientational dynamics and dye-DNA interactions in a dye-labeled DNA aptamer. J. R. Unruh, G. Gokulrangan, G. Lushington, C. K. Johnson, G. S. Wilson. Biophysical journal. 2005, 88(5): 3455-3465.

[117] Orientation control of fluorescence resonance energy transfer using DNA as a helical scaffold. F. D. Lewis, L. Zhang, X. Zuo. Journal of the American Chemical Society. 2005, 127(28): 10002-10003.

[118] L. Technologies ($R_0$ values for some Alexa Fluor dyes) http://www.lifetechnologies.com/fr/fr/home/references/molecular-probes-the-handbook/tables/r0-values-for-some-alexa-fluor-dyes.html

[119] W. Becker (2005) *Advanced time-correlated single photon counting techniques (Series in chemical physics, Vol. 81)* (Springer-Verlag).

[120] Synthesis and study of a mixed-ligand ruthenium (II) complex in its ground and excited states: bis (2, 2′-bipyridine)(dipyrido [3, 2-a: 2′, 3′-c] phenazine-N4N5) ruthenium (II). E. Amouyal, A. Homsi, J.-C. Chambron, J.-P. Sauvage. Journal of the Chemical Society, Dalton Transactions. 1990,(6): 1841-1845.

[121] Mixed phosphine 2,2'-bipyridine complexes of ruthenium. B. P. Sullivan, D. J. Salmon, T. J. Meyer. Inorganic chemistry. 1978, 17(12): 3334-3341.

# Bibliography

# List of figures

# List of tables